

Lymphoid tissue stromal cells regulate lymph node and Peyer's patch homeostasis and facilitate adaptive immune responses

A dissertation presented

by

Jonathan Chang

to

The Division of Medical Sciences

in partial fulfillment of the requirements

for the degree of

Doctor of Philosophy

in the subject of

Immunology

Harvard University

Cambridge, Massachusetts

April 2018

© 2018 Jonathan Chang

All rights reserved

Dissertation Advisors: Dr. Michael Carroll  
Dr. Shannon Turley

Jonathan Chang

**Lymphoid tissue stromal cells regulate lymph node and Peyer's patch homeostasis and facilitate adaptive immune responses**

**ABSTRACT**

The initiation of adaptive immune responses depends upon the careful maneuvering of lymphocytes and antigen into and within strategically placed lymphoid tissues. Non-hematopoietic stromal cells form the cellular infrastructure that directs this process. Once regarded as merely structural features of lymphoid tissues, these cells are now appreciated as essential regulators of immune cell trafficking, fluid flow, and lymph node homeostasis.

Recent advances in the identification and *in vivo* targeting of specific stromal populations have revealed important insights into the population heterogeneity and functional complexity of lymphoid tissue stromal cells. Here, we attempt to expand on these findings by describing a novel model of CXCL13-cre-directed cellular ablation. These studies have allowed us to characterize the specific contributions of the CXCL13-expressing stromal cell compartment to lymphoid tissue homeostasis.

We have additionally sought to provide new insights to the functions of stromal cells in intestinal Peyer's patches – an area which, until recently, has been largely overlooked. Peyer's patches (PPs) are B cell-rich lymphoid tissues situated throughout the small intestine which play

an important role in mucosal antibody responses. PP architecture and stromal cell composition closely resemble that of peripheral lymph nodes despite geographical and functional differences. Notably, fibroblastic stromal cells located in small intestinal PPs form a network of collagen-rich reticular fibers similar to the network of conduits found in lymph nodes. Unlike lymph nodes, PPs lack a conventional source of afferent lymph that would normally contribute fluid flow through the conduit network. Instead fluid flow through PP conduits depends largely on water absorbed across the intestinal epithelium. We find that by disrupting water absorption, we can limit or prevent the contribution of absorbed luminal fluids to the flow of PP conduits. Disruption of fluid absorption subsequently has profound effects on the structural integrity of the high endothelial venules and surrounding perivascular FRCs and correlates with a striking defect in the recruitment of naïve recirculating lymphocytes to the PP. Prolonged disruption additionally impacts mucosal antibody responses. We believe these findings reveal a critical role for conduit-mediated fluid flow in the maintenance of Peyer's patch homeostasis and mucosal immune function.

## Acknowledgements

**I am deeply grateful to my advisors, Mike and Shannon.** I have learned so much from them both. Without their encouragement, enthusiasm, and patience, none of this work could have been completed. Shannon – Thank you for guiding me into the field of stromal cell immunology, for helping me find and pursue my interests, and especially for sticking with me these last few years. Mike – Thank you so much for taking me in, for investing so much of your time and careful thought, and for your dedication to my training.

**I am grateful to my dissertation and thesis committee members** for their insightful suggestions and especially for taking time out of their very busy schedules to provide me guidance.

**Thank you to all my lab mates** for all the support and for making the lab such a great place to work.

**Thank you to my classmates, especially Ezana, Wilson, and David.** Any time grad school seemed endless and terrible, it was such a great relief to know I was not alone in my poor life choices.

**Thank you Mom and Dad** for working so hard to provide me with everything I could have ever needed, and for making me the person I am. Mom, thank you for always reminding me to not only work hard, but to have fun. Dad, thank you for the example you've set for me as a scientist and as a person.

**Thank you Laura** – I've always looked up to you.

**Thank you Cat** for making every day better.

To Grandma – you made us all succeed.

# Table of Contents

<b>Abstract</b> .....	iii
<b>Acknowledgements</b> .....	v
<b>Table of Contents</b> .....	vii
<b>Chapter 1: Introduction</b> .....	1
1.1: Introduction .....	2
1.2: Lymphoid tissue organogenesis .....	3
1.3: Lymphocyte recirculation and lymph node surveillance .....	6
1.4: Antigen transport to lymph nodes .....	15
1.5: Immune cell positioning and homeostasis in lymph nodes .....	21
1.6: Concluding remarks .....	27
<b>Chapter 2: CXCL13cre as a novel model of stromal cell manipulation</b> .....	30
2.1: Introduction .....	31
2.2: Results .....	32
2.3: Discussion .....	49
2.4: Materials and methods .....	55
<b>Chapter 3: Intestinal fluid absorption modulates Peyer's patch homeostasis and mucosal antibody responses.</b> .....	58
3.1: Introduction .....	59
3.2: Results .....	61
3.3: Discussion .....	92
3.4: Materials and methods .....	98
<b>Chapter 4: Discussion and future directions.</b> .....	106
4.1: Technological breakthroughs enable an acceleration of stromal cell immunology .....	106
4.2: Exploration of conduit networks and moving beyond descriptive research with new experimental approaches.....	109
<b>References:</b> .....	114

## Chapter 1: Introduction

***Adapted from:***

Jonathan E. Chang<sup>1,2</sup>, Shannon J. Turley<sup>3</sup>. **Stromal infrastructure of the lymph node and coordination of immunity.** *Trends in Immunology* 36, 30-39. 2015



## 1.1 Introduction

### **Stromal contributions to the initiation of adaptive immunity**

The immune system's enormous repertoire of antigen receptors provides a level of versatility to match the vast array of potential antigens one may encounter in a lifetime. Yet this versatility comes at the cost of pure numbers for any one antigen-specific cell. Each distinct population of naive lymphocytes is exceedingly rare. Naive T cell precursor frequencies for a given peptide-MHC range between just 1 cell per 100,000-1,000,000 and thus in some instances may number fewer than 100 cells per mouse <sup>1-6</sup>. Antigen-reactive naive B cell precursors are similarly quite rare <sup>7-9</sup>. The initiation of immunity depends upon the timely encounter of these rare lymphocytes with cognate antigen or antigen-bearing dendritic cell. If left to chance, such an encounter would likely never occur, yet adaptive immune responses are initiated with remarkable speed and reliability. This is made possible by an efficiently regulated system of lymphocyte recirculation, and by the consolidation of tissue-derived signals and antigen into strategically placed lymphoid tissues throughout the body.

Non-hematopoietic stromal cells direct every aspect of lymphocyte ingress, positioning, and egress, thereby allowing efficient surveillance of lymphoid tissues. Likewise, tissue stroma form the lymphatic ducts and vessels through which antigen and signaling molecules travel, as well as actively and dynamically regulate the passage of antigen-bearing dendritic cells (DCs). The combination of these functions efficiently facilitate the cellular and molecular interactions necessary for priming an adaptive immune response.

More recent studies have sought to understand the finer intricacies of how the lymphoid tissue microenvironment directs cellular movement and homeostasis. These studies have revealed a striking level of complexity and heterogeneity in stromal cell populations not previously appreciated. Yet in comparison to their hematopoietic counterparts, the role of these cells in supporting immune responses has, until recently, been largely overlooked.

In this section, I will introduce our current understanding of how lymphoid tissue stroma coordinate the homeostatic movement and positioning of immune cells. I will highlight recent findings that redefine the functional identity of previously described stromal cell subsets and discuss the emergence of newly defined populations. I will also discuss the evolving role of lymphoid tissue stroma in directing active immune responses and mechanisms that drive these functions. Finally, I will outline a few of the open questions regarding stromal cell function in immunity which we have attempted to experimentally address in the following chapters.

## **1.2 Lymphoid tissue organogenesis**

Non-hematopoietic stromal cells direct the formation of lymphoid tissues, and the mature LN is populated by a variety of endothelial and non-endothelial stromal cell subsets which provide the critical infrastructure necessary for controlled movement of leukocytes into and within the LN (**Table 1**).

**Table 1: Previously described stromal cell subsets of the lymph node**

Stromal Cell type	Molecular Identifiers	Description
Lymphoid Tissue organizer (LTo)	PDPN+, CD31-, MAdCAM+, RANKL+, ER-TR7+	LTo cells differentiate from mesenchymal cells upon interaction with LT $\alpha$ $\beta$ -expressing lymphoid tissue inducer cells during lymphoid tissue organogenesis. These cells recruit and retain hematopoietic cells to the lymph node anlagen and are thought to give rise to several major stromal cell types including FRCs and MRCs.
Follicular Dendritic Cell (FDC)	PDPN+, CD31-, ER-TR7-, CD35+	FDCs are found within the B cell areas of the lymph node cortex and play a critical role in organizing the B cell follicle through expression of CXCL13. FDCs are a major source of B cell survival factors, including BAFF and APRIL. FDCs efficiently acquire and retain antigen and are critical for the formation of germinal centers.
Fibroblastic Reticular Cell (FRC)	PDPN+, CD31-, ER-TR7+	FRCs densely populate the T cell areas of the lymph node. These cells produce and then ensheath extracellular matrix, forming a fiberoptic-like reticular structure. A large, interconnected network of these reticular structures permeate the lymph node parenchyma and facilitate the flow of lymph and transport of small molecules. FRCs are a heterogeneous group of cells that contribute distinct functions based on their anatomical location within the LN, including support of HEV integrity, recruitment and survival of T cells within the paracortex, and survival of B cells.
Marginal Reticular Cell (MRC)	PDPN+, CD31-, MAdCAM+, RANKL+, ER-TR7+	MRCs are a newly identified subset of stromal cells localized to the outer edge of LN follicles beneath the subcapsular sinus. MRCs constitutively produce CXCL13 and maintain many of the characteristics of LTo cells, though the precise immunological function of these cells remains unclear.
Integrin $\alpha$ 7 Pericytes (IAP)	PDPN-, CD31-, ITGA7+	IAPs are a newly identified subset of stromal cells that encircle blood vessels in the LN cortex and medulla. Little is known about the function of these cells, though transcriptional analysis suggests they are highly contractile and exhibit many characteristics similar to FRCs.
Blood Endothelial Cell (BEC)	PDPN-, CD31+,	BECs line the blood vessels within the LN. While a specialized subset of BECs that line the HEV have been extensively studied due to their role in lymphocyte ingress, little is known about the immunological functions of non-HEV BECs. Both HEV and non-HEV ECs proliferate extensively during immune responses, likely reflecting the need to increase blood flow to the growing LN.
High Endothelial Venule EC (HEV EC)	PDPN-, CD31+, PNA <sup>d</sup> +  MAdCAM+ (mucosal)	A specialized subset of blood endothelial cell lining the post-capillary venules within the paracortex of the LN. HEV ECs actively regulate the ingress of circulating lymphocytes to the LN parenchyma.
Lymphatic Endothelial Cell (LEC)	PDPN+, CD31+, LYVE-1+	LECs line the afferent and efferent lymphatic vessels, the medullary sinuses, and both the ceiling and floor of the LN subcapsular sinus.

The development of lymph nodes begins during embryonic development and is driven by the interactions of hematopoietic lymphoid tissue inducer (LTi) cells with non-hematopoietic mesenchymal cells. This process is initiated upon expression of the chemokine CXCL13 by mesenchymal cells<sup>10</sup>. Interestingly, these poorly defined mesenchymal cells have recently identified as adipocyte precursors that are reprogrammed to give rise to LN stromal cells<sup>11</sup>. The stimulus leading to their initial expression of CXCL13 is not yet entirely clear, though thought to depend on the production of retinoic acid by nearby nerve fibers<sup>10</sup>. Upregulation of CXCL13 in turn attracts CXCR5-expressing LTi cells.

LTi cells express both RANK and RANK-L, and clustering of these cells allows homotypic interaction through this signaling axis<sup>12</sup>. Signaling via RANK:RANK-L on LTi cells leads to their upregulation of LT $\alpha$ 1 $\beta$ 2, which then triggers differentiation of mesenchymal cells to lymphoid tissue organizer (LTo) cells (also known as stromal organizer cells)<sup>13-15</sup>. LTo cells then contribute to further recruitment of LTi cells, thus initiating a positive feedback loop that fuels the continued recruitment and development of lymph node tissue progenitors.

LTo cells additionally begin to attract and retain lymphocytes through production of CCL19 and CCL21 and expression of adhesion molecules ICAM-1, VCAM-1, and MAdCAM1<sup>16</sup>. LTo cells eventually give rise to the various major LN stromal cell subsets that populate the mature LN, including FDCs, FRCs, and MRCs. A more thorough examination of the mechanisms driving early LN development and the differentiation of various LN stromal cell subsets can be found in several topical reviews<sup>16-18</sup>.

Similar to LNs, the formation of intestinal Peyer's patches begins during roughly the same prenatal developmental window and involves  $LT\alpha 1\beta 2$ -mediated interactions between LTI cells and tissue mesenchymal cells, though subtle differences in the molecular and cellular mediators of this process exist. Initiation of PP development, for instance, is thought to involve the triggering of the receptor tyrosine kinase RET on CD11c+ cells, which in combination with LTI cells trigger the expression of chemotactic factors by LTO and the recruitment and retention of hematopoietic cell clusters <sup>16,19</sup>.

### **1.3 Lymphocyte recirculation and lymph node surveillance**

Rare antigen specific lymphocytes continuously survey lymphatic tissues, entering through specialized blood vessels termed high endothelial venules (HEVs, Table 1), exiting through the cortical and medullary sinus to the efferent lymph, and returning to circulation via the thoracic duct <sup>20,21</sup>. This entire process occurs within a matter of several hours, and thus millions of lymphocytes enter and exit each peripheral lymph node on a daily basis.

#### **1.3.1 Lymphocyte recruitment to the lymph node**

The timely initiation of adaptive responses is predicated on the efficiency of lymphocyte surveillance of lymphatic tissues and recirculation; hence significant efforts have been made to understand the mechanisms that drive this process. The consensus model of lymphocyte extravasation into lymphoid tissues involves a multi-step process which is initiated by lymphocyte capture and rolling, followed by firm adhesion and finally transmigration across the vessel wall. The step-wise interactions between lymphocytes and HEV ECs necessary for

lymphocyte ingress are largely mediated by the coordinated action of a distinct set of selectins, integrins, and chemokines<sup>22,23</sup> (Figure 1.1).

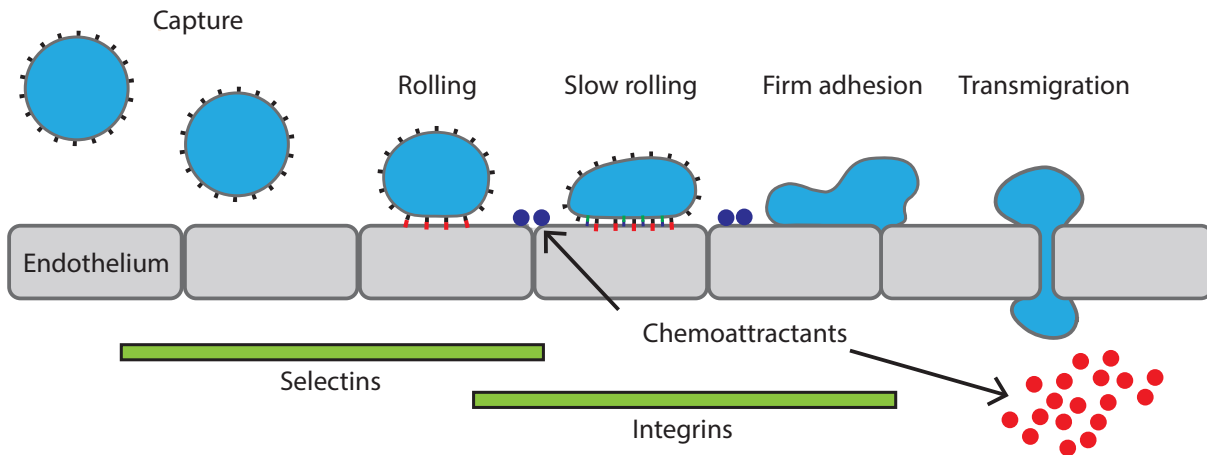


**Figure 1.1. Lymphocyte recruitment to lymphoid tissues through step-wise interactions with HEV ECs.** Initial capture and rolling of circulating lymphocytes is mediated by selectins. Chemokines displayed on the surface endothelium induce conformation changes to increase ligand affinity on rolling lymphocytes, allowing firm adhesion and eventually transmigration.

It is now understood that this is not a static process, but one involving numerous regulatory checkpoints. Identifying the cellular and molecular regulators of lymphocyte-endothelial interactions is thus an area of great interest.

Despite continuous population turnover, resting lymph node and splenic cellularity remains strikingly constant under resting conditions, and thus the drivers of lymphocyte ingress and egress must somehow equalize. Exactly how this occurs has largely been unclear. Evidence from Mionnet *et al* suggests that HEV endothelial cells (ECs) help maintain normal population homeostasis through the formation of temporary holding areas for incoming lymphocytes<sup>24</sup>. Close inspection of HEV EC morphology revealed that the distinctive cuboidal, or "high"

morphology of HEV ECs, may actually be a result of numerous lymphocytes nested within pockets formed on the abluminal side of the cell (Figure 1.2).

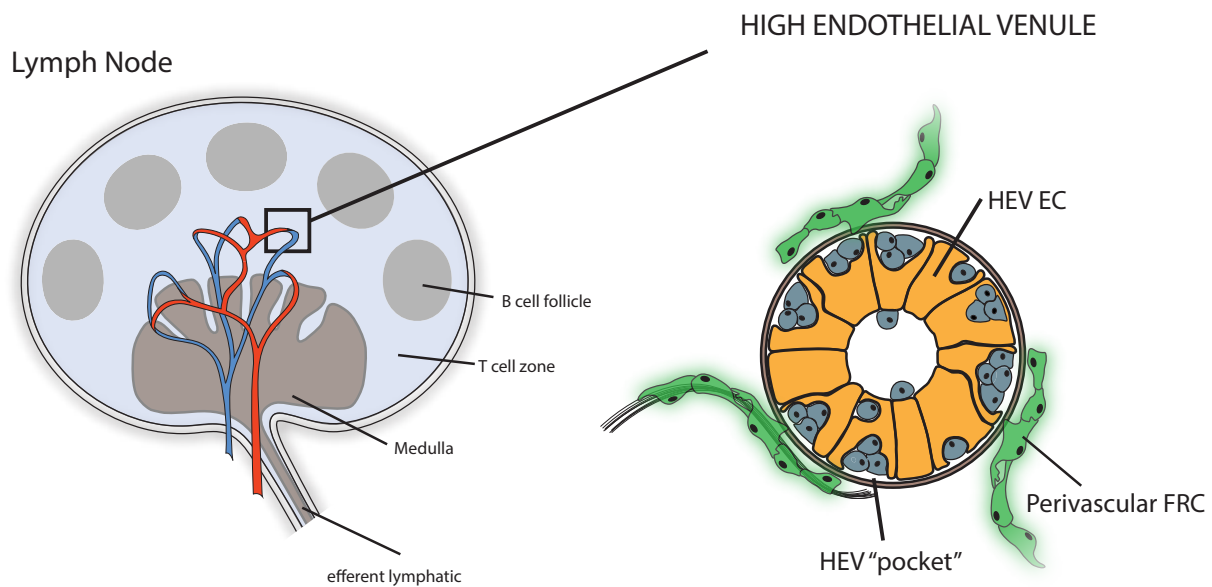


**Figure 1.2. High endothelial venule.** Circulating lymphocytes enter the LN through the high endothelial venule (HEV). Upon crossing the endothelium, lymphocytes are temporarily retained within pockets formed by specialized blood endothelial cells (BECs) lining the HEV until there is space to migrate into the LN. HEVs are encircled by FRCs, which direct lymph-borne signals to the HEV as well as help maintain HEV integrity.

These pockets allow migrating lymphocytes to exit the flow of circulation before being granted access to the lymph node. The subsequent transition from HEV pockets to lymph node parenchyma presumably depends upon physical constraints - when space is made available through cell egress in the lymph node sinus, new lymphocytes are permitted entrance across the HEV basal lamina. Hence, the rate of ingress is matched to the rate of egress, and the proper resting cellularity of lymphoid organs is maintained.

Whether this transition occurs passively, with lymphocytes stochastically moving to fill empty space, or is actively controlled by HEV ECs in response to environmental cues remains unclear. However there are other notable requirements for the extravasation of circulating lymphocytes across the HEV basal lamina into the lymphoid organ parenchyma. Movement of lymphocytes across the HEV basal lamina additionally depends on the activity of autotaxin (ATX), an endothelial cell-produced enzyme that catalyzes production of the lipid mediator lysophosphatidic acid (LPA) <sup>25,26</sup>. LPA in turn induces morphological changes to HEV ECs that appear necessary for movement of lymphocytes across the HEV. Local inhibition of the ATX/LPA axis results in an excess accumulation of lymphocytes within HEV EC pockets or in the sub HEV EC space.

Additional immune-stromal interactions may participate in the regulation of HEV function. Multiple studies have demonstrated that surgical deprivation of efferent lymph flow to a draining LN results in a "flattening" of the HEV, reduction in expression of glycocalyx, and perturbations in the recruitment of circulating lymphocytes <sup>27-29</sup>. The exact signals responsible for this phenomenon remain unclear, though it has been speculated that the loss of migratory DCs from efferent lymph vessels is a contributing factor <sup>30</sup>. Indeed, recent studies have demonstrated that DCs are required for the homeostatic maintenance of HEV EC function and lymphocyte homing to lymph nodes in a lymphotoxin-dependent manner <sup>31</sup>. Furthermore, in the absence of continuous lymphotoxin beta receptor (LT $\beta$ r) signaling, blood endothelial cells (BECs, table 1) in the lymph node fail to develop properties typical of HEV ECs, including expression of peripheral node addressins (PNAd) and MAdCAM, polarized ICAM expression and



production of CCL19 and CCL21<sup>32,33</sup>. Notably, lymphocytes are no longer found sequestered within HEV pockets and ingress of circulating lymphocytes largely is impaired.

Alternatively, evidence also exists which suggests stromal cells may also respond directly to shear force imposed by fluid flow via mechanosensation. Fibroblastic reticular cells (FRCs) grown in culture respond to interstitial fluid flow by upregulation of the lymphocyte chemoattractant CCL21. *In vivo* deprivation of fluid flow to the LN likewise impacts CCL21 expression by FRCs<sup>34</sup>. Whether and how mechanosensation of lymph flow in an intact lymph node may impact HEV function and recruitment of circulating lymphocytes remains to be determined.

It should also be emphasized that the HEV functions as a barrier as much as a port of entry. The continuous influx of lymphocytes across the HEV, particularly during initiation of immune responses, likely requires constant rearrangement of the junctions between ECs. Fibroblastic reticular cells (FRCs, Table 1) that encircle the HEV are believed to provide support of HEV integrity in a manner dependent on interaction with CLEC-2-expressing platelets<sup>35</sup>. Ligation of CLEC-2 with PDPN, a mucin-type glycoprotein expressed on the surface of FRCs and various other stromal subsets, mediates a number of immunologically important functions. In this particular instance, interaction of platelet-bound CLEC2 with PDPN on FRCs specifically induces the release of S1P by platelets, which in turn elicits an up-regulation of VE-cadherin on HEV ECs. In the absence of CLEC-2-PDPN signaling, HEV integrity is compromised and bleeding occurs within the node.

### 1.3.2 Lymphocyte egress from the lymph node

Egress of lymphocytes primarily begins at the blunt ended cortical sinuses populating the T zone of the LN, which then flow into the medullary sinus and the efferent lymphatics<sup>36,37</sup>. Transmigration across the sinus endothelium is thought to occur through specific portals, though this remains to be more thoroughly explored. However, the molecular requirements for egress have been thoroughly studied and found to be principally dependent on lymphocyte expression of sphingosine-1-phosphate receptor (S1PR1) and a differential concentration of S1P within lymph and LN tissue<sup>38-40</sup>. S1P is largely absent within the LN parenchyma, while high concentrations within the blood and lymph are established by hematopoietic cells and lymphatic endothelial cells (LECs, Table 1) respectively<sup>41,42</sup>. The S1PR1 receptor is rapidly internalized upon contact with S1P, and thus naive lymphocytes that enter the LN from the blood initially lack the capacity to respond to S1P, preventing immediate egress into the lymph<sup>43</sup>. Thus, while many of the cortical sinuses through which lymphocytes egress are found in close proximity to HEVs, direct migration from HEV into the sinus is not typically observed<sup>36</sup>. Instead, incoming lymphocytes must remain within the lymph node parenchyma until reacquiring expression of S1PR1 and gaining access to the sinus, a process which has been found to occur within 20 minutes to an hour<sup>36,44</sup>. Interestingly, the average dwell time of most T and B cells has been observed to be much longer, lasting roughly 6-10 hours for T cells and 12-24 hours for B cells<sup>36,45</sup>. This would suggest that the rate of egress is not limited by acquisition of S1PR1 expression but may instead reflect the competing effects from chemotactic retention signals such as the CCR7 ligands CCL19 and CCL21. In the absence of CCR7, for instance, egress from the LN occurs more rapidly<sup>42</sup>. It is thus hypothesized that CCR7

desensitization may play a role in the kinetics of lymphocyte retention and egress <sup>46</sup>. Ultimately, however, future studies will need to more thoroughly dissect the mechanisms governing lymphocyte dwell time and recirculation dynamics of naive lymphocytes.

### 1.3.3 Recruitment and retention of lymphocytes during immunity

While the lymphocyte population in resting lymph nodes is maintained at a fairly constant level, T and B cell numbers can increase substantially during an active immune response. Within hours of immunogenic challenge, lymphocyte recruitment is enhanced while egress is transiently shut down <sup>47</sup>. This process is largely initiated by innate signals originating from the effected peripheral tissues. Lymph-borne cytokines and chemokines are thought to be transported into the lymph node cortex through a reticular conduit network formed by FRCs that extends from the lymph node capsule to the HEVs <sup>48-52</sup> (Figure 1.3).

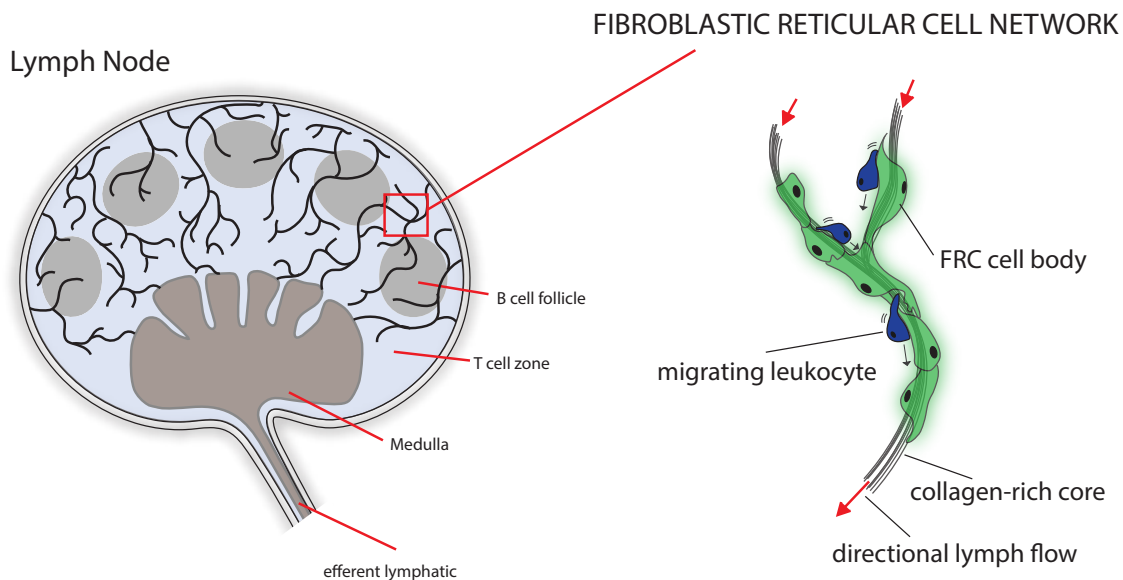


**Figure 1.3. Fibroblastic reticular cell network.** FRCs produce and ensheath organized bundles of fibers, forming a *conduit network* that facilitates the transport of fluid and fluid-borne signals and antigen through the LN. FRCs additionally provide the infrastructure for leukocyte migration within lymphoid tissue.

These factors can be transcytosed across the HEV EC and displayed on the luminal surface of the vessel, enhancing recruitment of naive circulating lymphocytes <sup>48</sup>. Concurrent up-regulation of CD69 on lymphocytes in response to inflammatory cues results in decreased responsiveness to S1P and a transient halt to cellular egress from the node <sup>53</sup>. This process effectively primes the lymph node for the ensuing immune response by increasing the pool of potential antigen-specific naive lymphocytes.

Massive alterations to the stromal network must take place within the first few days of immune activation to facilitate this net cellular influx and support the resulting enlarged population. Early stages of an immune response are associated with a proliferative expansion of the primary feed arteriole, bringing a greater supply of blood circulation to the lymph node <sup>54</sup>. HEVs also grow in both size and number <sup>55</sup>. Interestingly, though HEVs become more numerous, this occurs in proportion to the overall growth of the lymph node and thus the density of these vessels remains constant <sup>56</sup>.

This initial expansion of the lymph node vasculature is driven by innate immune factors and may occur in the absence of antigen <sup>54</sup>. Lymph node resident CD11c+ dendritic cells (DCs) appear to be critical for this stage of vascular expansion, but drive the process through mechanisms distinct from the direct triggering of LT $\beta$ r, which was found necessary for homeostatic maintenance of HEV ECs <sup>56</sup>. Instead, DCs are thought to indirectly influence vascular expansion by enhancing production of VEGF by FRCs <sup>57</sup>. In contrast, subsequent expansion and remodeling of the lymph node vasculature depends on B and T cells <sup>58</sup>. In the case of LCMV infection, continued lymph node expansion has been shown to occur

independently of VEGF, but instead requires B cell derived  $LT\beta$ <sup>59</sup>. This proposed biphasic expansion of lymph node ECs presumably mirrors the transition from innate activation to initiation of adaptive immune responses.

The FRC network likewise undergoes morphological changes and proliferative expansion to accommodate increases in lymphocyte numbers<sup>58,60</sup>. As with expansion of the blood vasculature, FRC growth appears to occur in two phases as well. Early expansion of FRCs is dependent on the presence of DCs and trapping of naive lymphocytes<sup>60</sup>. The exact mechanisms by which naive lymphocytes may drive this process are yet unclear. However, direct triggering of PDPN signaling in FRCs through interaction with DC-expressed CLEC-2 has recently been shown to reduce FRC contractility, allowing these cells to stretch and accommodate increases in LN volume<sup>61,62</sup>. Reduced contractility may additionally trigger proliferative expansion of the FRCs<sup>62</sup>. In contrast, late phase expansion of the FRC network depends upon interaction of the stromal network with activated lymphocytes through  $LT\alpha\beta$  and LIGHT<sup>60</sup>.

These studies collectively illuminate a generalized expansion of multiple components of the LN stromal cell support network in response to inflammation and infection, and highlight the influential role these cells play in driving the ensuing immune response. In contrast to the events leading up to an immune response, significantly less is known about the resolution of LN swelling and return to homeostasis. FRCs are believed to internalize PDPN upon signaling, and this may be one means through which LN swelling is limited or reversed<sup>61,62</sup>. Additionally, activated migratory DCs are relatively short-lived, and thus reduced FRC contractility may be

tied to the turnover rate of CLEC-2 expressing DCs in the inflamed node<sup>63,64</sup>. Similarly, B and T cell derived signals, which promote stromal cell expansion, may be similarly lost as these cells egress from the LN. However, there may also be alternative signaling pathways that attenuate stromal cell growth or proliferation that arise during the resolution of an immune response.

A recently reported study examining stromal cell responses in LNs following viral infection has provided new insight to the process of stromal cell activation, expansion, and recovery<sup>65</sup>. Having documented the kinetics of both transcriptional alterations and population expansion during and after immune responses, this study found that while transcriptional alterations in stromal populations resolved within 30 days of infection, the expanded network of FRCs and LECs remained. Moreover, the expanded stromal cell network did not appear to undergo additional expansion or remodeling upon subsequent infections. This may suggest that an immune "experienced" LN remains structurally primed to accommodate future immune reactions, as opposed to undergoing repeated expansions and contractions with each new immune response.

#### **1.4 Antigen transport to lymph nodes**

In addition to coordinating lymphocyte recruitment, stromal cells contribute to the initiation of adaptive responses by facilitating the transport of antigen to the lymph node. Antigen is brought from peripheral tissues to regional lymph nodes through an expansive system of lymph vessels. Collection of lymph begins with blind-ended lymphatic capillaries, which are formed of loosely-connected ECs with discontinuous "button"-like junctions<sup>66</sup> (Figure 1.4).

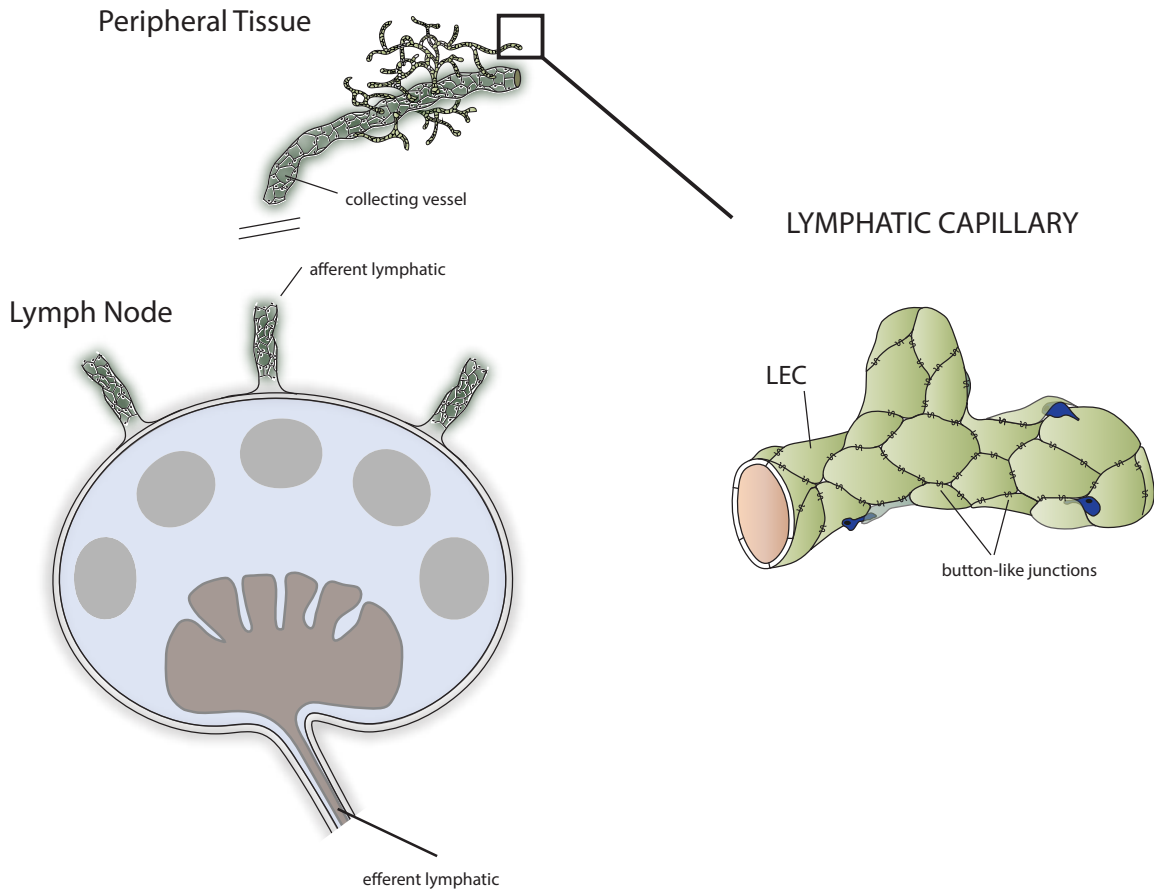


**Figure 1.4. Draining lymphatic vessels.** A) Antigen-bearing dendritic cells (DCs) and free soluble antigen enter the lymphatics through the initial lymphatic capillaries. These capillaries are formed from specialized lymphatic endothelial cells (LECs) joined with discontinuous, button-like junctions that allow the passage of fluid and cells without disrupting junction integrity.

These specialized junctions allow ECs to form overlapping flaps that ensure unidirectional uptake of fluid from surrounding interstitial space into the vessel lumen. Lymphatic capillaries eventually converge into collecting vessels which, unlike the initial capillaries, contain continuous junctions and are surrounded by smooth muscle cells<sup>67</sup>. Smooth muscle cells, along with movement of the surrounding tissue, provide the necessary pumping action to regulate

the movement of lymph, and a system of valves separating segments of lymph vessels ensures directional flow to the draining node <sup>68</sup>.

#### **1.4.2 Dendritic cell-mediated antigen transport**

Stromal cells function as a critical highway for tissue-derived migratory DCs. En route to the T cell zone of draining lymph nodes, antigen-bearing DCs must crawl along into and then along ECs lining afferent lymphatic vessels and FRCs lining the reticular network of the lymph node. The PDPN:CLEC-2 signaling axis has been identified as a key facilitator of these interactions <sup>69</sup>. Expression of PDPN extends throughout the stromal reticular network of the lymph node cortex as well as the lymphatic endothelium, and through its interactions with CLEC-2, functions as a critical factor driving the migration of DCs from peripheral tissues to the lymph node. While expression of CLEC-2 on DCs is normally low at a resting state, activation and maturation results in its up-regulation. Upon binding PDPN, CLEC-2 signaling induces formation of actin-rich protrusions and facilitates movement of DCs along the stromal cell network. This, in conjunction with chemotactic cues, guides the directional migration of DCs into the lymphatic vasculature as well as their positioning within the lymph node cortex.

The primary chemotactic cues directing peripheral migratory cells into lymphatics have been well established <sup>70,71</sup>. Both CCR7 ligands CCL19 and CCL21 have been implicated in DC migration to the lymph node, but contribute to chemotaxis by distinct mechanisms <sup>72</sup>. LECs constitutively produce CCL21, which is then immobilized on extracellular matrix or cell surfaces through interactions with heparin sulfate glycosaminoglycans (GAGs) <sup>73</sup>. Gradients of



immobilized CCL21 are formed around initial lymphatic vessels and these gradients direct DCs migration by haptotaxis <sup>74</sup>.

Interestingly, numerous inflammatory chemokines such as IL-8, RANTES, and MCP-1 have also been shown to bind GAGs and can presumably be displayed on LECs <sup>75</sup>. Yet inflammatory leukocytes do not accumulate around lymphatic vessels or migrate to the draining node. Rather, migration into lymphatic vessels is largely restricted to CCR7-expressing DCs. Recent studies have suggested that the accumulation of inflammatory cytokines on LECs is prevented by the scavenging activity of the atypical chemokine receptor D6, which is specifically expressed on the cell surface of LECs. D6 binds and internalizes numerous inflammatory chemokines, but does not interact with CCL19 or CCL21 <sup>76,77</sup>. In the absence of D6, inflammatory leukocytes are found to accumulate around lymphatic vessels and within the draining lymph node. This excess accumulation of inflammatory cells actually results in congestion of lymphatic vessels and impedes DC migration.

By contrast, CCL19 is not immobilized on cell surfaces, but freely diffuses <sup>78</sup>. In peripheral tissue, it has thus been suggested that DCs direct chemotaxis in an autologous manner by secreting CCL19, which then diffuses in the direction of interstitial fluid flow <sup>70</sup>. Migration of DCs within the initial lymphatic capillaries depends on active crawling along the surface endothelium, and directionality of movement within these vessels has been linked to the rate of fluid flow <sup>73</sup>.

Once in the larger collecting vessels, DCs are passively swept along by the flow of lymph until reaching the lymph node subcapsular sinus (SCS) <sup>73</sup>. Upon arriving at the draining lymph node,

migrating DCs must next traverse the SCS - a process which involves a recently described transition from migration along the endothelium lining ceiling of the lymph node sinus (termed cLECs) to the floor-lining endothelium (fLECs) <sup>79</sup>. This process is also driven by CCR7-directed migration along a CCL21 gradient. Interestingly, this gradient is established by the expression of the atypical chemokine receptor CCRL1, which functions as a scavenger receptor for CCL19 and CCL21 <sup>79-81</sup>. Expression of CCRL1 is restricted to cLECs, thus preventing surface display of CCR7 ligands on the SCS ceiling and effectively directing migration of DCs through the fLECs and into the lymph node parenchyma (Figure 1b).

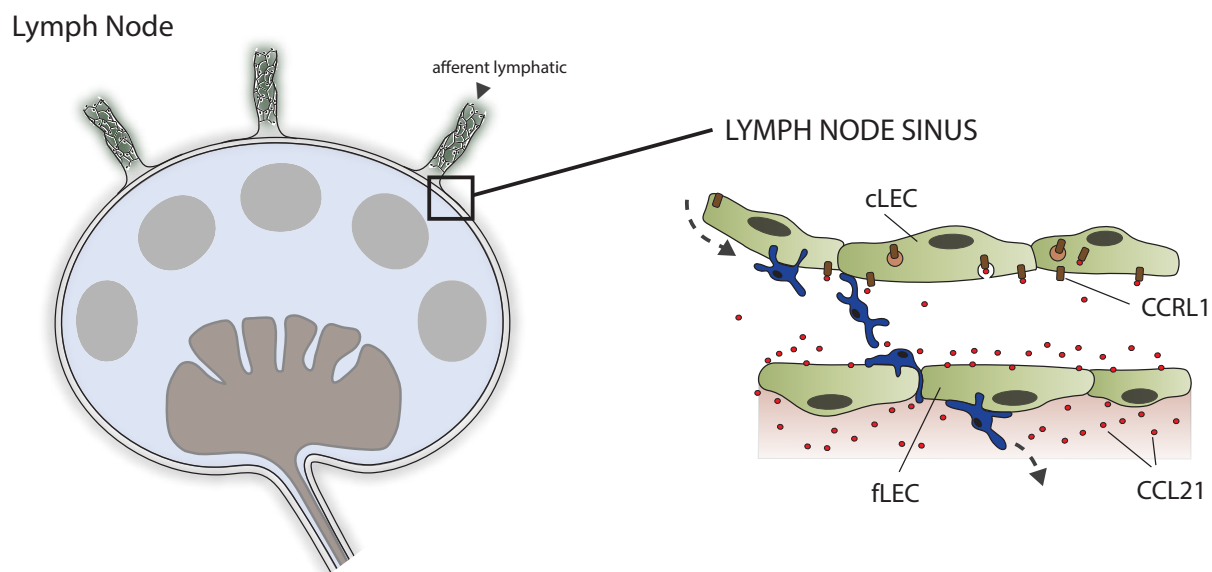


**Figure 1.5. Lymph node sinus.** Afferent lymph and migrating DCs enter through the LN sinus. As DCs migrate into the lymph node (LN), they must traverse the subcapsular sinus. The atypical chemokine receptor CCRL1, which is expressed exclusively by LECs lining the ceiling of the subcapsular sinus (cLECs), scavenges CCL21 and establishes a gradient that is most concentrated on LECs lining the floor of the subcapsular sinus (fLECs) and the LN cortex. This gradient directs DCs to transition from migrating along cLECs to fLECs, and finally passing into the LN cortex. Lymph and lymph-borne soluble material pass through transendothelial channels in the LN sinus and enter the FRC conduit network.

### 1.4.3 Cell-independent antigen transport

While uptake and transport via migratory DCs is typically recognized as the major avenue of antigen delivery from non-lymphoid tissues into lymph nodes, soluble antigen can also freely drain via the afferent lymph. This occurs rapidly, with antigen arriving at the lymph node within a matter of minutes. Upon arriving at the lymph node, smaller antigens with a hydrodynamic radius of less than ~4nm (or MW of less than 70kDa) rapidly permeate the lymph node cortex through FRC conduits, making these antigens readily accessible to resident DCs, cognate B cells, and follicular dendritic cells (FDCs, table 1) that are in close contact to the FRC network<sup>82-84</sup>. By contrast, larger particles, such as viruses and bacterium, are excluded from the conduit network. This size cut-off may serve as a form of protection against allowing unprocessed pathogens access to the FDC network. Larger material is instead primarily captured by medullary and subcapsular sinus macrophages<sup>85</sup>, and can then be transferred to B cells in the lymph node cortex<sup>86-88</sup>. The vast majority of material present in the afferent lymph is captured and filtered out as it passes through the lymph node<sup>89</sup>. This process that has been found to not only influence adaptive immune responses, but prevent systemic dissemination of lymph borne pathogens<sup>87,90,91</sup>. Recent evidence suggests that LECs residing along the subcapsular sinus may also capture and store antigen. Interestingly, this archiving function appears to be restricted to proliferating LECs which emerge under inflammatory conditions<sup>92</sup>. This would suggest that archiving of free antigen by LECs occurs only in conditions of immunogenic challenge.

The immunological consequence of DC-borne antigen transport versus soluble antigen transport to the LN will need to be more thoroughly examined. DCs carrying antigen to the LN

may be conditioned by signals derived from the site of infection or the stromal cells upon which they migrate. Cell-free antigen lacks this additional information and thus may elicit a distinct immunological outcome upon arrival within the LN. Indeed, it has been reported that following subcutaneous immunization, soluble antigen reaches the LN first and is presented by resident DC populations, while tissue derive DCs bearing antigen subsequently initiate a second wave of antigen presentation. These two distinct waves of antigen transport to the LN appear to have differing consequences on T cell activation<sup>93</sup>. However, it should be noted that, while cell independent trafficking of antigen to the lymph node has been convincingly shown to occur during model immunization, the extent to which this occurs during a natural infection, in which antigen is introduced in more limiting quantities, is less clear.

### **1.5 Immune cell positioning and homeostasis in lymph nodes**

The basic concept of stromal cell-mediated recruitment, compartmentalization and homeostatic maintenance of immune cells has long been appreciated. Pioneering research in the late 1990s established critical roles for stromal-cell produced chemokines CCL19, CCL21, CXCL12, and CXCL13 in the attraction, retention, and organization of circulating lymphocytes within lymphoid tissues<sup>94-97</sup>.

The expression of CCL19 and CCL21 in lymphatic vessels has likewise been linked to the migration of antigen-bearing dendritic cells<sup>98</sup>. However, these findings alone do not sufficiently address the exquisite spatial and temporal control of leukocyte movement and antigen transport observed in the lymph node. Rather there is a complexity to the ordering of stromal cell architecture and the shaping of the directional cues they produce that has remained largely

unaddressed. Moreover, active immune responses are accompanied by large scale changes to LN architecture and alterations to leukocyte migration patterns, suggesting that stromal cells are not static structures, but must be dynamically regulated.

Lymphoid organs are carefully organized into discrete functional compartments. This compartmentalization is critical for optimal resource management and efficient generation of adaptive immune responses. Significant progress has been made in the last several years toward deciphering the physical and chemical cues that direct immune cells to their proper destination within the lymphoid tissue parenchyma. Entry and movement of lymphocytes within the densely packed lymph node depends on close physical interactions with the stromal network<sup>99</sup>. Lymphocytes appear to crawl along the lymph node stroma, but largely remain within strictly defined geographical regions that are delineated by specific chemokine expression patterns<sup>99</sup>. Entry and retention of lymphocytes in the paracortical T cell zone is dependent on the expression of CCR7 and interaction with its ligands CCL19 and CCL21, while incoming naive B cells additionally depend upon CXCR5-mediated homing toward CXCL13-rich follicles<sup>95,98,100</sup>. The role of stromal cells in orchestrating this process has long been appreciated, however the specific contributions of FRCs, FDCs, and other stromal subsets, as well as the precise means by which they shape the lymphoid tissue landscape are only recently coming to light.

Studies in which FRCs were specifically ablated *in vivo* (via administration of diphtheria toxin to mice conditionally expressing the diphtheria toxin receptor in CCL19-expressing cells) have confirmed the pivotal role these cells serve in both organizing lymphocyte positioning within

lymphatic tissues as well as maintaining cell homeostasis and viability <sup>101,102</sup>. FRC-depleted lymph nodes lose segregation of B and T cell compartments, fail to maintain normal T cell numbers, and are rendered incapable of mounting virus-specific CD4 and CD8 T cell responses. Interestingly, only naive lymphocytes require FRC-derived signals for retention within the lymph node, as depletion of FRCs during an ongoing immune response did not result in a loss of activated lymphocyte numbers or failure to mount antiviral immunity <sup>102</sup>. Failure to support T cell survival is likely due to the loss of FRC-produced IL-7 <sup>103</sup>. This phenomenon is similarly observed following long term fibrosis of LNs in HIV/SIV infected subjects in which the FRC network is damaged or inaccessible <sup>104,105</sup>. Unexpectedly, Cremasco *et al* also found that the loss of FRCs was equally devastating to resident B cell populations, and likewise resulted in impaired germinal center formation and humoral immunity <sup>101</sup>. FRCs localized to the B cell follicle were found to be major producers of the B cell survival factor BAFF, thus indicating that FRCs may not only organize and maintain the paracortical T cell zone, but help establish and maintain B cell homeostasis in the follicle as well. Whether BAFF-expressing FRCs in the B cell follicle represent a distinct population of stromal cells remains to be addressed. Recent work by Mionnet *et al* has suggested that a previously unidentified population of stromal cells, distinct from conventional FRCs (based on transcriptional profile), populate the T cell area of the LN <sup>106</sup>. Moreover, these cells, termed "versatile stromal cells" (VSCs) could be instructed via interactions with B cells to produce CXCL13. A phenotypically distinct, CXCL12-expressing population of reticular stroma (CRCs) has also been found to populate the T-zone proximal region of the primary B cell follicle as well the germinal center dark zone <sup>107</sup>. The contribution of these newly identified stromal populations to immune cell compartmentalization and

homeostasis will ultimately need to be more thoroughly parsed out in future studies. However, these findings nevertheless indicate a greater level of heterogeneity to the LN reticular stroma than previously thought.

Maintenance of B cell homeostasis and the organization of discrete follicles had previously been attributed to the function of FDCs. Indeed FDCs are producers of both B cell chemotactic cues (CXCL13) as well as BAFF, APRIL, and other survival factors, and the loss of these cells results in failure to maintain strict primary follicle organization <sup>108,109</sup>. However, the specific ablation of FDCs alone results in no appreciable decreases in BAFF production in the spleen and lymph node, and only modest decreases in CXCL13 in the spleen <sup>109</sup>. FDCs were also found to be dispensable for resting B cell homeostasis. Nevertheless, were unable to support germinal center formation upon immune activation. Interestingly, loss of FDCs was found to result in encroachment of CCL21-expressing FRCs into the B-cell rich areas, which might suggest that FDCs may additionally contribute to maintenance of strict follicle borders through repression of T cell chemotactic cues or by repelling T zone FRCs <sup>109</sup>.

Marginal reticular cells (MRCs), a recently described stromal cell subset localized to the subcapsular sinus overlying B cell follicles, have also been implicated in the production of BAFF and CXCL13 <sup>110,111</sup> (Table 1). However their definitive contributions to lymph node organization and homeostasis remain to be determined. Failure to maintain B cell homeostasis in the absence of FRCs suggests that MRC-derived BAFF and CXCL13 alone are not sufficient for maintaining B cell follicles. Interestingly, while little is known about the direct functional

contributions of MRCs, fate mapping studies have suggested that this population gives rise to FDCs, and thus may serve as important stromal cell progenitors <sup>112</sup>.

### **1.5.2 Immune cell redistribution upon initiation of adaptive immune responses**

The significance of stromal cells in coordinating immune cell positioning and migration within resting lymphoid tissues is fairly well established. However the contributions of stroma to immune responses are only more recently coming into focus. The failure to mount antiviral T and B cell responses upon acute FRC ablation presents new evidence that the lymph node stroma is indispensable during immunity <sup>101</sup>. However, it is unclear whether failure to mount effective immune responses following FRC ablation results from impaired cellular positioning or because the collapsed lymph node architecture can no longer regulate normal cellular ingress or maintain the survival of B and T cell populations.

Using a model of conditional LTBR ablation in CCL19-expressing FRCs, Chai *et al* describe the formation of an intact, but functionally immature T zone reticular network <sup>113</sup>. Though slightly reduced in size and cellularity, the basic architectural features of the lymph node remain largely normal, including formation of distinct B and T cell zones as well as a functional conduit network. However, the loss of LTBR on lymph node FRCs nevertheless resulted in a loss of immunocompetence and increased susceptibility to viral infection. Failure to establish antiviral immunity in this model was associated with impaired expression of interleukin 7 and homeostatic chemokines CCL19 and CCL21 by FRCs. Whether the loss of FRC-produced chemotactic cues is causal remains unclear, though *plt* mice, which lack both CCL19 and CCL21, exhibit a similar delay in antiviral response.



The importance of stromal produced homeostatic chemokines during immune activation is an intriguing question, as numerous reports suggest that immune cell compartmentalization is transiently disrupted during the initial stages of immune response to infection <sup>114-120</sup>. This is a general phenomenon found to occur following exposure to a number of viral, bacterial, and parasitic protozoan infections. Though in some instances this appears to be due to direct targeting and destruction of the FRC network <sup>121</sup>, many of these pathogens have been found to elicit a specific transcriptional down-regulation of CCL21 and CXCL13 <sup>118</sup>. Disruption of immune cell compartmentalization has also been found to occur in response to administration of LPS or in the presence of certain immune adjuvants such as CFA <sup>118,122</sup>.

Whether this transient down-regulation occurs by design, or represents a commonly exploited means of subverting host adaptive immunity remains unclear. In most instances, adaptive immunity does not appear to be impaired following this transient alteration in lymph node or splenic architecture. However, in the case of Salmonella, LPS-induced disruption of CCL21 and CXCL13 in draining lymph nodes enhances the virulence of this pathogen <sup>120</sup>. Moreover, the loss of these organizational cues during a variety of infections appears to render the host more susceptible to secondary infection <sup>118</sup>.

It has been suggested that a temporary down-regulation of CCL21 and CXCL13 may benefit the host adaptive immune response by limiting the recruitment of additional naive lymphocytes after initial immune activation, thereby reducing the competition for limited space and resources <sup>118</sup>. An alternative possibility is that CCL21 or CXCL13-mediated retention of lymphocytes within their respective compartments must be relieved to allow favorable intra-

nodal repositioning for antigenic priming. For instance, recent reports suggest that the chemokine receptor CXCR3 mediates T cell localization within the inter-follicular and medullary zones and enhances interactions with antigen-bearing DCs <sup>123,124</sup>. This occurs through interaction with stromal cell-derived CXCL9 and DC-derived CXCL10 <sup>123</sup>. Both CXCL9 and CXCL10 are transiently expressed upon exposure to LPS/PolyI:C and follow a close reciprocal expression pattern to that of CCL21 and CXCL13. Whether this represents a coordinated response to redirect immune cells to regions rich in antigen-bearing APCs will need to be specifically examined.

## **1.6 Concluding remarks**

Stromal cells orchestrate adaptive immune responses by directing the recruitment and positioning of lymphocytes, delivery of antigen, and maintenance of cell populations within secondary lymphatic tissues. These are not static functions, but are dynamically regulated in response to complex cellular or molecular cues.

Recent advances in high powered imaging techniques and the development of new genetic tools for specific targeting of stromal cell subsets have reshaped the field of stromal cell biology and enabled the study of these cells at far greater depth than ever before. New studies demonstrate clearly that stromal cells are more heterogeneous and functionally versatile than previously credited. The contributions of newly described endothelial (cLECs and fLECs) and non endothelial (MRCs, IAPs, VSCs, and CRCs) stromal cell populations to immune cell trafficking and homeostasis are intriguing and warrant future investigation (Table 1).

Moreover, our understanding of many previously established stromal populations, including HEV ECs, FDCs, and FRCs is continuously evolving.

Upon immunogenic challenge, lymph node stroma undergoes marked expansion and reorganization. The mechanisms driving this process and the consequences of these alterations are not fully understood, though we have discussed here the involvement of a variety of key signaling pathways known to drive phenotypic and proliferative expansion of LN stroma. A thorough understanding of these processes may have relevant implications for vaccine design. Additionally, significantly less is known about what regulates these pathways during immune responses or how LN homeostasis is restored. Addressing these questions may yield findings relevant to the control of long term disruption of LN homeostasis and fibrosis resulting from conditions of chronic infection or inflammation.

The topics covered in this section have largely focused on the contribution of LN stroma to immunity. This is largely reflective of the lymph node-centric focus of the stromal cell research to date. However, it is important to note that stromal cells are likely just as critical to immunological functions of other lymphoid organs and peripheral tissues. Many of the same populations of stromal cells may be found in other secondary lymphoid organs, including the spleen and Peyer's patch. Whether these stromal cells are functionally similar to those that populate the LN will need to be directly examined. However, given the environmental and architectural differences of these other lymphoid tissues, there will almost certainly be functional differences.

Ultimately, it has become clear that stromal cells constitute a fundamental, though oft-overlooked component of the immune system. Recent studies discussed herein have brought better resolution to the complex picture of the LN microenvironment, and have opened the door to a bevy of exciting new avenues to be explored. Ultimately, discovering the precise means by which these cells coordinate the cellular interactions necessary for the initiation of adaptive responses will have important biological and clinical implications.

## Chapter 2

### **CXCL13cre as a novel model of stromal cell manipulation**

Advances in the identification and *in vivo* targeting of specific stromal populations have resulted in striking new insights to the function of stromal cells and revealed a level of complexity previously unrealized. Recent studies involving the specific genetic targeting and ablation of CD21- and CCL19-expressing stromal cell populations have help to redefine the specific roles of LN follicular dendritic cells (FDCs) and fibroblastic reticular cells (FRCs) respectively <sup>101,109</sup>. These studies have highlighted the utility of this experimental approach toward understanding the population heterogeneity and functional complexity of lymphoid tissue stromal cells. We have expanded on these findings by describing a recently generated mouse model of CXCL13cre-directed cellular ablation. These studies have allowed us to characterize the specific contributions of the CXCL13-expressing stromal cell compartment, which we show to include B-zone FRCs, FDCs, and marginal reticular cells (MRCs). Despite some population overlap with both CD21 and CCL19-expressing cells, depletion of the CXCL13-expressing stromal subset resulted in a alterations to lymphoid tissue architecture and immune cell composition that was clearly distinct from previously described models of stromal cell manipulation.

## 2.1 Introduction

The conventional understanding of lymph node organization is that fibroblastic reticular cells (FRCs) and follicular dendritic cells (FDCs) establish the T and B cell zones respectively. FRCs facilitate CCR7-mediated homing of T cells to the LN paracortex through production of CCL19 and CCL21, while FDCs establish B cell follicles through production of CXCL13 and recruitment of CCR5-expressing B cells and T-follicular helper cells <sup>95,96,99,108,125</sup>. Likewise, FRCs are understood to support T cell survival through production of IL-7, while FDCs provide key B cell survival factor BAFF <sup>103,126</sup>. However, two recently published studies in which either FDCs or FRCs are specifically targeted for ablation have revealed this previously accepted model to be overly simplistic <sup>101,109</sup>.

Following specific ablation of FDCs, germinal center reactions disappear and B cells no longer cluster into distinct, rounded follicles <sup>109</sup>. However, the majority of B cells nevertheless remain specifically localized to the LN cortex, where other CXCL13-expressing stromal cell populations were found to remain. Moreover, total B cell numbers remain consistent after FDC ablation, and whole tissue BAFF levels are largely unaffected. These studies reveal that FDCs, though necessary for GC reactions, are only partially responsible for B cell chemotaxis and are largely dispensable for homeostatic B cell survival.

By contrast, specific ablation of FRCs (through CCL19cre-driven expression of diphtheria toxin receptor) results in dramatic loss of both B and T lymphocyte cell numbers as well as a loss of B/T zone separation in the lymph nodes <sup>101</sup>. FRCs along the periphery of the B cell zone

(hereafter referred to as B-zone FRCs) were found to be an unexpected source of BAFF, suggesting the existence of regionally and functionally distinct FRC subsets.

The full extent of LN stroma heterogeneity remains to be more thoroughly addressed, but at minimum now include T-zone FRCs, B-zone FRCs, FDCs, pericytes, marginal reticular cells (MRCs), blood endothelial cells (BECs), and lymphatic endothelial cells (LECs). How each specific subset contributes to LN function is not fully understood due to the limited number of genetic tools for studying these cells *in vivo*.

Here we attempt to expand on the above mentioned studies through the use of a newly developed mouse model in which cre-recombinase is driven by the CXCL13 promoter. The CXCL13-expressing lineage is then specifically ablated by cre-driven expression of diphtheria toxin receptor and administration of DTx. We find that depletion of this stromal lineage has dramatic effects on lymphoid tissue structure, organization and immune cell composition, and that these effects are unique from previously established models of stromal cell manipulation.

## **2.2 Results**

### **CXCL13cre targets multiple stromal populations of the LN cortex**

To determine the role of the CXCL13-expressing lineage of stromal cells in supporting lymphoid tissue homeostasis and function, we made use of a newly generated mouse line expressing the transgene CXCL13-cre/TdTomato (generously provided by the laboratory of Burkhard Ludewig, unpublished). These mice were crossed to the ROSA26-iDTR line in which the simian diphtheria toxin receptor transgene is expressed downstream of a loxP-flanked transcriptional stop

element. Cre-mediated excision of the “stop” sequence irreversibly triggers expression of DTR and thus allows the specific ablation of the CXCL13-expressing stromal cell lineage upon administration of diphtheria toxin (DTx) (Figure 2.1a).



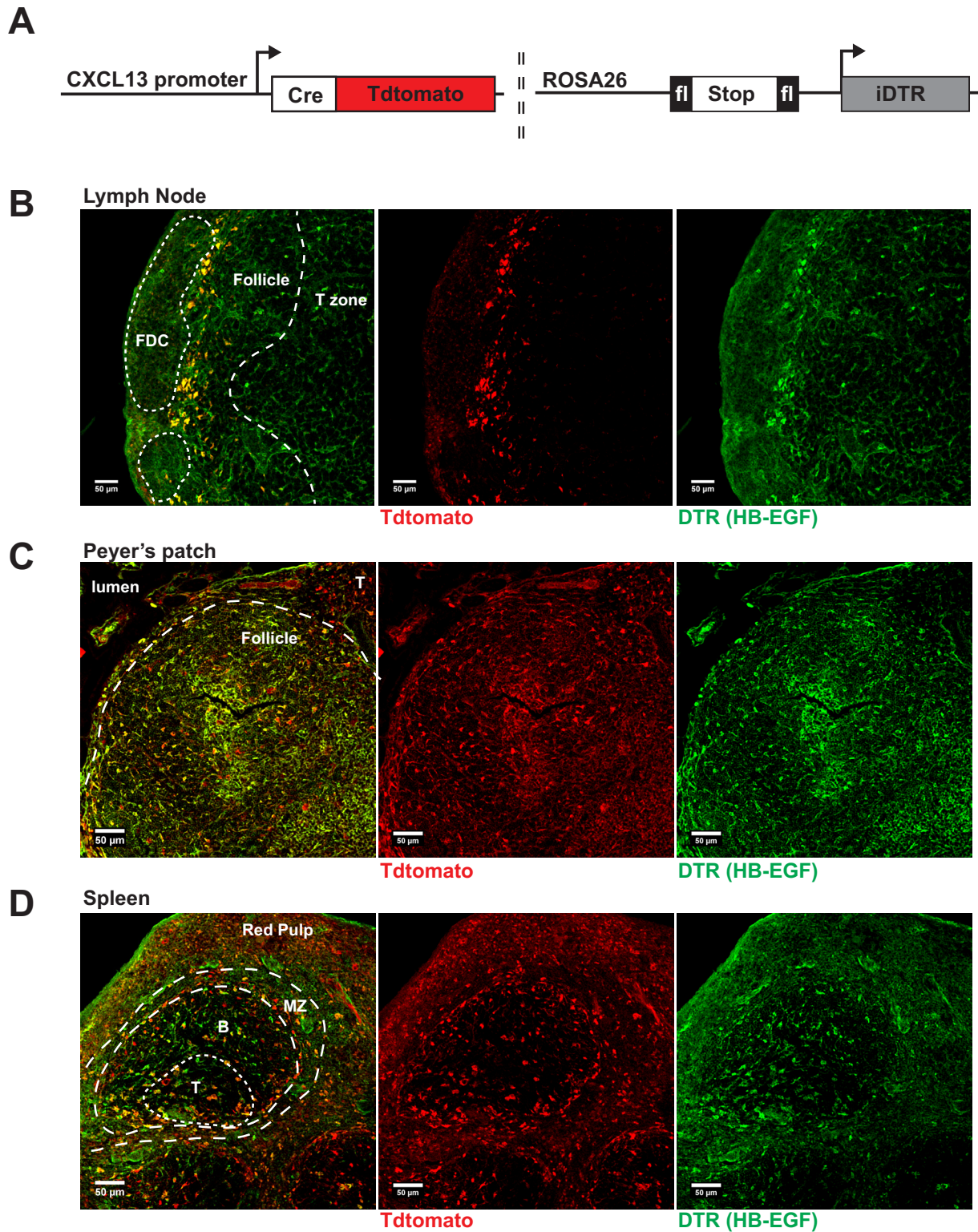


**Figure 2.1** *CXCL13cre*-directed expression of *DTR*. (a) Schematic design of *CXCL13cre*/*Tdtomato* transgene. These mice were bred to *ROSA26iDTR* strain (b-d) Confocal microscopy of tissue sections from *CXCL13cre-iDTR* mice, counterstained with anti-*DTR* (HB-EGF). Tissues imaged include (b) inguinal LN (c) Peyer's patch (d) Spleen.

Expression of CXCL13 is thought to be largely restricted to follicular dendritic cells and B zone FRCs. Unsurprisingly, confocal imaging of these mice reveals that active expression of CXCL13, as indicated by a tdTomato reporter gene, is largely restricted to a subset of stromal populations in the B cell follicle and lining the LN sinus (Figure 2.1 b). The total lineage of cells having undergone cre-mediated recombination and expression of DTR, however, is significantly more widespread. Some expression of DTR is found among the reticular network of both the cortex and paracortex, though expression appears most strongly present in stroma surrounding the B zone follicles.

In contrast to the lymph node, presence of both tdTomato and DTR appears more ubiquitous in the PP and spleen (Figure 2.1 c,d). The hematopoietic compartment of the PP is more than 80% comprised of naive B cells, and CXCL13 is the principle chemokine directing their homeostatic homing and retention <sup>127</sup>. As such, it is unsurprising that both active expression of CXCL13 and CXCL13cre-triggered DTR expression is more wide-spread than that of the LN. More surprising is the pattern of active CXCL13 expression in the spleen. tdTomato signal is apparent not just in the B cell follicle of the splenic white-pulp, but along stromal cells lining the marginal zone and to some extent within the red pulp as well.

### ***In vivo* ablation of the CXCL13-expressing structural support network of lymphoid organs.**

Ablation in CXCL13cre-iDTR mice is effectively achieved within 3 days of administration of DTx. We first sought to identify the specificity of CXCL13cre-directed ablation and the overall impact on lymphoid tissue structure. Stromal cell populations of the lymph node can be distinguished by their expression of gp38 and CD31 (table 1) <sup>128</sup>. Upon administration of diphtheria toxin, we

find substantial alterations to the composition of lymph node stroma, with a roughly 2-fold decrease in the frequency of gp38+CD31<sup>-</sup> cells (which may include FRCs, FDCs, and MRCs) and a corresponding increase in proportion of gp38+CD31<sup>+</sup> lymphatic endothelial cells (LECs) and gp38-CD31<sup>+</sup> blood endothelial cells (BECs) (Figure 2.2 a). Quantification of absolute cell numbers reveals that this primarily reflects a decrease in the total cellularity of gp38+CD31<sup>-</sup> stroma, while the absolute cell numbers of LECs and BECs are unchanged (Figure 2.2b). These results confirm the specificity of this model in targeting non-endothelial LN stroma.

Confocal imaging of the lymph node following diphtheria toxin-mediated ablation reveals several striking alterations to the structure and distribution of gp38<sup>+</sup> stroma (Figure 2.2 c). Notably, LNs from CXCL13<sup>cre+</sup> mice exhibit an apparent loss of gp38<sup>+</sup> reticular cells specifically in the LN cortex. Additionally, ablation in CXCL13<sup>cre</sup> x iDTR mice appears to result in disruptions to gp38<sup>+</sup> stroma underlying the lymph node sinus. By contrast, the reticular network of the paracortex appears to be largely intact and structurally normal. Together, these data suggest that CXCL13<sup>cre</sup>-directed ablation primarily targets stromal populations supporting the B cell follicle, including B-zone FRCs, but not T-zone FRCs. These data largely reflect the expected distribution pattern of CXCL13-expressing stroma. It is notable that while we observed some level of DTR expression (visualized by anti-HB-EGF, Figure 2.1b) on FRCs of the T-cell zone, the FRC network supporting this region remains largely intact following DTx treatment.

In comparison to lymph nodes, stromal ablation in intestinal PPs was far more extensive. However, the full extent of stromal ablation in PPs could not be quantified, as 3 days after administration of DTx, no remaining PPs could be macroscopically identified (data not shown).

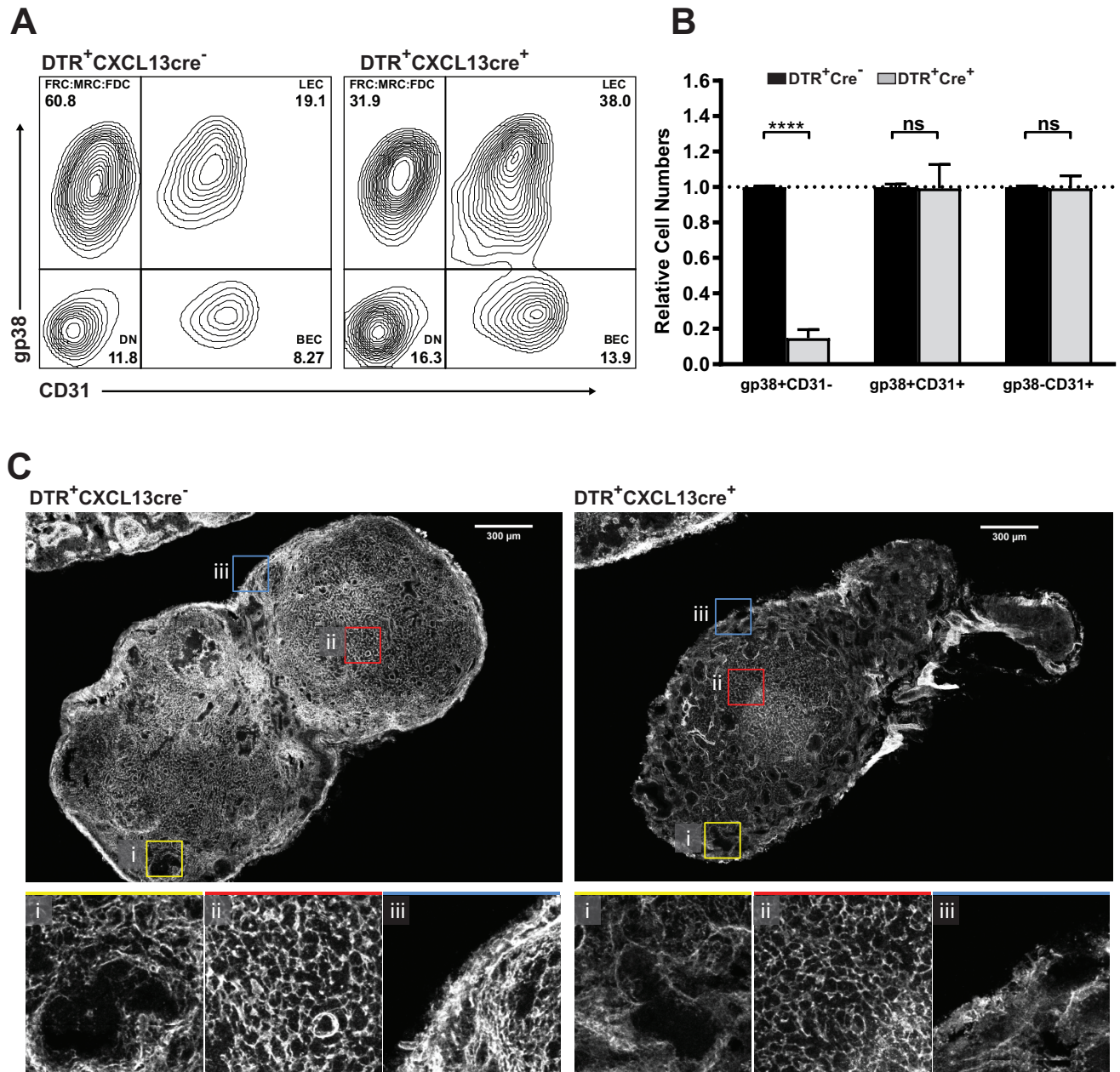


**Figure 2.2** *CXCL13cre-iDTR targets gp38+CD31<sup>-</sup> stromal cells for ablation.* (a-c) Analysis of inguinal lymph nodes of CXCL13cre<sup>+</sup>DTR<sup>+</sup> or CXCL13cre<sup>-</sup>DTR<sup>+</sup> mice 3 days post DTx injection. (a) Flow cytometric analysis of key stromal cell populations. (b) Relative cell counts of LN stromal cell populations (n ≥ 4). (c) Confocal microscopy of inguinal lymph nodes stained with anti-gp38. insets = i) cortex ii) paracortex iii) LN sinus (representative of at least 3 mice per group).

### **Ablation in CXCL13cre-iDTR mice specifically targets FDCs, MRCs, and B-zone FRCs.**

Stromal cells populating the LN cortex include FDCs, MRCs, and B zone FRCs, with each population occupying a distinct region: FDCs roughly localize to the center of each individual B cell follicle, MRCs line the LN sinus covering the follicles, and B zone FRCs form largely along the perimeter of the FDC network (Figure 2.3a). Confocal imaging of LNs from CXCL13cre-iDTR mice following administration of DTx reveals a loss of MRCs at the LN sinus, as indicated by an absence of both RANKL+ and MAdCAM+ staining (Figure 2.3b). Some gp38+ staining remains, likely reflecting the persistence of lymphatic endothelium organizing the LN sinus itself. Likewise, subcapsular sinus macrophages, which occupy roughly the same physical space as MRCs, also remain after DTx treatment (Figure 2.3c). However, it is notable that these macrophages, which normally form a single layer of cells underneath the sinus, appear to project into the LN cortex following ablation of the MRCs. These data may reflect an important role for MRCs in directing the physical retention and organization of SCS macrophages.

Ablation in CXCL13cre-iDTR mice also results in a complete loss of FDCs, as indicated by a loss of CR1/CR2 staining (Figure 2.3d). In total, these alterations to the LN stromal cell network have dramatic effects on lymphocyte organization. B cells fail to form distinct follicles, but rather form a continuous, disorganized band around the periphery of the T zone. Additionally, these B cells appear to collapse inward from the cortex to the outer edge of the paracortex. Surprisingly, segregation of B and T cell zones in the LN is maintained, with T cells localizing to the remaining FRC network in the paracortex, and B cells localizing along the outer fringe of this network.

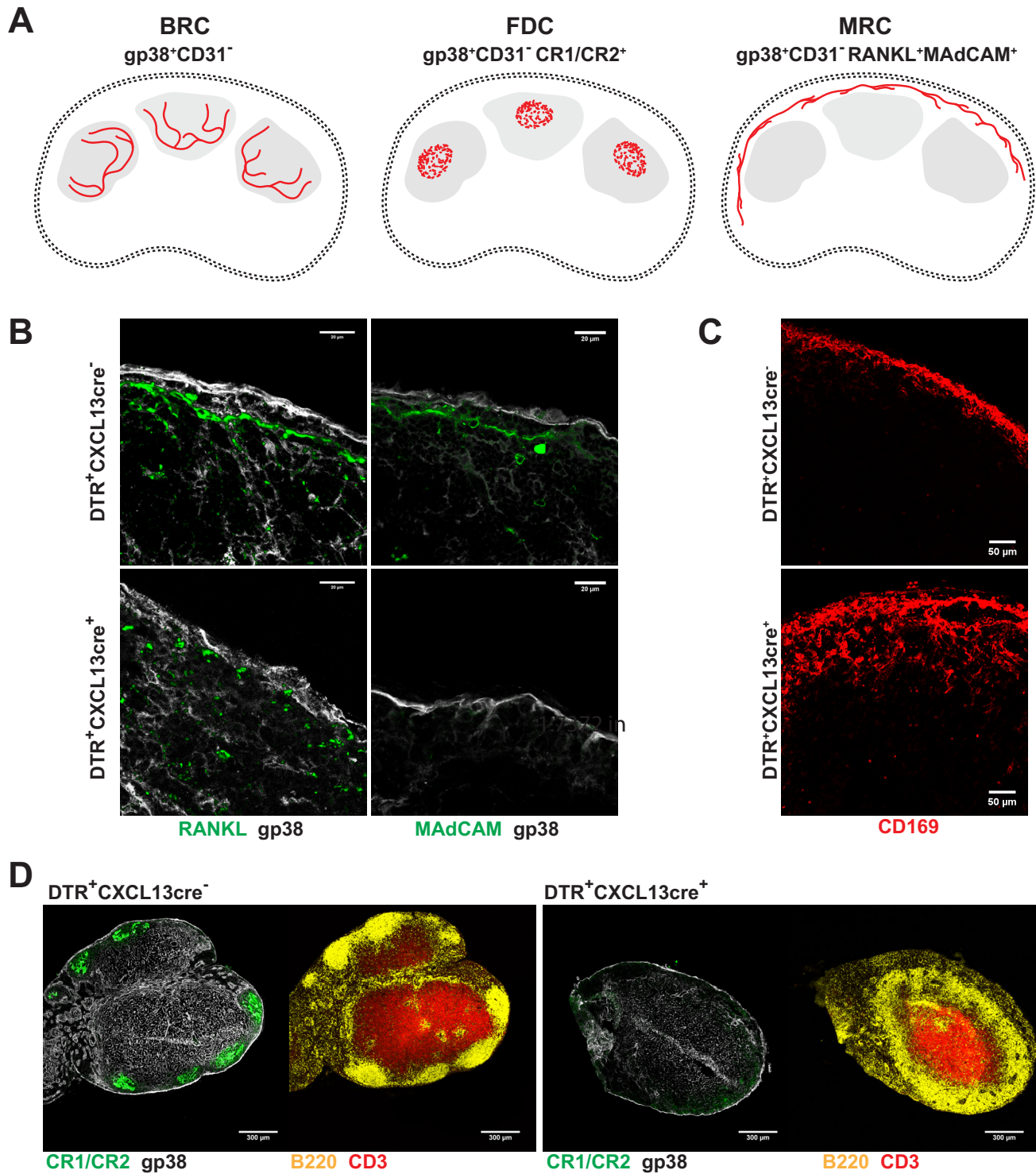


**Figure 2.3** *CXCL13cre-iDTR* target MRCs and FDCs for ablation. (a) Schematic representation of B zone FRCs, FDCs, and MRCs (b-d) Confocal microscopy of inguinal LNs from Cre<sup>+</sup> and Cre<sup>-</sup> mice 3 days post injection with DTx. (b) MRCs lining the LN sinus counterstained with anti-gp38 and anti-RANKL (left panels) or anti-MAdCAM (right panels) (c) Sinus-lining macrophages, stained with anti-CD169. (d) Representative images of the FDC and FRC network (anti-CR1/CR2 and anti-gp38, left) or B and T cell zone (anti-B220 and anti-CD3, right).

## **Ablation of CXCL13cre-expressing stroma triggers redistribution of blood and lymphatic vessels.**

While we have established that CXCL13cre-directed ablation in these mice specifically targets the gp38+CD31<sup>-</sup> non-endothelial compartment of stromal cells, we nevertheless observe significant alterations to the regional distribution of both blood and lymphatic vessels following the ablation of CXCL13cre-expressing stroma. High endothelial venules (identified in LNs by expression of peripheral node addressins, PNA<sup>d</sup>) function as the site of lymphocyte entry into the LN and are normally distributed throughout the paracortical T cell zone and along the border of the T cell zone and B cell follicle (Figure 2.4a,c)<sup>129,130</sup>. Few, if any HEVs pass directly into the B cell follicles. However, upon ablation of CXCL13cre-expressing stroma, the vast majority of HEVs redistribute to the outer LN cortex and B cell zone, while few HEVs remain in the T cell zone. A similar redistribution of lymphatic vessels (identified by expression of LYVE-1) is also observed following ablation of CXCL13cre-expressing stroma. Localization of lymphatic endothelium in the LN is typically restricted to a thin layer of afferent lymphatics lining the LN sinus and a network of lymphatic vessels comprising efferent lymphatics of the inner LN medulla (Figure 2.4b,c). Upon ablation in CXCL13cre-iDTR mice, LYVE-1 staining appears to expand throughout the LN cortex. However, it is unclear whether these lymphatic vessels permeating the cortex arise from an inward migration of LN sinus-lining afferent lymphatics or a spreading of the medulla.

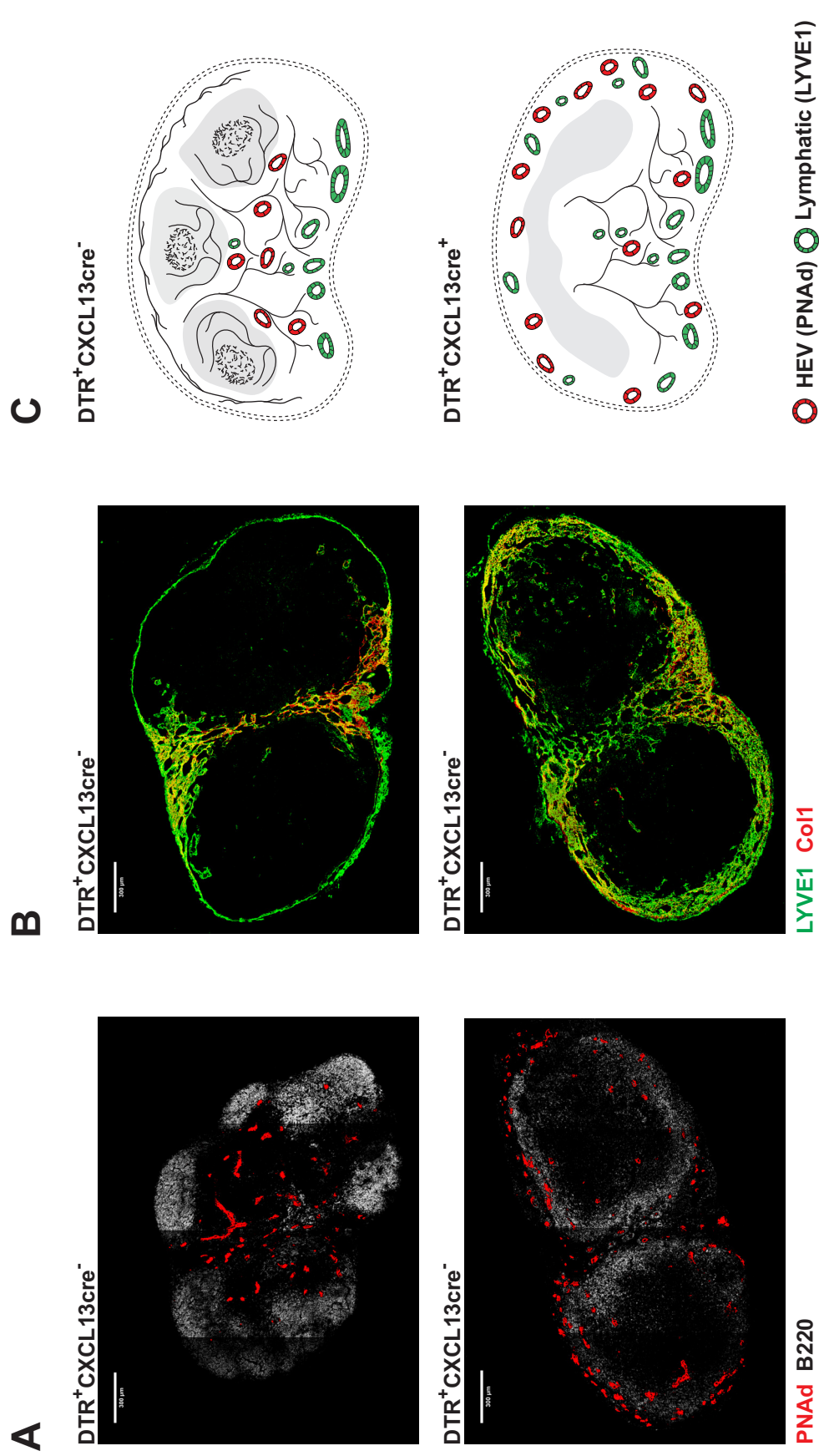


**Figure 2.4** Altered blood and lymphatic vessel localization following CXCL13cre-directed ablation (a-b) Confocal microscopy of inguinal lymph nodes from Cre+ and Cre- mice 3 days post DTx injection. (a) HEVs were stained with anti-PNAd. B cell zone is identified with anti-B220. (b) Lymphatic vessels were stained with anti-LYVE1 and Col1. (c) Schematic representation of the LN from DTR+CXCL13cre+ and DTR+CXCL13cre- mice illustrating alterations to blood and lymphatic vessel localization.



### **Ablation of CXCL13-expressing stromal lineage specifically disrupts B cell homeostasis.**

Despite structural alterations, we find little difference in LN or splenic size following administration of DTx. However, flow cytometric analysis of lymphocyte populations in lymph nodes 3 days post DTx treatments shows a substantial and specific loss of B cells (Figure 2.5a). By contrast, absolute T cell numbers remain constant, likely reflecting the persistence of a supporting T-zone FRC network. In mesenteric lymph nodes, which normally harbor ongoing germinal center reactions, ablation in CXCL13cre-iDTR mice appears to additionally result in a nearly complete loss of germinal center B cells, identified as B220+GL7+CD38- (Figure 2.5b).

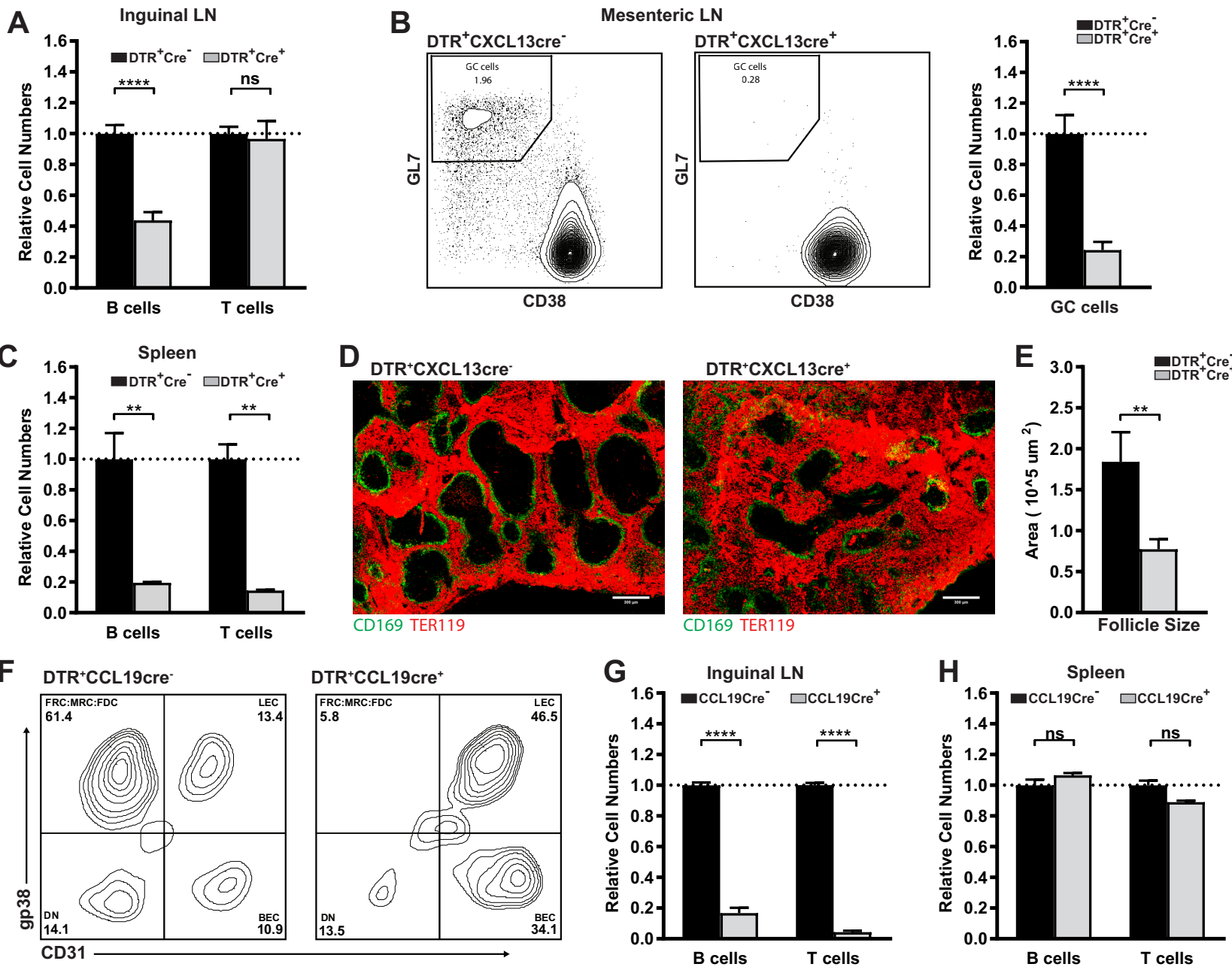
Whereas ablation results in a selective loss of B cell homeostasis in LNs, the effect on lymphocyte homeostasis in the spleen extends to both B and T cell populations (Figure 2.5c). Furthermore, the extent of B cell loss appears more dramatic in the spleen. We find a nearly 10-fold decrease in total B220+ B cells and CD3+ T cells within three days of DTx treatment. Imaging of spleen sections reveals a partial collapse of the splenic white pulp (Figure 2.5d,e), as follicle size is dramatically decreased. However, separation of white pulp and red pulp (identified by TER119 staining) remains, as do the marginal zone macrophages. This suggests at least some of the structural support network remains intact.

The effect of ablation in CXCL13cre-iDTR mice on lymphocyte homeostasis is strikingly different from that of CCL19cre-iDTR mice. As with CXCL13cre, CCL19cre-directed ablation specifically targets the gp38+CD31- population of stromal cells (Figure 2.5f). However, whereas CXCL13cre is limited to B zone FRCs, CCL19cre has been reported to target all FRC populations of the LN<sup>101</sup>. This is reflected by the greater decrease in gp38+CD31- cell frequency than seen following

depletion in CXCL13cre-iDTR mice. In line with previous reports, we also find that both B and T cell numbers are dramatically decreased in the LN of CCL19cre-iDTR mice within 3 days of DTx treatment, while splenic lymphocyte populations are not significantly impacted (Figure 2.5g,h). Furthermore, CCL19cre-iDTR mice were reported to exhibit only moderate decreases in lymphocyte populations of the intestinal PPs, whereas CXCL13cre-iDTR mice exhibit complete ablation of the PP (data not shown). Cumulatively, these data suggest very different roles for CXCL13cre and CCL19cre-expressing stroma in support of lymphocyte homeostasis in different immune organs.

**Figure 2.5** *Loss of B cell homeostasis in CXCL13cre-iDTR ablated mice.* (a-e) CXCL13cre-iDTR mice 3 days post DTx injection. (n ≥ 10) (f-h) CCL19cre-iDTR mice 3 days post DTx injection. (n ≥ 3) (a) Flow cytometric analysis: relative cell counts of B220+ B cells and CD3+ T cells from inguinal LN. (b) Flow cytometric analysis of germinal center B cells from mesenteric lymph nodes, gated on B220+ cells. Quantification of relative cell numbers (right) (c) Relative cell counts of B220+ B cells and CD3+ T cells from spleen. (d,e) Confocal microscopy of spleen sections stained with CD169 and TER119. (e) Quantification of follicle size calculated in ImageJ (n ≥ 10 F.O.V from 3 mice) (f) Flow cytometric analysis of stromal cell populations from CCL19cre-iDTR mice. (g) Relative cell numbers from inguinal LN of CCL19cre-iDTR mice (h) Relative cell numbers from the spleen of CCL19cre-iDTR mice.

Figure 2.5 (Continued)



## **Ablation of CXCL13cre-expressing stroma disrupts B cell retention**

Stromal populations of the lymph node produce several key chemotactic and survival factors supporting naive lymphocyte homeostasis. Previously reported findings from CCL19cre-iDTR mice which exhibit significant loss of LN B and T cell populations largely attributed these changes to a loss of FRC-produced BAFF and IL-7, respectively<sup>101</sup>. We similarly find a significant decrease in BAFF transcript from LNs of CXCL13cre-iDTR mice, however decreases in IL-7 did not reach statistical significance (Figure 2.6a). These data largely reflect the specific loss of B cells and retention of T cells observed following ablation.

As expected, CXCL13cre-targeted ablation also results in a complete loss of detectable CXCL13 transcript, thus likely accounting for a loss of B cell chemotaxis and localization to the LN cortex (Figure 2.6b). Interestingly, ablation was also associated with statistically significant decreases in transcript levels of CCL19, but not CCL21. These data may suggest that, while CXCL13 and CCL21 expression is more restricted to B and T zone FRCs, respectively, CCL19 is widely expressed by all FRC populations.

The observed alterations to B cell localization likely results directly from the loss of CXCL13 production. However, it remained unclear whether decreases in the total number of B cells is likewise a consequence of perturbed B cell chemotaxis, or if B cells are recruited and retained in the LN normally, but fail to survive in the absence of sufficient levels of BAFF. To address this question, we examined the efficiency of short-term lymphocyte recruitment to the LN. Fluorescently labeled splenocytes were adoptively transferred to CXCL13cre-iDTR mice 3 days post DTx injection. One hour after transfer, we find significantly fewer lymphocytes

accumulating in the LN of CXCL13cre+iDTR mice relative to controls (Figure 2.6c). This was largely due to a specific loss of B cell recruitment, as T cell recruitment was largely normal.

We previously noted that HEVs and lymphatic vessels in the LNs of CXCL13cre-iDTR mice localize in close proximity to each other in the LN cortex (fig 2.4). Given this unusual distribution, we additionally explored the possibility that decreases in accumulation of adoptively transferred B cells may be a factor of impaired retention rather than a defect in the initial entry across the HEV. To address this question, we additionally treated CXCL13cre-iDTR mice with the S1PR1 agonist FTY720 prior to adoptive transfer, thereby restricting lymphocyte access to efferent lymphatics<sup>46</sup>. We find that addition of FTY720 completely restores the accumulation of adoptively transferred B cells to the LN in ablated mice (Figure 2.6d). Cumulatively, these data suggest that B cell recruitment to the LNs of ablated CXCL13cre-iDTR mice is normal, but that in the absence of B cell chemoattractants, these cells cannot be retained and immediately egress through nearby efferent lymphatic vessels. Interestingly, while FTY720 restored short-term retention of transferred B cells, it did not significantly restore total B cell numbers (Figure 2.6e). This may suggest that even if B cells can be retained in the ablated LN, the vast majority of these cells will not survive due to the absence of BAFF.

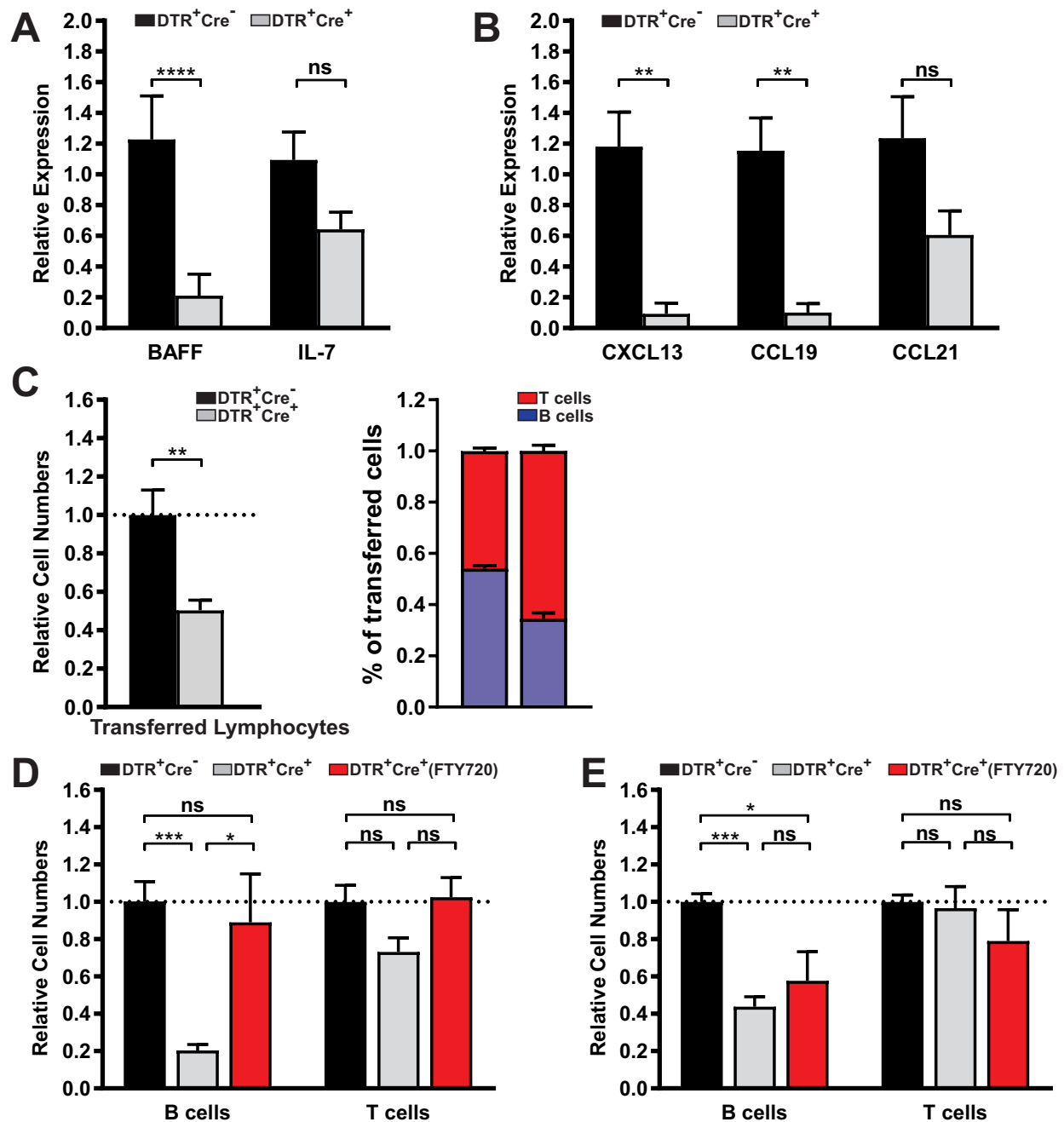


**Figure 2.6** Lymphocyte recruitment and retention in *CXCL13cre-iDTR* ablated mice. (a) qPCR analysis of transcript levels for survival factors BAFF and IL-7 from whole LN mRNA. (n ≥ 5 mice) (b) qPCR analysis of transcript levels for chemokines CXCL13, CCL19, and CCL21 from whole LN mRNA. (n ≥ 5 mice) (c) CMFDA labeled lymphocytes were adoptively transferred into Cre<sup>+</sup> or Cre<sup>-</sup> recipients 3 days post DTx injection. LNs were harvested 1 hour after adoptive transfer and quantified by flow cytometry. Data represented are relative transferred cell numbers (left) and percentage of B and T cells (of transferred lymphocytes). (n ≥ 6 mice per group) (d) CMFDA labeled lymphocytes were adoptively transferred into Cre<sup>+</sup> or Cre<sup>-</sup> recipients 3 days post DTx injection. A subset of mice were additionally treated with FTY720 12 hours before adoptive transfer. LNs were harvested 1 hour after adoptive transfer and quantified by flow cytometry. (n ≥ 3 mice per group)

## 2.3 Discussion

Recent studies involving the specific genetic targeting and ablation of CD21- and CCL19-expressing stromal cell populations have established specific roles for FDCs and FRCs respectively<sup>101,109</sup>. These studies have highlighted the utility of this experimental approach toward understanding the population heterogeneity and functional complexity of lymphoid tissue stromal cells. We have expanded on these findings by describing a model of CXCL13-cre-directed cellular ablation in which FDCs, MRCs, and B-zone FRCs are specifically targeted.

Despite some population overlap with both CD21 and CCL19-expressing cells, depletion of the CXCL13-expressing stromal subset resulted in alterations to lymphoid tissue architecture and immune cell composition that was clearly distinct from previously described models of stromal cell manipulation. Comparison of these results to previously reported models of stromal cell ablation may offer clearer insight into the specific role each stromal population may fill in supporting lymphoid tissue homeostasis and immune function.

The short-term effects of ablating LN and splenic FDCs have been previously reported through use of a CD21cre-iDTR mouse model. Similar to these reports, we find that ablation of the CXCL13cre-expressing stromal lineage results in impaired B cell follicle formation and a loss of germinal center cells. Despite the loss of distinct follicles, B and T cells remain distinctly compartmentalized, with T cells remaining in the LN paracortex and B cells forming a disorganized band surrounding the T cell zone. However, unlike CD21cre-directed ablation of FDCs, our results additionally demonstrate substantial and specific decreases in B cell numbers.



Similar deficiencies in supporting B cell homeostasis have been reported following CCL19cre-directed ablation of FRCs. Thus the combination of these findings is in line with the proposed model that FDCs organize B cell follicles and support GC reactions, while FRCs provide the necessary support for B cell chemotaxis and homeostasis. However, whereas ablation in CCL19cre-iDTR mice (which broadly targets all FRC populations) results in a decrease in both B and T cell numbers, the ablation of CXCL13cre-expressing FRCs only impacts B cell homeostasis. Additionally, CCL19cre-directed ablation reportedly results in a disruption to B and T cell compartmentalization, whereas separation of B and T cell zones is maintained following CXCL13cre-directed ablation. This discrepancy thus provides new experimental evidence of heterogeneity within the FRC population and supports the notion of functionally distinct B-zone and T-zone FRC populations.

The maintenance of distinct B and T cell zones following depletion of CXCL13-expressing stroma raises an interesting question of what role CXCL13 plays in the organization of immune cell populations. The conventional understanding of B cell chemotaxis within lymphoid tissues is that CCL19 and CCL21 initially aid in the recruitment of both B and T cells across the HEV, while CXCL13 then specifically diverts CXCR5-expressing B cells out of the T-cell zone and into the follicles. Our data suggests that CXCL13 is dispensable with regard to B cell exclusion from the T cell zone, though whether there exist other active chemotactic cues directing B cells to leave the T cell zone is unclear. An alternative explanation may be that T cells more readily respond to homeostatic or chemotactic signals provided by T-zone FRCs, and thus simply out-compete B cells for physical space in the paracortex. B cells may then be subsequently "pushed" outward toward the cortex.

It should be noted, however, that although B cells remain distinctly excluded from the T cell zone, their distribution to the LN cortex nevertheless appears abnormal. B cell follicles are normally positioned immediately beneath the MRCs lining the LN sinus. Even when FDCs are specifically ablated and follicles fail to form (as in CD21cre-iDTR mice), the B cell zone appears to remain similarly situated near the MRCs. However, ablation of all CXCL13-expressing stroma results in a clear area of separation between B cell zone and the LN sinus. This phenomenon has not previously been observed in either CD21- or CCL19-directed models of ablation, and unlike CXCL13cre-directed ablation, neither of these models have been shown to target MRCs. It is thus possible that MRCs play some critical role in orienting the B cell zone along the LN sinus.

Finally, while CXCL13 may be dispensable for separation of B and T cell zones, we suggest that it may be essential for the retention of B cells within lymphoid tissues. B cell numbers in both LN and spleen decrease substantially following CXCL13cre-directed ablation, and this may partly be a consequence of cell death following the loss of stromal cell-derived BAFF, as was reported in the CCL19cre-DTR model of FRC depletion. However, our results suggest that loss of B cells is at least partly a consequence of failed B cell immigration as well. We show that adoptively transferred B cells, but not T cells, fail to accumulate in the LNs of ablated mice. However, simultaneous blockade of lymphocyte egress (by administration of FTY720) during adoptive transfer rescues short-term B cell accumulation. We suggest that CCL19 and CCL21 may be sufficient to direct initial immigration of B cells into the LN, but that CXCL13 is critical for their retention. In the absence of CXCL13, immigrating B cells immediately egress through nearby efferent lymphatics.

Beyond these observed alterations to lymphocyte recruitment and localization, we also report that ablation of the CXCL13-expressing stromal lineage causes substantial reorganization of blood and lymph vessels. In the absence of MRCs, FDCs, and B-zone FRCs, the LN cortex is largely devoid of structural elements, likely permitting the redistribution of blood and lymphatic vessels to fill this space. The immunological consequence of this stromal reorganization on LN function is currently unclear, though one might speculate dramatic alterations to lymph flow dynamics in the LN and thus alterations to antigen trafficking. Lymph nodes function as an intersection between blood and lymph, and one important architectural feature of the LN is that afferent lymphatics of the LN sinus connect to the HEV in the paracortex via a network of FRC conduits <sup>49,131</sup>. This is thought to permit the directional flow of lymph and lymph-borne material into the LN parenchyma. As such, one potentially important consequence of HEV redistribution away from the LN paracortex (and the remaining FRC network populating the paracortex) is a disruption of normal lymph transport and loss of FRC-HEV interactions. The full extent to which this occurs, and the immunological consequence, will require further investigation. Moreover, it will be important to determine whether remaining FRCs maintain functional conduits in the LN at all following ablation.

Ultimately, we believe that CXCL13cre-directed cellular ablation will prove to be a useful tool in furthering our understanding of various lymphoid tissue stromal subsets. There are specific advantages to this model which may provide information not attainable in previously described models. Firstly, this is the first reported model in which MRCs can be genetically targeted. While it cannot be described as MRC-specific, as FDCs and B-zone FRCs are also targeted, we suggest that important insights to MRC function may nevertheless be attained by direct

comparison to CD21cre and CCL19cre mouse lines, which target FDCs and FRCs, but not MRCs. One important question which may be directly addressed through ablation of MRCs is understanding the lineage relationship between MRC, FRC, and FDC. No clear lineage relationship between MRC and FRC has been experimentally established, though it has recently been reported that most of the FDC network derives from MRCs <sup>112</sup>. Additional insight to the lineage relationship between these stromal subsets may be found by characterizing the recovery kinetics of each stromal subset after ablation.

Secondly, no other mouse model has yet been described which allows the study of long-term effects of FDC ablation. CD21-driven cre is expressed not only by FDCs in lymphoid tissues, but in the brain and kidney as well <sup>109</sup>. Consequently, DTx-mediated ablation in this model results in severe illness and paralysis shortly after treatment. DTx can access lymphoid tissues more rapidly than the brain, and thus these adverse effects can be temporarily delayed by administering DTx-neutralizing antibody shortly following DTx treatment, while still allowing efficient ablation of FDCs. However, these experiments are nevertheless limited to a maximum duration of 2 days. By contrast, in the CXCL13cre-iDTR model of stromal ablation, we have observed no apparent adverse effects to the animal's health up to one month following administration of DTx (data not shown). This offers a unique opportunity to follow the long term effects of FDC ablation not possible through the use of CD21cre mice.

Finally, while CXCL13cre-iDTR and CCL19cre-iDTR mice both target subsets of FRCs, the extent of FRC ablation and the effects on homeostatic maintenance of lymphocyte populations appears to vary by organ. In the lymph node, CCL19cre-directed ablation targets all FRC

populations and has dramatic effects on both B and T cell populations, while CXCL13cre-directed ablation results specifically in a loss of B-zone FRCs and B cell homeostasis. By contrast, CXCL13cre-directed ablation results in a complete loss of intestinal PPs and dramatic decreases to both B and T cell populations of the spleen, while CCL19cre-directed ablation has only moderate effects on stromal and lymphocyte populations of the PP and spleen. CXCL13cre and CCL19cre mouse models can therefore be alternatively used to variably target FRC populations in different lymphoid organs.

## 2.4 Materials and methods

**Mice.** *CXCL13cre*-tdTomato mice (unpublished) and *CCL19cre* mice were generously provided by Dr. Burkhard Ludewig. *CCL19-Cre* mice were previously described<sup>113</sup>. These mice were crossed with *Rosa26-DTR* mice (iDTR, stock number 007900, purchased from Jackson Laboratory) to generate *CXCL13cre-iDTR* and *CCL19cre-iDTR* mice respectively. Mice were maintained under specific pathogen-free conditions in accordance with institutional and National Institute of Health guidelines and used at 6-8 weeks of age. For each of the experiments performed, age-matched mice of both sexes were analyzed. Experiments were approved by the Boston Children's Hospital and Harvard Medical School institutional animal use and care committee in accordance with NIH guidelines for the humane treatment of animals

**Antibodies.** The following antibodies were used:  $\alpha$ CD45 (30-F11),  $\alpha$ CD31 (390),  $\alpha$ PDPN (8.1.1),  $\alpha$ MadCAM-1 (MECA-367),  $\alpha$ B220 (RA3-6B2),  $\alpha$ CD3e (145-2C11),  $\alpha$ PNA<sub>D</sub> (MECA-79),  $\alpha$ TER119 (TER119),  $\alpha$ RANKL (IK22/5),  $\alpha$ CD169 (3D6.112),  $\alpha$ CR1/CR2 (7E9),  $\alpha$ GL7 (GL7), and  $\alpha$ CD38 (90) from Biolegend,  $\alpha$ LYVE-1 (ALY7) from ebioscience,  $\alpha$ Col1 (millipore sigma),  $\alpha$ HB-EGF (R&D systems)

**Stromal ablation *in vivo*.** *CXCL13creTdtomato* or *CCL19cre* mice were bred to *Rosa26-iDTR* mice to generate *CXCL13creDTR* and *CCL19creDTR* mice respectively. DTR+Cre<sup>+</sup> and DTR+Cre<sup>-</sup> control mice were injected i.p. with 8 ng/g DTx and sacrificed 72 hours post injection.

**Adoptive transfer of lymphocytes.** A single-cell suspension of naive lymphocytes was prepared from spleens from C57Bl/6 donor mice and immediately labeled with CellTracker Green CMFDA dye (ThermoFisher Scientific C2925). Lymphocytes were adoptively transferred to recipient

mice by retro-orbital injection in 50ul of sterile saline. Tissues were harvested for analysis by flow cytometry 1 hour after transfer.

**FTY720 treatments.** To prevent cell egress, mice were injected with 1 mg/kg FTY720 (Fingolimod, R&D) i.p. 12 hours before adoptive transfer of labeled lymphocytes.

**Enzymatic digestion of lymphoid organs.** Single cell suspensions of LN, PP, and spleen were prepared for analysis by flow cytometry. *Lymph nodes:* LNs were dissected and incubated at 37 °C in RPMI containing 0.1 mg/ml Dnase I (Invitrogen), 0.2 mg/ml Collagenase P (Roche) and 0.8 mg/ml Dispase (Roche) for 50–60 minutes, as previously described<sup>132</sup>. Cells were collected in medium containing 2% FBS and 5 mM EDTA every 15–20 min, and replaced with fresh digestion medium. *Peyer's patches:* Intestines were dissected and washed by lavage with ice cold PBS. PPs were removed from the intestine and washed in a solution 2 mM EDTA and 5% DTT in PBS for 20 minutes at 37°C to remove the epithelium. PPs were then enzymatically digested (as with the LN). *Spleen:* Lymphocyte were extracted from the spleen by mechanical disruption and passage through a 70um cell strainer. Red blood cells were lysed with ACK buffer before analysis by flow cytometry.

**Immunohistochemistry and confocal microscopy.** Isolated tissues were fixed in 4% paraformaldehyde (PFA) for 4 hours and placed in 30% sucrose until saturation. Tissue was embedded in OCT medium (Optimal Cutting Temperature), frozen, and cut into 20 µm sections. Sections were stained and imaged using Inverted Olympus IX 81 confocal microscope.

**Statistical analysis.** Statistical tests were performed using GraphPad Prism software. Differences were considered to be statistically significant when  $P < 0.05$ . For graphs, data are shown as mean  $\pm$  SEM. Statistical significance is indicated with the following: \* ( $p \leq 0.05$ ), \*\* ( $p \leq 0.01$ ), \*\*\* ( $p \leq 0.005$ ), \*\*\*\* ( $p \leq 0.001$ ). Sample size was not specifically predetermined, but the number of mice used was consistent with prior experience with similar experiments.



## Chapter 3

### **Intestinal fluid absorption modulates Peyer's patch homeostasis and mucosal antibody responses.**

Peyer's patches (PPs) are B cell-rich lymphoid tissues situated throughout the small intestine which play an important role in mucosal antibody responses. PP architecture and stromal cell composition closely resemble that of peripheral lymph nodes despite geographical and functional differences. Notably, fibroblastic stromal cells located in small intestinal PPs form a network of collagen-rich reticular fibers similar to the network of conduits found in lymph nodes. In the PP, these conduits extend from the basement membrane of the intestinal epithelial cell lining into the PP follicle, and terminate along blood and efferent lymphatic vessels.

Unlike lymph nodes, PPs lack a conventional source of afferent lymph that would normally contribute fluid flow through the conduit network. Instead fluid flow through PP conduits depends largely on water absorbed across the intestinal epithelium. We find that by disrupting water absorption, we can limit or prevent the contribution of absorbed luminal fluids to the flow of PP conduits. Disruption of fluid absorption subsequently has profound effects on the structural integrity of the HEV and surrounding perivascular FRCs, and display of the mucosal addressin MAdCAM1 within the HEV lumen is reduced. These alterations correlate with a striking defect in the recruitment of naïve recirculating lymphocytes to the PP.

Prolonged blockade of water absorption additionally impacts mucosal antibody responses. Antigen-specific fecal IgA titers are reduced, and germinal center responses are decreased in

scale. We believe these findings reveal a critical role for conduit-mediated fluid flow in the maintenance of PP homeostasis and mucosal immune function.

### **3.1 Introduction**

Fibroblastic reticular cells (FRCs) provide the architectural framework supporting lymphoid tissues. In lymph nodes, FRCs deposit and ensheath organized bundles of collagen fibers to form an intricate network extending from the subcapsular sinus to the high endothelial venule (HEV) and efferent lymphatics <sup>51,131</sup>. The anatomy of these structures allows for two functionally distinct compartments. The surface of the reticular network, comprised of interconnected FRC cell bodies, facilitates leukocyte attachment, cellular interactions and directional migration of leukocytes within the LN parenchyma. This aspect of the reticular network is functionally essential for the proper compartmentalization and survival of lymphocytes, as well as the initiation of adaptive immune responses <sup>95,99,101,103,125,126</sup>. In contrast, the inner collagen core of the reticular network has been described as a conduit network, directing the flow of lymph from the LN sinus into the LN parenchyma <sup>131</sup>. The functional and biological relevance of this latter aspect of the reticular network is less established.

Soluble, lymph-borne mediators have long been known to penetrate the LN cortex and reach the high endothelial venule (HEV) just minutes after upstream subcutaneous inoculation. The speed at which these molecules have been found to traverse the densely packed LN parenchyma from capsule to HEV suggests a mode of transport beyond passive interstitial diffusion of fluid. LN conduits have thus been proposed to function as an efficient and rapid

pathway for the transport of immunologically important soluble mediators from upstream tissues.

Multiple reports have now demonstrated that antigen injected into the footpad of mice rapidly enters the LN conduit network where it can be directly sampled by resident DCs and follicular B cells through gaps in the FRC sheath<sup>83,84,133</sup>. Likewise, soluble chemokines injected subcutaneously are rapidly delivered via the conduit network to the abluminal surface of the HEV, whereupon these molecules are transcytosed and decorate the vascular lumen<sup>48-50</sup>. This process leads to an increase in leukocyte homing within minutes of injection. This latter example has led to a predicted model in which conduits facilitate a form of “remote control” wherein soluble mediators from upstream tissues can prime the lymph node for the initiation of adaptive immune responses.

The concept of FRC conduits mediating rapid and selective transport of soluble, small MW material is now widely accepted. However, the necessity for conduit-mediated molecular and fluid transport for either LN homeostasis or initiation of adaptive immune responses has not been experimentally addressed. To date, no models exist in which to interrogate lymph node function in the absence of conduits. Even acute ablation of FRCs fails to eliminate the conduit network once formed<sup>101</sup>. Nor have any physiological means of altering afferent lymph flow been developed, though surgical manipulation of upstream lymphatics has been reported<sup>27-29</sup>. Interestingly, lymph nodes that have been surgically deprived of afferent lymph have been reported to exhibit a gradual “flattening” of the high endothelial venule, loss of glycamin expression on the vascular endothelium, and a corresponding decrease in lymphocyte immigration. However, the specific contribution of conduit-mediated lymph flow to this

phenomenon cannot be ascertained, as surgical deprivation of afferent lymph additionally impacts cellular migration of antigen-experience DCs and macrophages from upstream tissues.

Few advances have been made in recent years towards establishing a better understanding of the biological importance of conduit-mediated fluid flow and molecular transport due to these experimental limitations. Additionally, the existence of conduit networks in lymphoid tissues not exposed to continuous lymph flow has not yet been addressed.

Here we identify FRC conduit networks in the intestinal Peyer's patches. Peyer's patches (PPs) are B cell-rich lymphoid tissues situated throughout the small intestine which play an important role in the initiation of mucosal antibody responses. Unlike lymph nodes, PPs lack a conventional source of afferent lymph that would normally contribute fluid flow through the conduit network. Instead we demonstrate that fluid flow through PP conduits depends largely on water absorbed across the intestinal epithelium and that this process can be disrupted in a physiological, non-inflammatory way. Prolonged disruption of conduit flow led to profound alterations to homeostatic lymphocyte recruitment to the PP and a reduced capacity to mount mucosal antibody immune responses.

### **3.2 Results**

#### **PP conduit network conducts fluid absorbed from the intestinal lumen.**

Despite lacking a conventional source of afferent lymph flow, characterization of stromal components in the small intestinal PP reveals that these lymphoid organs are supported by an intricate network of collagen-rich reticular fibers, structurally similar to the conduit network

found in lymph nodes (Figure 3.1). These fibers extend from the subepithelial dome and project into both follicle and interfollicular region. Scanning electron micrographs of alkali-water macerated PPs reveal that these reticular fibers emerge directly from the disorganized meshwork of collagen overlying the PP dome and eventually terminate directly along the blood vasculature (Figure 3.1a). As with LN conduits, PP reticular fibers are ensheathed by a basement membrane and an interconnected network of fibroblastic reticular cells (FRCs), identified by expression of perlecan and gp38, respectively (Figure 3.1b). In total, this three-dimensional structure exhibits many of the same microanatomical features as previously described in LN FRC conduits.

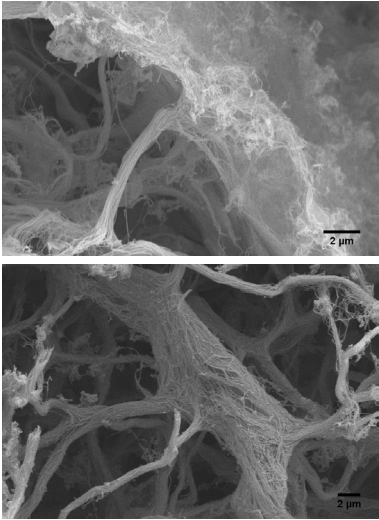
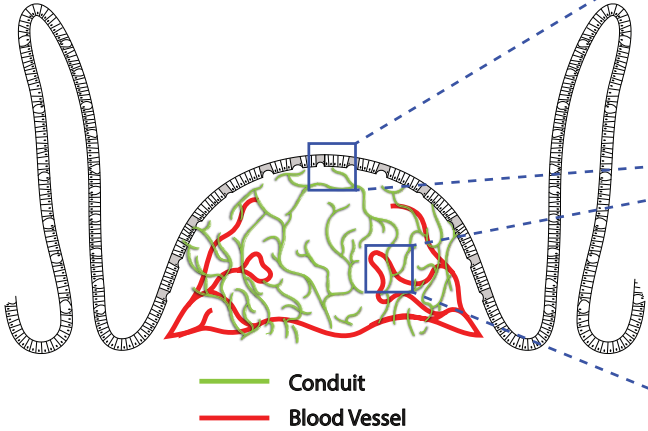
A functional hallmark of LN FRC conduits is the ability to direct lymph flow from the lymph node sinus into the dense parenchyma of the cortex and paracortex, additionally facilitating the delivery of soluble signaling molecules and antigen. The PP conduit network appears to perform a similar function, though drawing in fluid absorbed from the intestinal lumen in place of afferent lymph. Fluid uptake through PP conduits is identifiable through oral administration of soluble FITC. Within two hours of gavage, FITC was detectable throughout the PP and selectively localized within the collagen-rich core of the conduit network (Figure 3.1c).

High magnification confocal imaging additionally confirmed that FITC-bearing conduits interface with blood vessels in the interfollicular region of the PP (Figure 3.1d). Moreover, FITC signal is detectable along the blood vessel wall, suggesting a path of directional fluid flow from the intestinal lumen to PP vasculature mediated by the PP conduit network.

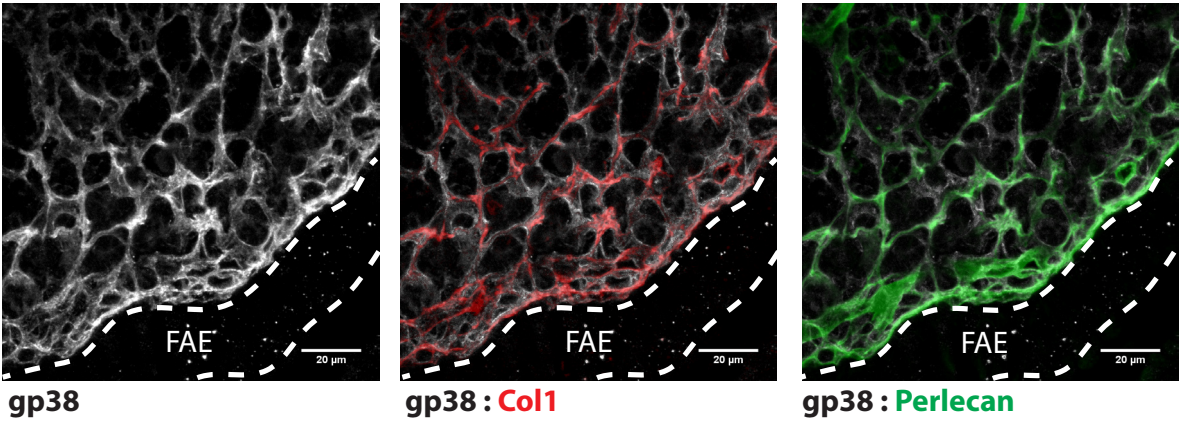
**Figure 3.1** *The FRC conduit network of intestinal Peyer's patches.* **(a)** Scanning electron micrograph of PP following alkali-water maceration to remove cells. top, PP dome region underlying the epithelium. bottom, blood vessel in the PP follicle. **(b)** Confocal microscopy of the dome region of a Peyer's patch stained with anti-gp38, anti-Collagen Type I, and anti-Perlecan. Follicle associated epithelium marked by dotted lines. **(c)** Multiphoton microscopy of a Peyer's patch from a villin-cre-SSB(BFP) mouse after oral gavage with soluble FITC and counterstained with anti-EpCAM1. **(d)** Multiphoton microscopy of a cleared Peyer's patch. The mouse was orally gavaged with soluble FITC and the HEV is stained by in vivo labeling with anti-MAdCAM before perfusion fixation.

Figure 3.1 (Continued)

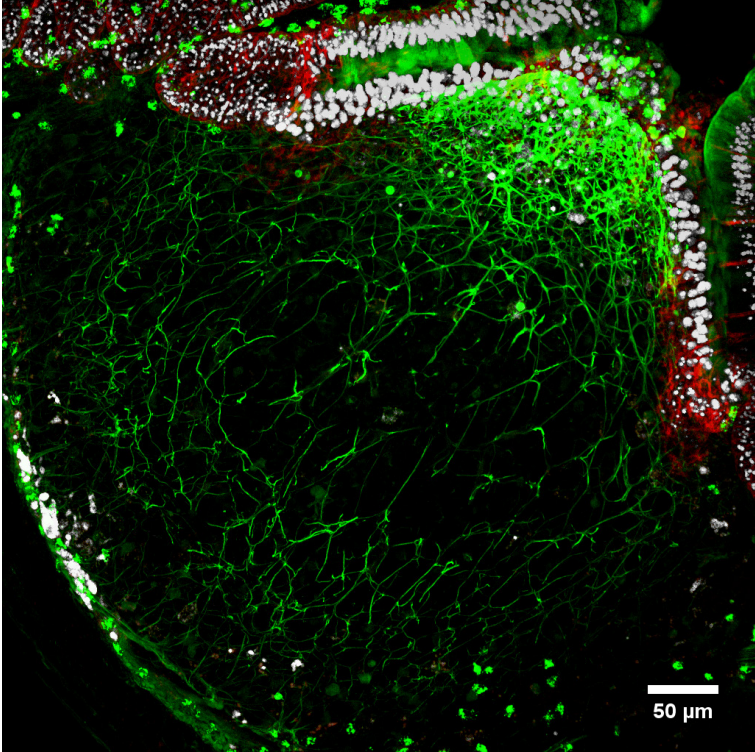
**A**



**B**

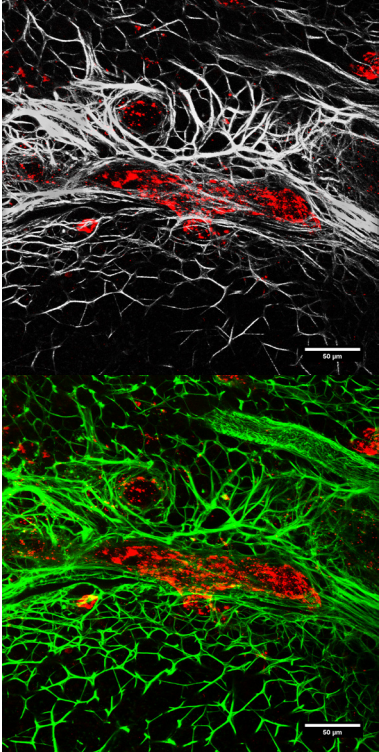


**C**



Villin-cre-SSB : EpCAM1 : FITC

**D**



SHM : MAdCAM1 : FITC

### **Perturbation of intestinal fluid absorption disrupts PP conduit flow**

In lieu of afferent lymph, fluid taken in from the intestinal lumen appears to be a major contributor to directional flow through the PP conduit network. This process is thus uniquely dependent on fluid absorption across the absorptive intestinal epithelium, a process which is tightly regulated by the maintenance of local osmotic gradients through ion transport (Figure 3.2a). The functional consequences of perturbed conduit fluid flow in the PP can thus theoretically be addressed by means of blocking fluid absorption. Here, altered fluid absorption was achieved by two mechanistically distinct treatments – first by administration of a 10% solution of a high M.W. polyethylene glycol (PEG), and secondly by oral treatment with amiloride hydrochloride. PEG is a non-absorbable, non-metabolized osmotically active substance which increases the osmolarity of ingested fluid and promotes its retention in the intestinal lumen (Figure 3.2b). By contrast, amiloride acts by selectively disrupting the function of epithelial Na<sup>-</sup>/H<sup>+</sup> exchangers, thereby disrupting the establishment of sufficient osmotic gradients for directional water transport (Figure 3.2c). Both models of disrupted fluid absorption were found to restrict fluid uptake into PP conduits, as visualized by uptake of soluble FITC after gavage (Figure 3.2c-e).

### **Prolonged blockade of fluid absorption disrupts HEV structure**

Extended periods of treatment with PEG in drinking water does not result in gross changes to the overall architecture or organization of the PP (data not shown), nor are there any apparent changes to the morphology or total numbers of FRCs, suggesting that fluid flow is not necessary



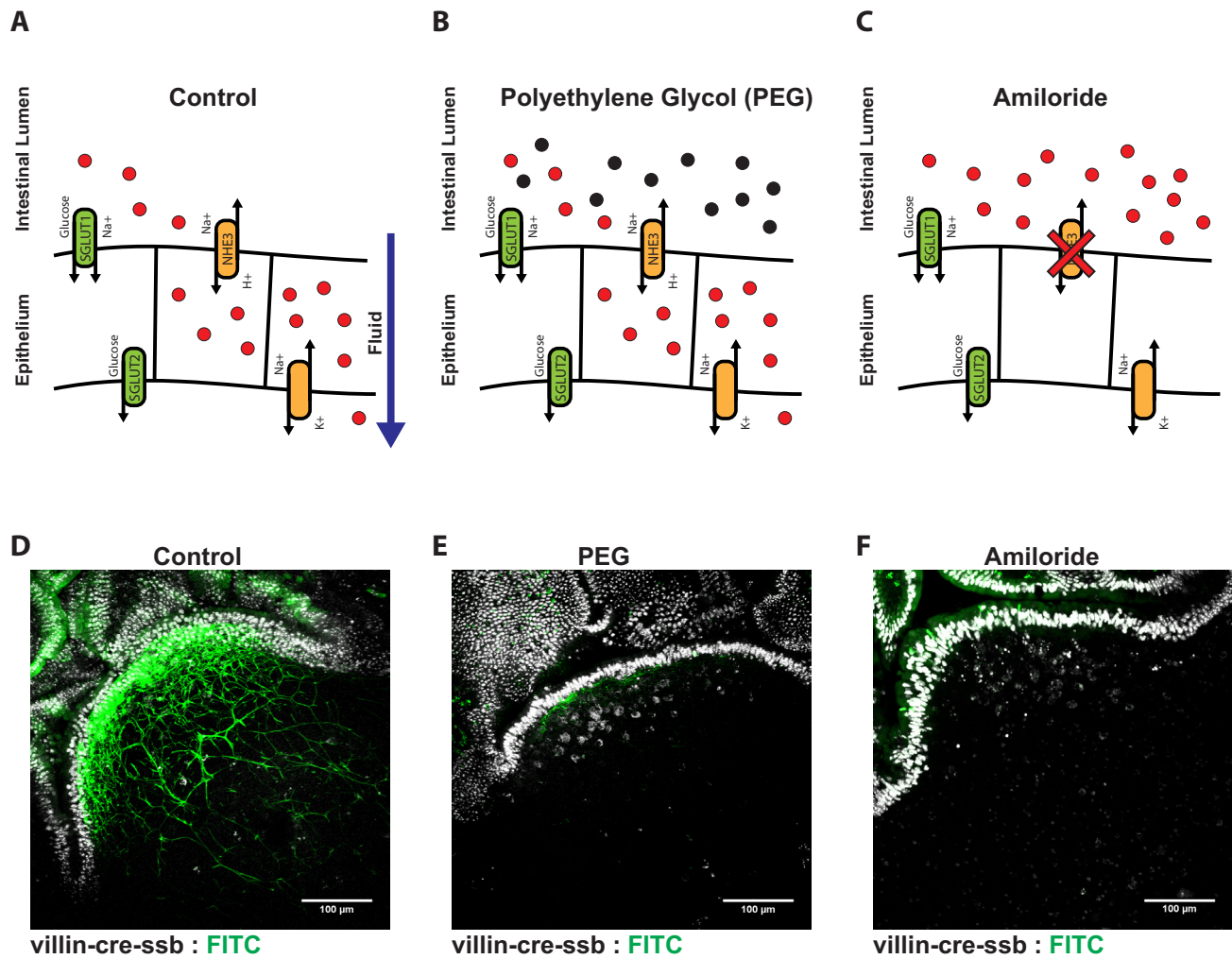


**Figure 3.2** Impaired fluid absorption limits fluid flow into Peyer's patch conduits. (a) Schematic representation of the establishment of osmotic gradients by Na<sup>+</sup>/H<sup>+</sup> transporters in absorptive epithelium. Establishment of this gradient is the primary means of directing fluid uptake. (b) Oral delivery of high molecular weight polyethylene glycol (3350 kDa) disrupts the establishment of effective osmotic gradients. PEG is a non-absorbable, non-metabolized, osmotically active agent. (c) Amiloride hydrochloride is an inhibitor of the Na<sup>+</sup>/H<sup>+</sup> transporters NHE1, NHE2, and NHE3. (d-f) Multiphoton microscopy of Peyer's patches from a villin-cre-SSB(BFP) mouse after oral gavage with soluble FITC in saline (d), FITC in PEG (e), or FITC in saline+amiloride.

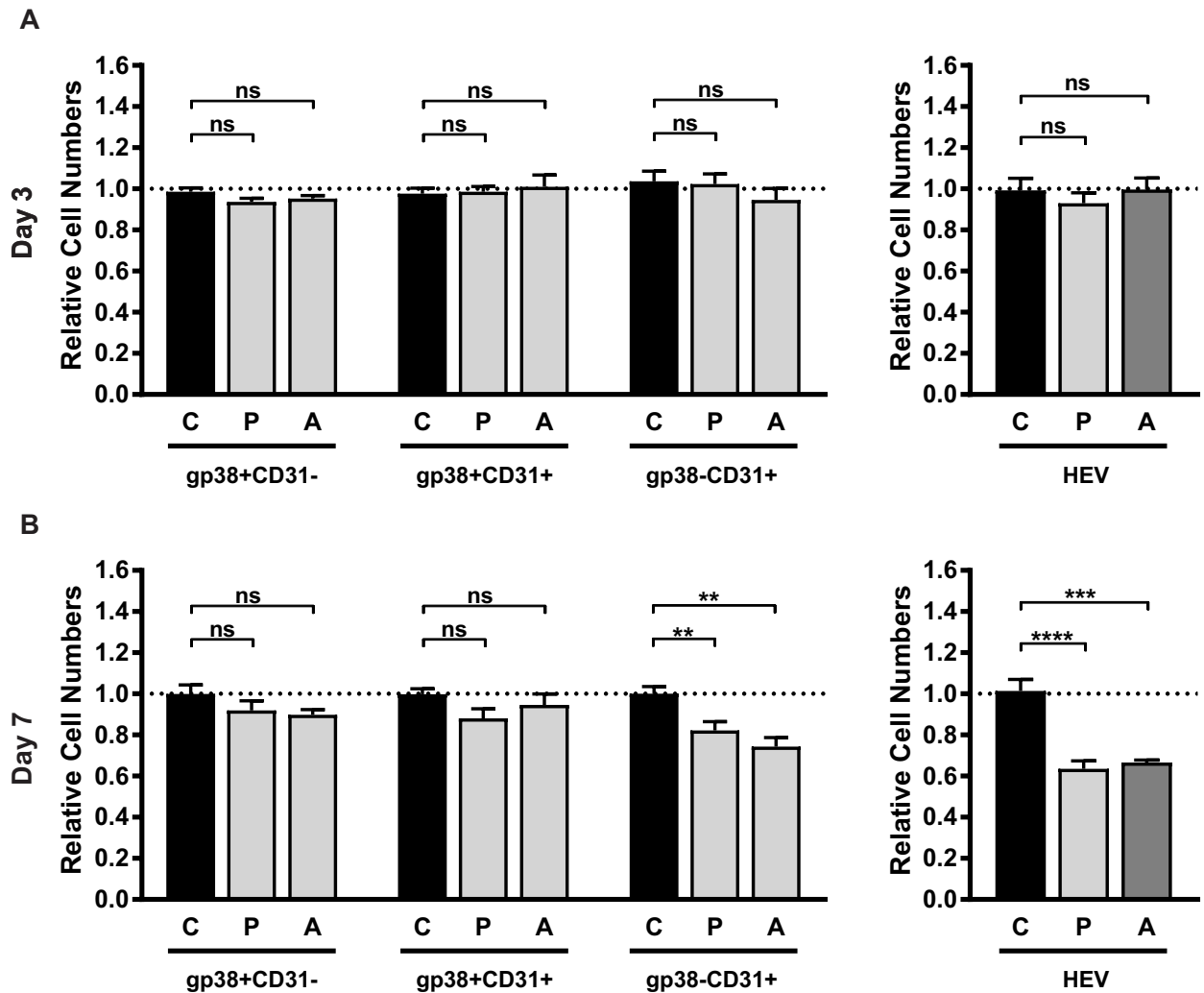


**Figure 3.3** Peyer's patch stroma numbers following treatments with PEG or amiloride. (a,b) Flow cytometric analysis PP stromal cell populations (CD45-TER119-) following treatment with PEG or amiloride. Mice were treated for a period of 3 days (a) or one week (b). Data are graphed as relative cell counts. The following populations are represented: gp38+CD31- (FRC, MRC, FDC), gp38+CD31+ (LEC), and gp38-CD31+ (BEC). Frequency of MAdCAM1+ HEV ECs among BECs. Data represents at least 2 independent experiments with at least 4 mice per treatment group each.

for the maintenance or organization of the FRC network itself (Figure 3.3a). However, treatment with PEG for periods beyond one week resulted in a specific decrease in blood endothelial cell (BEC) numbers, including MAdCAM-expressing endothelial cells of the PP high endothelial venule (Figure 3.3b).

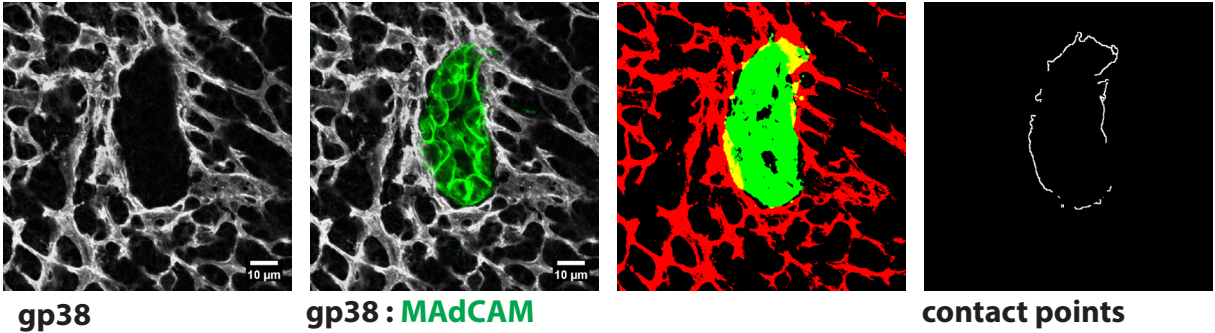
Changes to HEV EC cell numbers is preceded by a striking alteration in HEV structure. An intact PP HEV is structurally comprised of MAdCAM-expressing endothelium closely encircled by a ring of perivascular FRCs (Figure 3.4 a,f). Confocal imaging of the PP HEV following a 3-day treatment period with PEG revealed an apparent disruption in the normally continuous perivascular FRC ring and a quantifiable decrease in contact points between perivascular FRCs and HEV ECs (Figure 3.4b,c). These structural alterations are also apparent by high magnification transmission electron microscopy (TEM) of the PP HEV, which show distinct points of separation between the HEV ECs and surrounding basement membrane (Figure 3.4d). Interestingly, TEM imaging of the PP HEV after three days of PEG treatment additionally revealed an apparent dearth of leukocyte interactions with the vascular endothelium, as few cells were found either attached to the HEV lumen or within HEV pockets. This latter observation suggests a potential functional deficiency in HEV-mediated leukocyte immigration corresponding to perturbations in HEV structural integrity.

In total, these data suggest that the absence of directional conduit flow to the HEV results in disrupted alignment of perivascular FRCs and/or a loss of physical interaction between perivascular FRCs and HEV ECs (Figure 3.4 e,f). Aberrant HEV structure appears to additionally correspond to a loss of lymphocyte arrest in the vascular lumen. Loss of these interactions may contribute to decreasing BEC cell numbers following long-term blockade of fluid absorption.

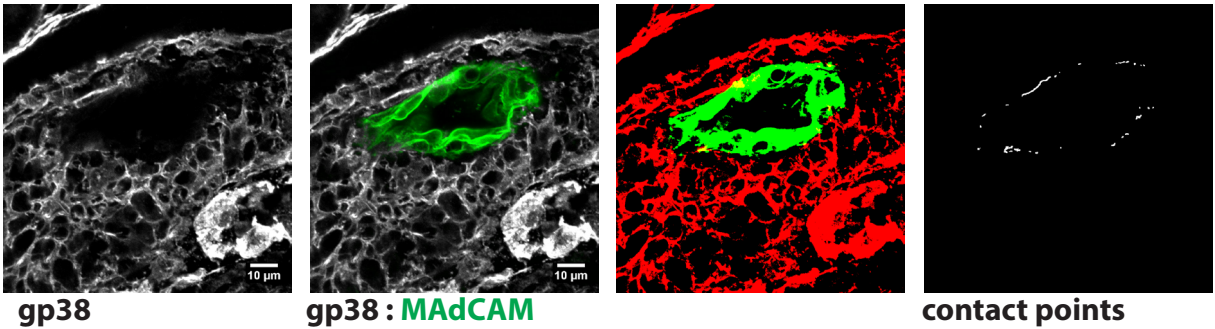
**Figure 3.4** *Disruption of HEV structure following blockade of fluid absorption.* (a-c) Confocal microscopy of an HEV from the PP of an untreated mouse (a) or a mouse treated for 3 days with PEG in drinking water (b). left two panels: FRCs and HEVs were marked by staining with anti-gp38 and anti-MAdCAM1 respectively. right two panels: overlay of image threshold to highlight FRC:HEV overlap (yellow). Perimeter contact points depicted in the far-right panel. (c) Quantification of FRC:HEV contact points from confocal imaging. (d) Transmission electron micrograph of PP HEVs. left panel: untreated. right panel: treated for 3 days with PEG in drinking water. (e,f) Schematic representation of HEV structure in PPs from untreated (e) and PEG-treated (f) mice.

Figure 3.4 (Continued)

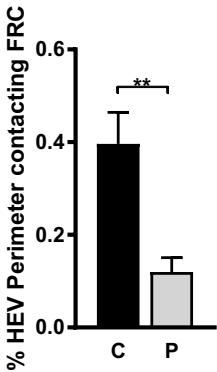
**A Untreated**



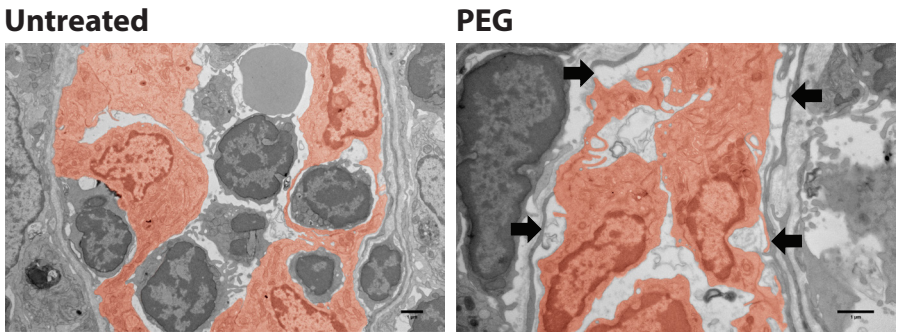
**B PEG**



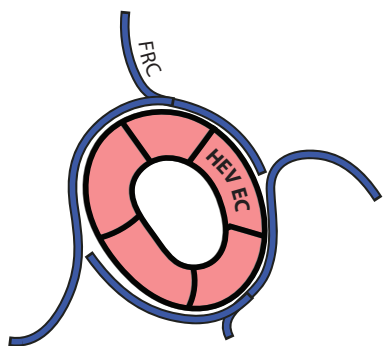
**C**



**D**

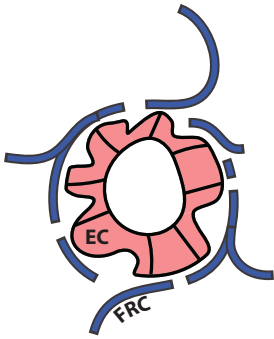


**E**



Untreated - Normal HEV

**F**



PEG - Disrupted HEV

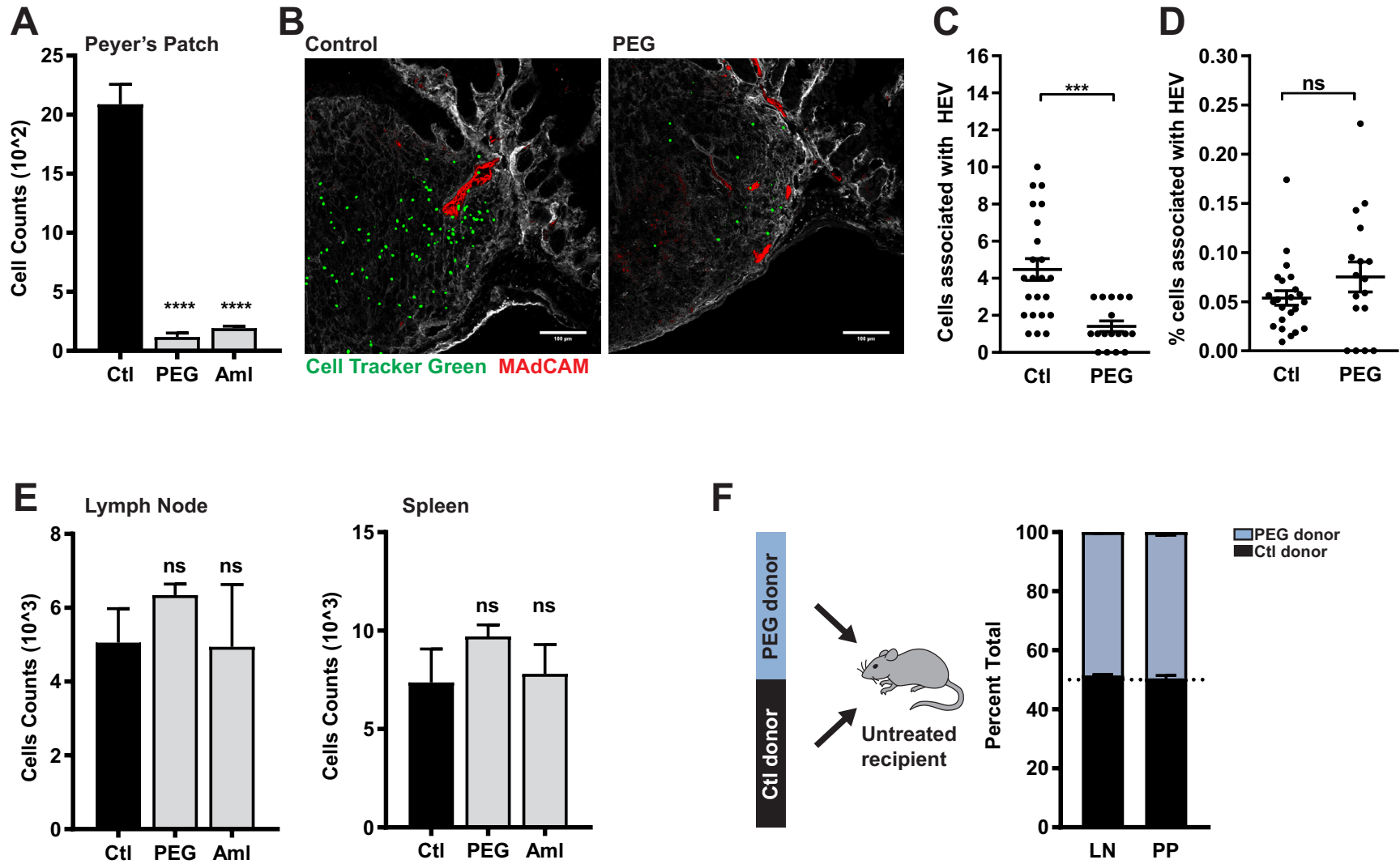
## **Prolonged blockade of fluid absorption disrupts PP lymphocyte recruitment and immune homeostasis**

The HEV is the main port of entry for naive recirculating lymphocytes to lymphoid organs, including both lymph nodes and PP. Concurrent with the observed PEG-induced changes to HEV structure was a significant decrease in naïve lymphocyte recruitment to the PP. Adoptive transfer of fluorescently labeled splenocytes to either PEG or amiloride-treated recipient mice showed significantly fewer T and B lymphocytes accumulating in the PP one hour after transfer relative to untreated control recipients (Figure 3.5a). Confocal imaging of these PPs reveals significantly fewer total lymphocytes directly associated with the HEV in PEG-treated recipients (Figure 3.5b,c). However, while the total numbers of these cells is decreased, the frequency of immigrating cells that remain associated with the HEV is unchanged (Figure 3.5d). This suggests that while fewer circulating lymphocytes successfully adhere to the HEV endothelium, there is likely no defect in migration from the HEV into the PP parenchyma.

In contrast to the PP, short term recruitment of transferred lymphocytes to skin draining lymph nodes and spleen remained normal, suggesting a specific deficiency in lymphocyte trafficking to the PP (Figure 3.5e). Additionally, equal ratio co-transfer of lymphocytes from untreated and PEG-treated donors to untreated recipients demonstrates no lymphocyte-intrinsic deficiency in homing to the PP (Figure 3.5f). Rather, the defect in short-term lymphocyte homing originates from the PP tissue environment itself.

**Figure 3.5** *Impaired lymphocyte immigration to the PP following treatment with PEG.* (a) Flow cytometric analysis of adoptively transferred splenocytes accumulating in the PP one hour after transfer into control (ctl), PEG-treated, or amiloride (Aml)-treated recipients. Donor splenocytes were labeled with CellTracker Green for identification prior to transfer (n=6 mice) (b-d) Confocal microscopy of PPs from control or PEG-treated recipient mice one hour after adoptive transfer of CellTracker Green-labeled splenocytes. (b) Representative images, co-stained with anti-gp38 (grey) and anti-MAdCAM1 (red). (c,d) Quantification of imaging (n=23 (ctl) or 17 (PEG) PPs, from 5 mice per group). (c) The total number of adoptively transferred cells co-localizing with MAdCAM1+ HEVs (d) The percentage of adoptively transferred cells co-localizing with MAdCAM1+ HEVs. (e) Flow cytometric analysis of adoptively transferred splenocytes accumulating in the LN and spleen of control, PEG-treated, or amiloride-treated recipients. (f) Flow cytometric analysis of adoptively transferred splenocytes accumulating in the PP and LN of an untreated recipient mouse. Adoptively transferred splenocytes were obtained from control and PEG-treated donor and transferred in a 1:1 ratio. (n=5 mice).

Figure 3.5 (Continued)



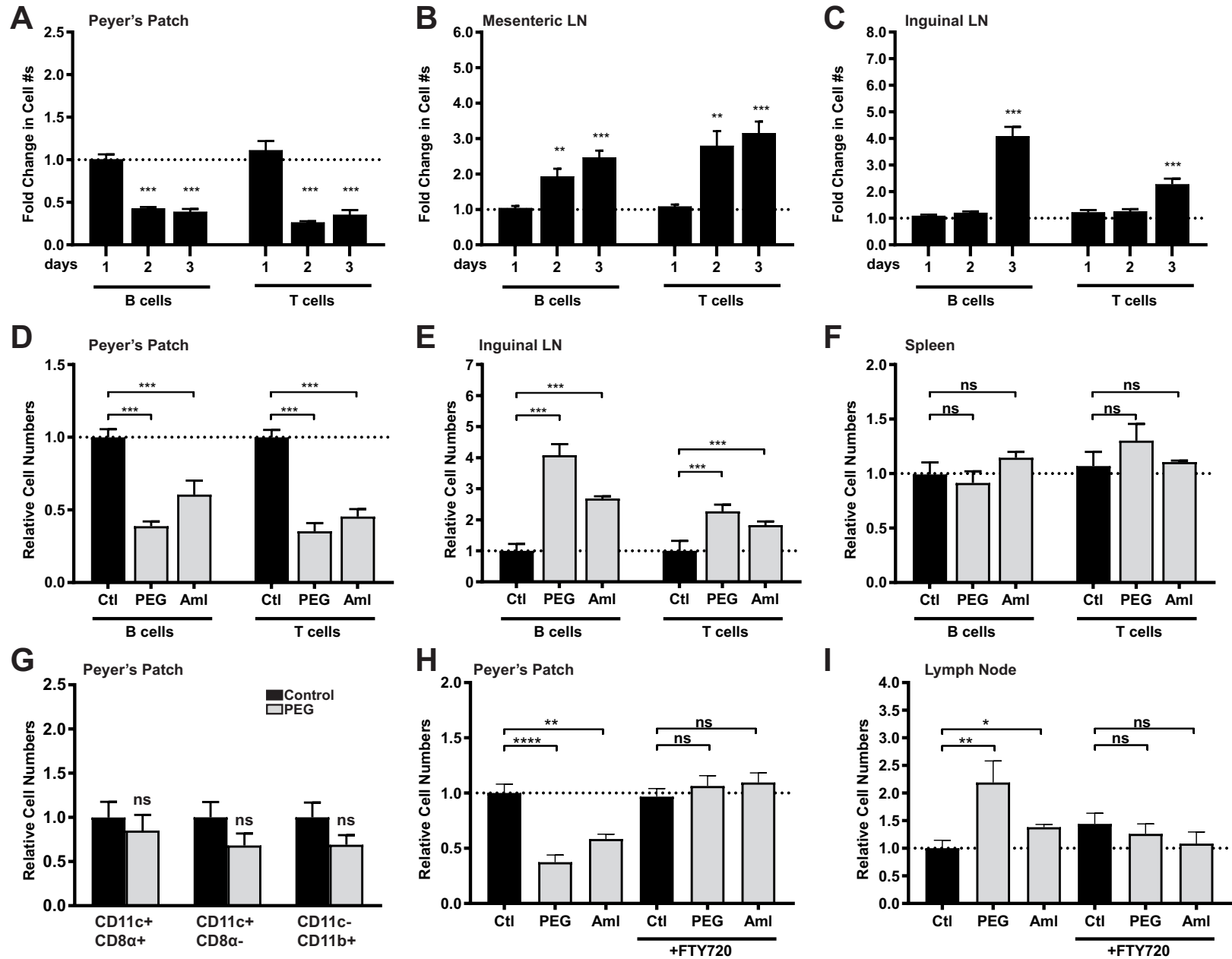


Inefficient lymphocyte homing to the PP eventually culminates in a roughly 2-3 fold decrease in total lymphocyte cellularity within 2 days of disrupted intestinal fluid absorption (Figure 3.6a). Interestingly, while we have observed no changes to recruitment of adoptively transferred lymphocytes to lymph nodes, total B and T cell numbers of the mesenteric LNs increases within 2 days of PEG treatment, and skin-draining LNs exhibit increased cellularity by day 3 (Figure 3.6b,c). These changes to PP and LN cellularity are observed in response to both PEG and amiloride-induced disruption to fluid absorption (Figure 3.6d,e). Both B and T lymphocytes are affected equally, and spatial compartmentalization of lymphocytes within the PP appears normal following treatment (data not shown). In contrast to the PP and LN, splenic B and T cell numbers appear largely unchanged following either treatment (Figure 3.6f). Additionally, alteration to PP cellularity appears to be limited to lymphocyte populations, as the numbers of resident myeloid cell subsets appear normal (Figure 3.6g).

Pre-treatment of mice with the S1PR1 agonist FTY720, which limits lymphocyte recirculation and promotes retention in lymphoid tissues, effectively reversed PEG or amiloride-induced alterations to both PP and LN cellularity (Figure 3.6h,i). These data further suggest that regular trafficking of recirculating lymphocyte populations through intestinal PPs are affected by prolonged disruption of fluid absorption.

**Figure 3.6** *Blockade of fluid absorption causes alteration to PP and LN cellularity.* (a-c) Flow cytometric analysis following a 1, 2, or 3-day treatment period with PEG. Lymphocyte cellularity is analyzed from (a) PP, (b) mesenteric LN, and (c) inguinal LNs. B cells are identified as CD45+B220+. T cells are identified as CD45+CD3+. Data are represented as fold change relative to untreated control mice. (n=10 mice per group). (d-f) Flow cytometric analysis following a 3-day treatment period with PEG or amiloride. Cells were analyzed from (d) PP, (e) iLN, and (f) spleen. Data is represented as relative absolute cell counts. (n=5 mice per treatment group). (g) Flow cytometric analysis of myeloid cell populations from the PP of control or PEG-treated mice (n=3 mice per treatment group). (h,i) Flow cytometric analysis of mice following a 3-day treatment period with PEG or amiloride. Mice were additionally treated with either FTY720 or PBS on day 0 and day 2. Lymphocyte cellularity was analyzed from (h) PP and (i) iLN. (n=5 mice per treatment group).

Figure 3.6 (Continued)



**Altered lymphocyte cellularity is directly related to the process of fluid absorption.**

We have demonstrated that blockade of fluid absorption by PEG and amiloride impacts conduit-mediated directional fluid flow to the HEV and that HEV structure is perturbed. However, we acknowledge that these treatments may adversely impact lymphoid tissue homeostasis through other means, including intestinal epithelial dysbiosis or inflammation, alterations to the intestinal microbiota, or general dehydration.

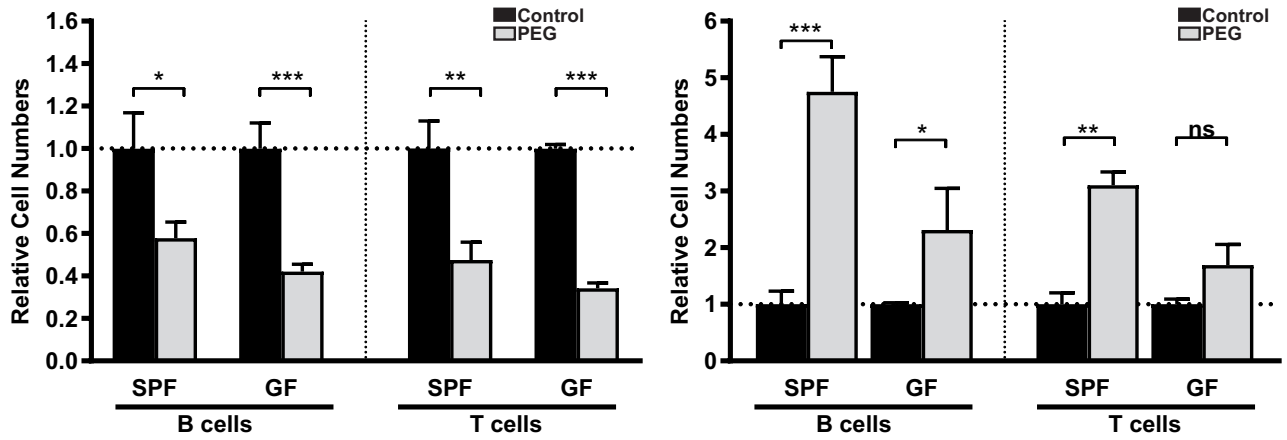
Importantly, neither treatment with PEG or amiloride was associated with any observable intestinal inflammation or epithelial disruption (data not shown). Additionally, similar effects of PEG treatment on PP and LN cellularity were found to occur in germ free mice, suggesting that altered lymphocyte migration is not secondary to any PEG-induced alterations to the microbiota (Figure 3.7a).

We find that altered migration of lymphocytes to the PP and LN following a 3-day period of treatment with PEG is rapidly reversible upon restoring normal intestinal fluid absorption. Within 12 hours of returning PEG-treated mice to normal drinking water, we find that PP and LN cellularity recovers to normal levels (Figure 3.7b). By contrast, supplementing PEG or amiloride-treated mice with fluids by subcutaneous injection had no apparent effect on either decreases in PP cellularity or increases in LN cellularity (Figure 3.7c). Together, these data suggest that altered PP and LN cellularity following blockade of fluid absorption is not a secondary effect of dehydration. Rather, the process of fluid uptake via the oral route appears to be necessary for the maintenance of normal lymphocyte migration and homeostasis.

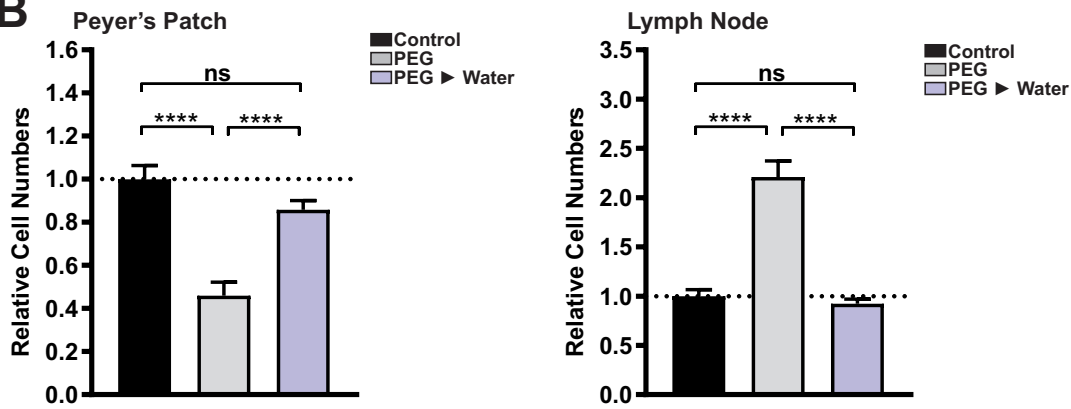
**Figure 3.7** *Altered LN and PP cellularity is not a consequence of dehydration or altered microbiota.* (a) Flow cytometric analysis of B and T lymphocyte numbers from conventional specific pathogen free (SPF) or germ free (GF) mice, either untreated or treated with PEG for 3 days. (n=5 mice per treatment group). (b) Flow cytometric analysis of total lymphocyte counts from PP and LN of mice after the following treatments: control untreated, PEG for 3 days, PEG for 3 days then restored to normal drinking water for 12 hours (PEG > Water). (n≥10 mice per treatment group). (c) Flow cytometric analysis of total lymphocyte counts from PP and LN after the following treatments: control untreated, PEG for 3 days, amiloride for 3 days, PEG or amiloride for 3 days with twice daily subcutaneous injection of saline. (n≥8 mice per treatment group).

Figure 3.7 (Continued)

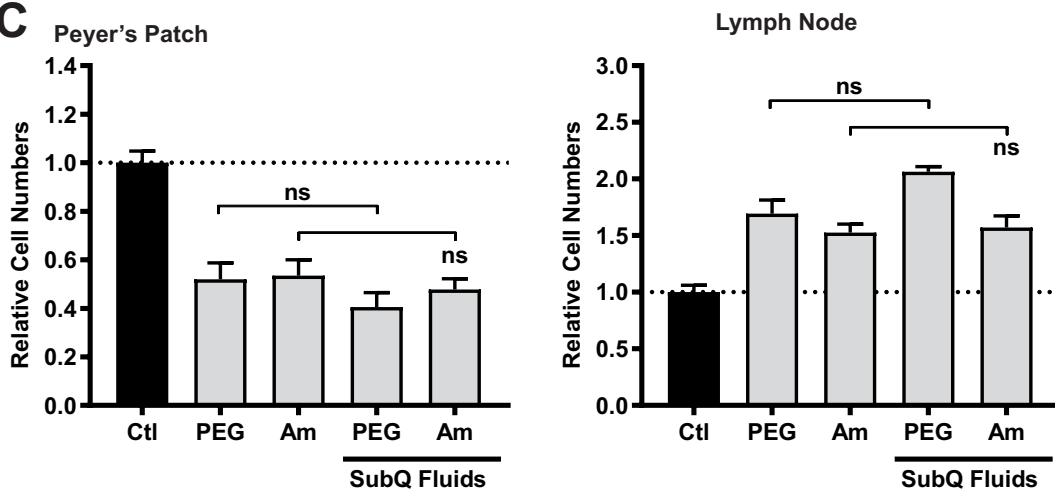
**A**



**B**



**C**



### **Impaired recruitment to the PP results from a loss of lymphocyte rolling on the HEV.**

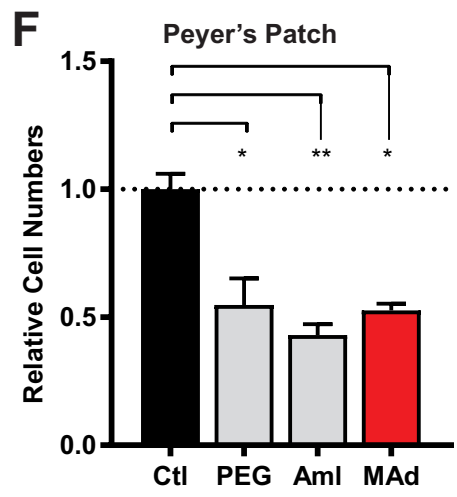
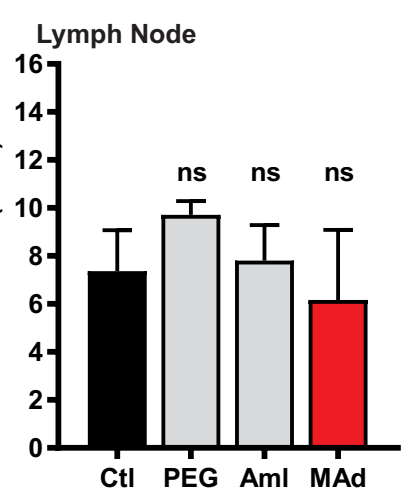
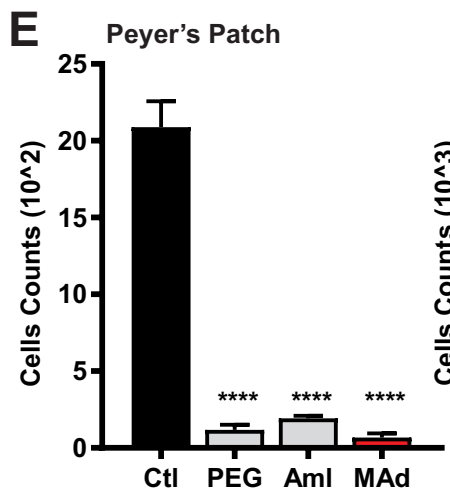
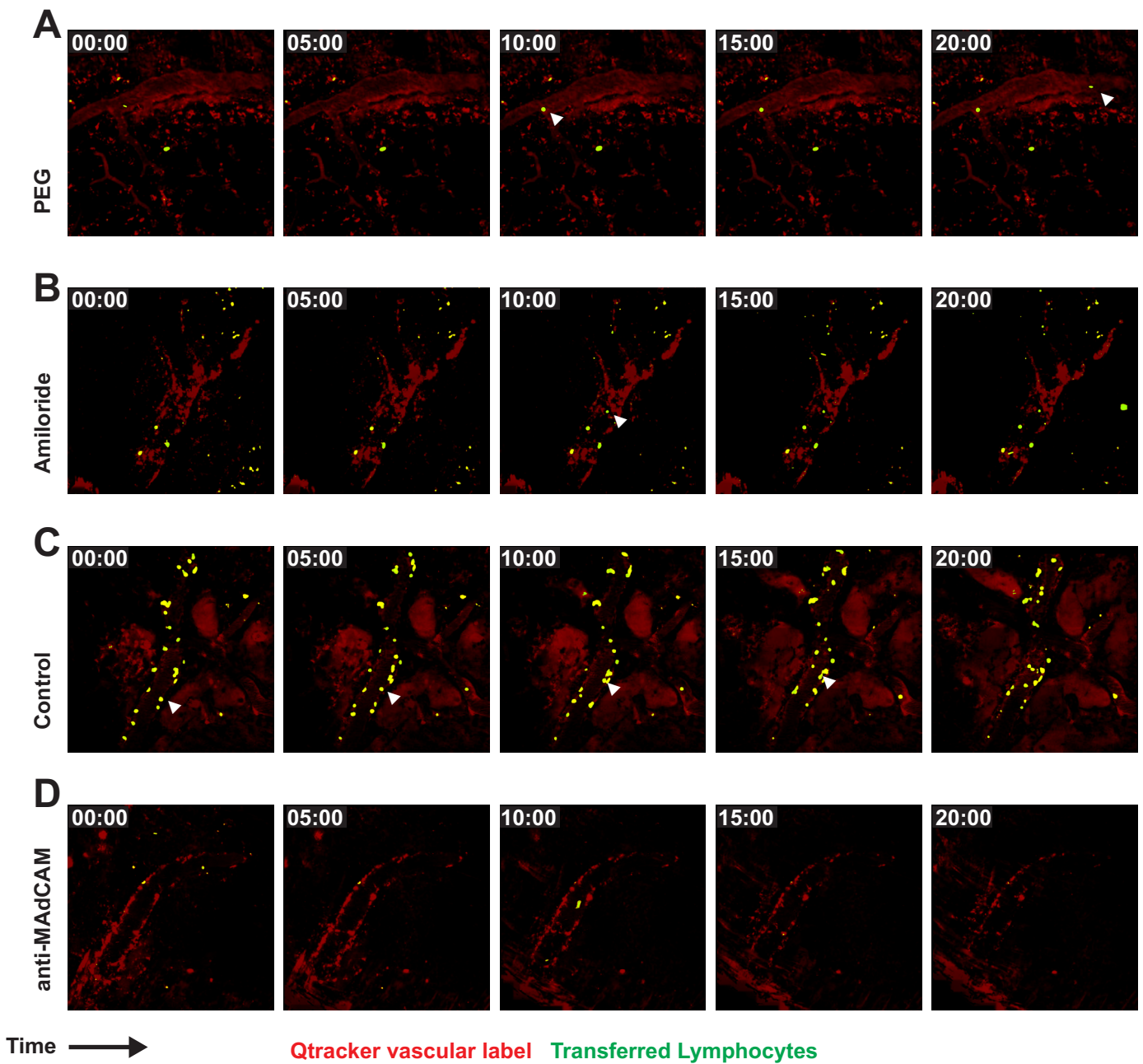
Lymphocyte ingress across the HEV to lymphoid tissues is a multistep process which involves first selectin-mediated capture and rolling along the vascular endothelium, followed by integrin- and chemokine-mediated firm arrest and transmigration through endothelial cell junctions. The specific molecular mediators of each step are well established. Intravital multiphoton imaging of the PP following adoptive transfer of labeled lymphocytes reveals a near complete absence of lymphocyte rolling events on the HEV lumen of mice treated with PEG or amiloride (Figure 3.8a,b). By contrast, several lymphocyte rolling and adhesion events are identifiable within the HEVs of control mice (Figure 3.8c).

Lymphocyte rolling in intestinal PPs is largely mediated through interaction between the mucosal addressin cell adhesion molecule 1 (MAdCAM1) expressed by HEV ECs, and either L-selectin or the integrin  $\alpha 4\beta 7$  on recirculating lymphocytes<sup>134</sup>. Similar to treatments with PEG or amiloride, intravenous administration of anti-MAdCAM1 antibody eliminates lymphocyte rolling events on the HEV, as confirmed by intravital imaging (Figure 3.8d). Moreover, anti-MAdCAM1 treatment limits short-term B and T lymphocyte accumulation in the PPs but not LNs (Figure 3.8e), and anti-MAdCAM1 blockage over the course of 3 days results in an overall decrease in PP lymphocyte cellularity that is comparable to that seen following PEG and amiloride treatment (Figure 3.8f).

**Figure 3.8** *Blockade of fluid absorption impacts lymphocytes rolling on HEV.* (a-d) Multiphoton intravital imaging of intestinal PPs following adoptive transfer of labeled splenocytes into (a) PEG-treated, (b) amiloride-treated, (c) untreated control, or (d) anti-MAdCAM treated recipients. Donor splenocytes are labeled in CellTracker Green (green) and blood vasculature is illuminated by Qtracker vascular label (red). White arrows identify newly captured/rolling lymphocytes. Representative images are shown at 5 minute intervals up to 20 minutes of total imaging. (e) Flow cytometric analysis of donor lymphocyte accumulation in control, PEG-treated, amiloride-treated, or anti-MAdCAM-treated recipient mice 1 hour after transfer. (f) Flow cytometric analysis of relative lymphocyte counts in the PP of control, PEG-treated, amiloride-treated, or anti-MAdCAM-treated mice on day 3 of treatment.



Figure 3.8 (Continued)



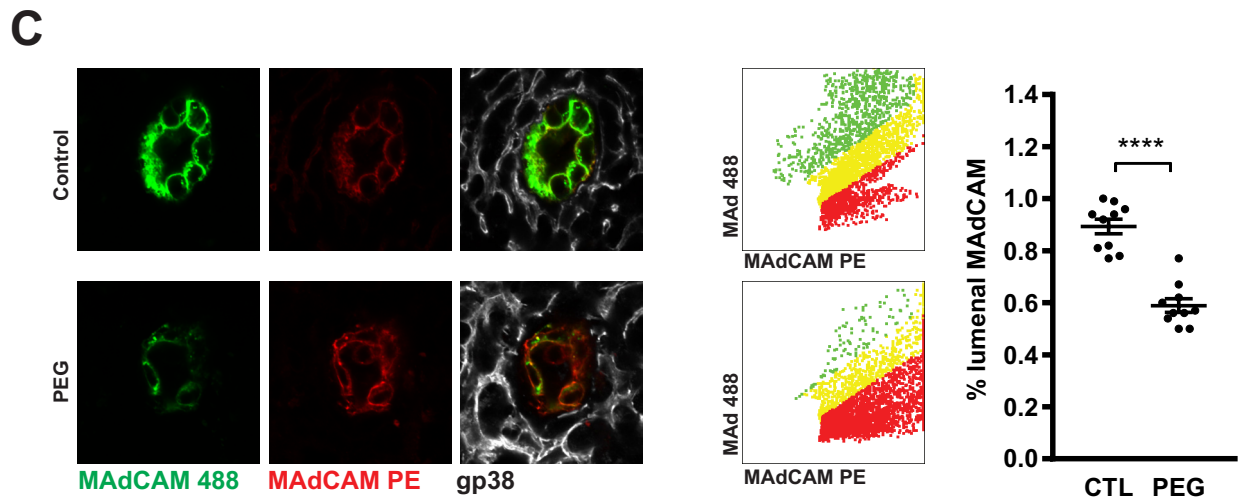
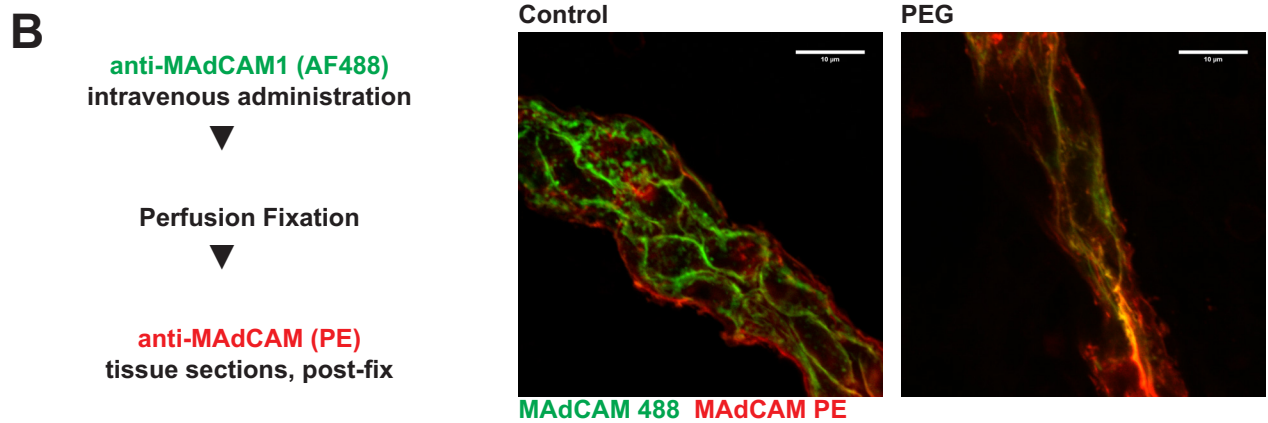
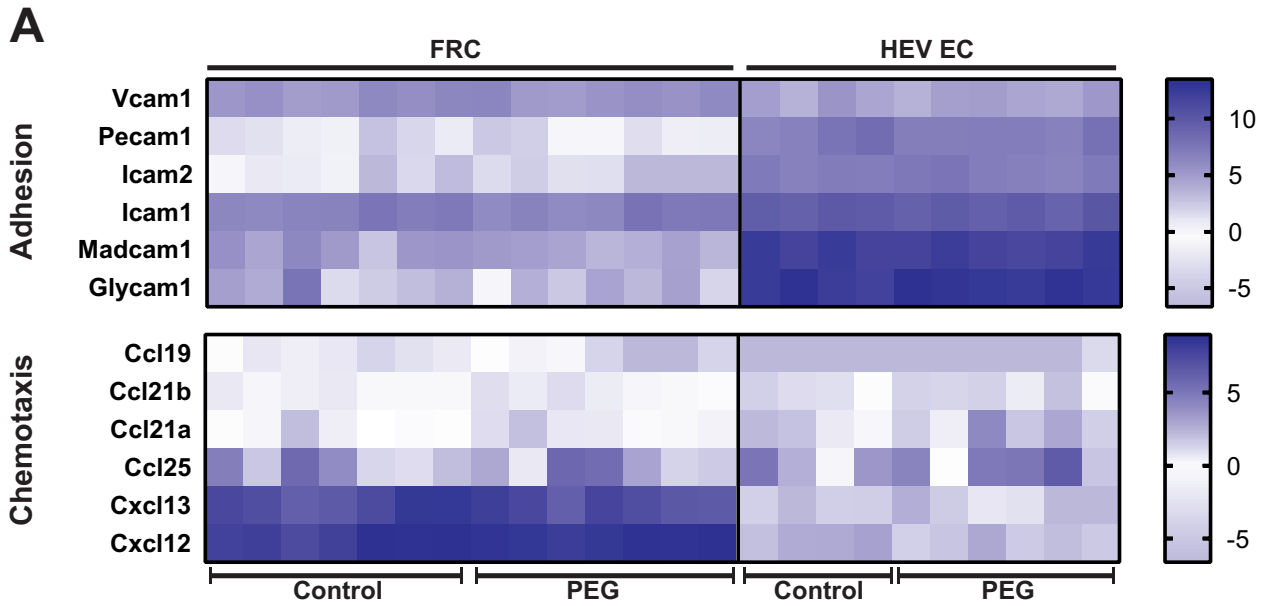
### **Blockade of fluid absorption influences MAdCAM1 localization, but not expression**

Despite noticeable changes to HEV structure following a three-day treatment with PEG, RNAseq analysis of FACS sorted HEV ECs and FRCs at this time point revealed few significant alterations in transcriptional profile. Notably, HEV EC expression of key adhesion molecules involved in lymphocyte capture and recruitment, including MAdCAM1, was not significantly impacted by PEG treatment (Figure 3.9a). Likewise, PP FRCs, which direct lymphocyte migration across the HEV, showed no significant alteration in transcript levels for any known chemotactic signal involved in lymphocyte homing to the PP, including CCL19, CCL21, CXCL12, and CXCL13.

While production of MAdCAM1 appears unaffected by altered PP conduit flow, there was a striking difference in the amount of MAdCAM1 protein exposed on the luminal surface of the HEV. Lumenally exposed MAdCAM1 was specifically visualized by a short pulse of anti-MAdCAM1 delivered intravenously to control and PEG-treated animals. Confocal imaging of PP tissue sections from these mice reveal significantly less *in vivo* labeling with anti-MAdCAM1 in PEG-treated animals relative to control (Figure 3.9b). Quantification of the percentage of lumenally-exposed MAdCAM1 was performed by comparing *in vivo* labeled anti-MAdCAM1 signal to total anti-MAdCAM1 (visualized by post-fix staining). We find that under normal conditions, nearly all MAdCAM1 is exposed on the luminal surface of the HEV. By contrast, this frequency drops to roughly 60% following PEG treatment (Figure 3.9c).

**Figure 3.9** *Blockade of fluid absorption impacts luminal display of MAdCAM on HEV surface.* (a) RNAseq was performed on FACS sorted FRCs and HEV ECs from both control and PEG-treated animals. Data represented as a heat-map of select adhesion molecules and chemokines involved in lymphocyte recruitment. (n≥4 mice per group). (b) Control and PEG-treated mice were in vivo labeled with anti-MAdCAM in alexafluor 488 by intravenous injection. Mice were perfused with fixative and tissue sections from PPs were restained with anti-MAdCAM in PE. right: representative confocal microscopy of an HEV. (c) Confocal microscopy of PP HEVs (cross-sectional orientation). left: representative images. second from right: graphical representation of pixel intensity in AF488 vs. PE. far right: cumulative data quantified as percentage of pixels positive in MAdCAM-AF488 out of total MAdCAM+ pixels (% luminal MAdCAM).

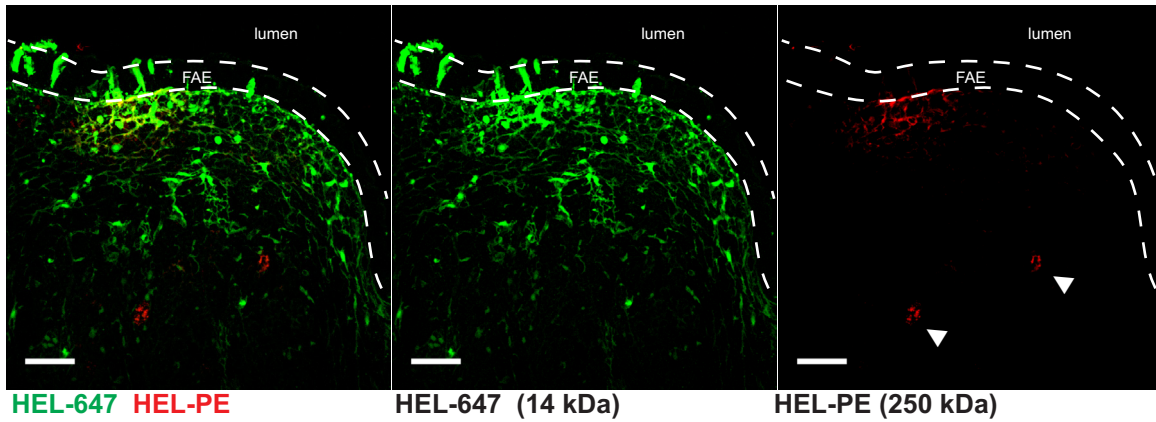
Figure 3.9 (Continued)



## **Blockade of fluid absorption impairs mucosal antibody responses**

Conduit-mediated transport in lymph nodes is limited to fluid and soluble molecules below a molecular weight cutoff of roughly 70 kDa<sup>49</sup>. We find that PP conduits are similarly restrictive. Hen egg lysozyme (HEL) labeled with alexafluor 488 (HEL-488, M.W. 14 kDa) and HEL labeled with phycoerythrin (HEL-PE, M.W. 250 kDa) were co-administered to the lumen of explanted intestinal loops. Confocal imaging of the PPs reveals that HEL-488 rapidly penetrates the PP dome and tracks along the FRC conduit network, while HEL-PE primarily remained near the epithelial surface and was carried into to PP follicle by myeloid cells (Figure 3.10a). The specific size exclusion cutoff of PP conduits was assessed by tracking the uptake and localization of several fluorescently labeled proteins and dextrans of different sizes and was determined to be roughly similar to that of LN conduits at roughly 50-70 kDa (Figure 3.10b). Thus, as with LNs, conduit-mediated antigen transport within intestinal PPs appears to be limited to small molecular weight molecules.

The importance of this conduit-mediated route of antigen transport has long been speculated, however the immunological impact of altered conduit flow on adaptive immune responses has not been previously addressed. Here we examine the effect of PEG-mediated blockade of fluid absorption into the PP conduits on mucosal antibody responses to orally delivered antigen. Mice were orally immunized with two NP-haptenated protein antigens of differing molecular weights: 14kDa NP-haptenated HEL (NP-HEL) and 150kDa NP-haptenated chicken gamma globulin (NP-CGG).

**A****B**

Molecule	Molecular Weight	Access to conduit
Dextran	10 kDa	Included
Dextran	40 kDa	Included
Dextran	500 kDa	Excluded
Hen Egg Lysozyme	14 kDa	Included
Ovalbumin	45 kDa	Included
Cholera Toxin $\beta$	57 kDa	Excluded
Phycoerythrine	250 kDa	Excluded

**Figure 3.10** *Size exclusion of PP conduit network.* (a) Confocal microscopy of a PP following intraluminal injection HEL-647 and HEL-PEG in explanted intestinal loops. Follicle associated epithelium (FAE) marked by dashed line (b) List of fluorescent tracers of various sizes and whether they are found to enter the PP conduit network following intraluminal injection ("Included") or not ("excluded").

Oral immunization during PEG treatment resulted in less potent NP-specific antibody responses relative to control animals. Anti-NP fecal IgA titers were lower in PEG-treated mice after immunization (Figure 3.11a). Interestingly, antibody responses to NP-HEL and NP-CGG were equally affected by treatment with PEG, despite the molecular weight of NP-CGG theoretically limiting its access to conduit-mediated transport even under control conditions. These data suggest that while limitations in conduit flow can impact antigen-specific humoral responses in the PP, this is not necessarily related to alterations in the mode of antigen transport. In addition to decreased anti-NP IgA titers, we find a moderate decrease in NP-specific B cell numbers in the intestinal lamina propria (Figure 3.11b,c). Together, these data suggest a decrease in the initiation and activation B cells following oral immunization.

Under normal conditions, PPs are continuously exposed to a wide range of food and microbial antigen and are characterized by a continuous ongoing germinal center (GC) reactions. We find that perturbation of fluid absorption over the course of 2 weeks results in a decrease in baseline GC cell numbers (Figure 3.11d,e). While GC activity was significantly decreased, the PP FDC network remained intact (Figure 3.11e). This general decrease in GC activity corresponds with an overall decrease in total fecal IgA titers (Figure 3.11f). PEG-treated mice also exhibit a decrease in intestinal lamina propria plasma cells (Figure 3.11g), but not total B220+ B cells (Figure 3.11h).

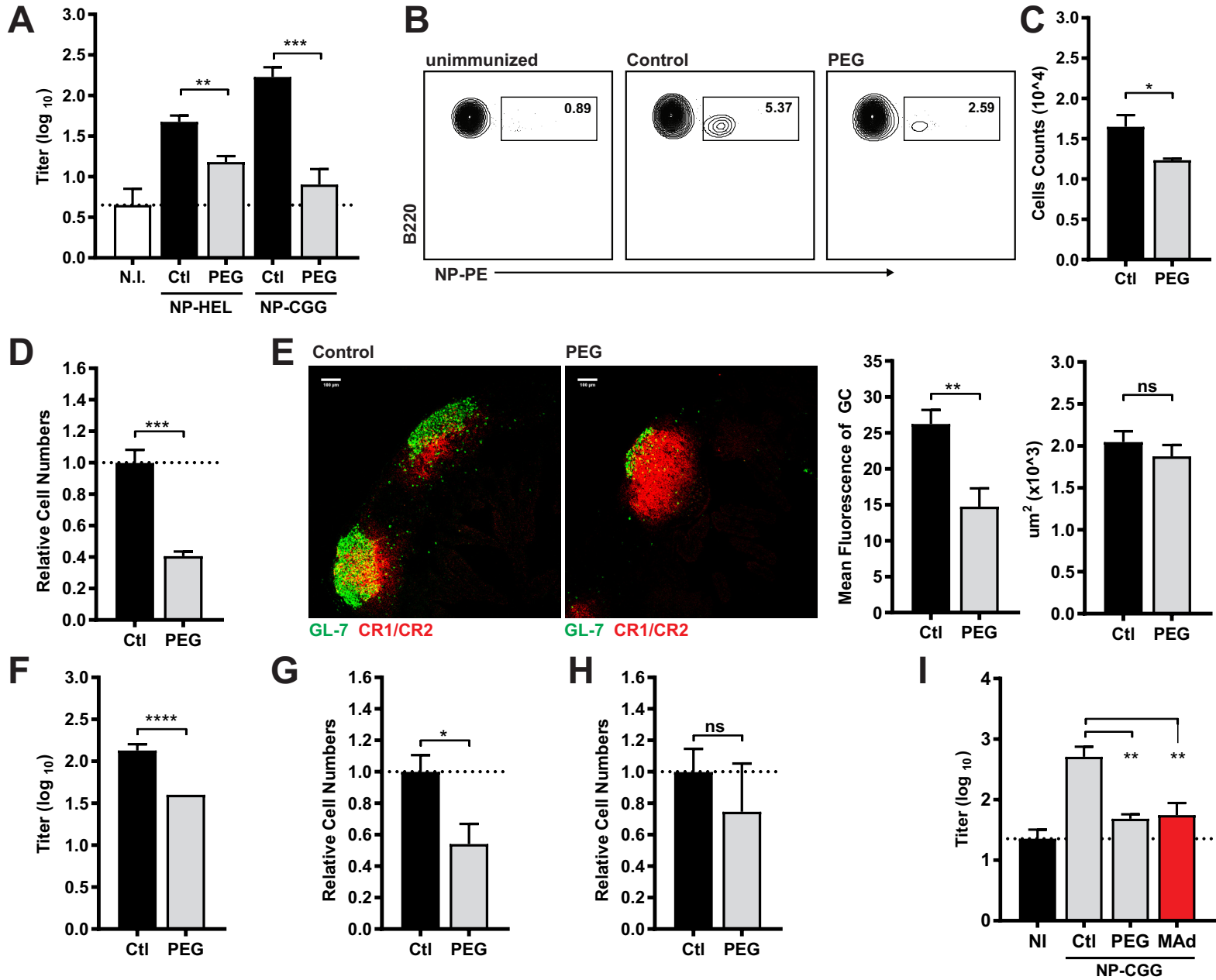
As previously established, anti-MAdCAM treatment directly impacts lymphocyte recruitment to the PP in a manner similar to PEG or amiloride treatment, but does so without any additional effects that might be associated with perturbed fluid absorption. To test whether PEG-induced

decreases in antibody responses may be a direct consequence of altered naïve lymphocyte trafficking through PP tissues, we tested antigen-specific antibody responses in mice treated with anti-MAdCAM1 blockade during oral immunization. Under these conditions, anti-NP IgA titers were also reduced relative to control animals (Figure 3.11i). Moreover, this reduction in antibody response was similar to that seen in mice immunized during PEG treatment.



**Figure 3.11:** *Blockade of fluid absorption impacts mucosal humoral responses.* (a-c) Experiments comparing the following treatment groups: normal drinking water and unimmunized (N.I.), normal drinking water and immunized (control, Ctl), PEG-treated and immunized (PEG). Antigens used for immunization were either NP-HEL (14kDa) or NP-CGG (150kDa). (n ≥ 4 mice per treatment group). (a) anti-NP fecal IgA titers quantified by ELISA. (b) Representative flow cytometric analysis of the frequency of NP-specific lamina propria B cells following oral immunization against NP-CGG (n=5 mice per treatment group). (c) Absolute number of NP-specific lamina propria B cells (n=5 mice per treatment group) following oral immunization against NP-CGG. (d-h) Experiments comparing control mice and mice treated with PEG for a duration of 2 weeks. (d) Relative number of GL7+CD38- germinal center cells (n=5 mice per group). (e) Confocal microscopy of PPs stained to identify the FDC network (anti-CR1/CR2) and GC B cells (anti-GL7). (right 2 panels) Quantification of GL7 mean fluorescence intensity; Area of the FDC network. (n=8 mice per treatment group) (f) Total fecal IgA quantified by ELISA. (n=5 mice per group) (g) Relative number of B220-IgA+ lamina propria plasma cells. (h) Relative number of B220+ lamina propria B cells (i) anti-NP fecal IgA titers following oral immunization against NP-CGG quantified by ELISA. Treatment groups: normal drinking water and unimmunized (N.I.), normal drinking water and immunized (control, Ctl), PEG-treated and immunized (PEG), anti-MAdCAM-treated and immunized.

Figure 3.11 (Continued)



### 3.3 Discussion

The fibroblastic reticular network simultaneously provides a platform for cellular migration and an isolated inner compartment for the rapid movement of lymph and lymph-borne mediators. The specific importance of FRCs in mediating homeostatic lymphocyte movement and immune interactions is broadly accepted, though perhaps incompletely understood. By contrast, the impact of conduit-mediated lymph flow is largely speculative. Attempts to establish direct experimental evidence that conduits support either homeostatic maintenance of lymphoid tissues or the initiation of adaptive immune responses have been stymied by an inability to specifically and physiologically modulate lymph flow.

To date, the only means of depriving a draining lymph node of conduit flow relies on the surgical ligation of afferent lymph vessels – a process which not only deprives LNs of lymph flow and lymph-borne soluble mediators, but of migrating dendritic cells as well. Thus the specific contributions of disrupted conduit flow cannot be definitively established by this experimental approach. However surgical ablation of afferent lymph vessels have nevertheless yielded some preliminary insights to the homeostatic state of a lymph-deprived LN; the endothelium of LN HEVs lose their characteristic cuboidal appearance and down-regulate adhesion molecules involved in the capture and recruitment of circulating lymphocytes, and total LN cellularity is reduced. Similar effects on HEV morphology and LN cellularity have been shown to result from systemic blockade of LT $\beta$ r signaling, as well as through specific ablation of lymphotoxin-expressing dendritic cells <sup>31-33</sup>. These latter findings might suggest that one possible explanation for the loss of normal HEV morphology following lymphatic vessel ligation may be

the loss of lymphotoxin signaling derived from migrating dendritic cells, rather than impaired conduit flow.

In contrast to draining lymph nodes, we have found that the flow of fluid into PP conduits can, at least in part, be disrupted by means of blocking fluid uptake across the epithelial border. Under these conditions, we find that HEV structure is disrupted and lymphocyte recruitment and cellularity decrease substantially, despite no apparent change to the resident myeloid population. PP conduits physically connect the site of fluid uptake at the intestinal epithelium to the abluminal wall of the HEV, and thus we postulate that these observed phenomenon result specifically from a loss of conduit-mediated directional fluid flow. However, the precise molecular mechanism directing these alterations to HEV structure and function remain unclear.

Previous reports have demonstrated that conduits can facilitate the rapid transport of tissue-derived chemoattractive factors to the HEV, thereby modulating lymphocyte recruitment<sup>48-50</sup>. In this way, an inflamed tissue may exert "remote control" over the draining lymph node, priming it for an impending immune response. For a PP which does not drain tissue, the intestinal lumen is one potential source of "upstream" signaling mediators, and thus we considered the possibility that alterations to the microbiome or the uptake and transport of microbial-derived signals (perhaps through conduits) might account for the observed alterations to HEV function in the PP. However, we find that PPs from germ free mice exhibited the same response to blockade of fluid absorption, suggesting a mechanism independent of microbial signals.

An alternative potential explanation for these observed effects is the loss of mechanical cues derived from directional fluid flow through the PP FRC conduits. Applying interstitial fluid flow to cultured FRCs *in vitro* has been shown to influence FRC morphology, organization, and expression of *CCL21*, thus showing FRCs to be responsive to mechanical force<sup>34</sup>. It is possible that directional fluid flow is necessary for the proper alignment or organization of the FRC network, particularly at the terminus of PP conduits along the HEV. By disrupting the flow of absorbed luminal fluids into the PP conduit network, this organizational cue may be lost, consequently impacting structural integrity or interactions at the FRC-HEV junction. While we have not specifically observed any transcriptional changes to *CCL21* in PP FRCs following blockade of fluid absorption, it should be noted that unlike LN FRCs, baseline expression of T cell chemoattractants *CCL19* and *CCL21* in the PP are already very low.

In endothelial cells, signaling through a mechanosensitive ion channel Piezo1 is triggered in response to shear force imposed by vascular flow – a process that has been found to be critical for proper alignment of endothelial cells and vascular integrity<sup>135,136</sup>. Preliminary findings from our lab suggest that *Piezo1* transcript is specifically decreased in PP FRCs (but not HEV ECs) of mice treated with PEG (data not shown). The possibility that Piezo1 may function on FRCs or HEV ECs as a mechanosensor of lymph flow through conduits is an attractive possibility that warrants further investigation.

Cumulatively, these findings suggest that conduits may be functionally important for the homeostatic maintenance of lymphoid tissues. However, we have additionally demonstrated that blockade of fluid absorption and directional conduit flow negatively impacts the amplitude

of active antigen-specific mucosal IgA responses. When fluid absorption is disrupted by treatment with PEG, we observed a general decrease in PP GC activity following prolonged PEG-induced blockade of fluid absorption, as well as decreases in antigen specific IgA responses in mice orally immunized against NP-haptinated protein.

It has also been proposed that conduits may contribute to immune responses by providing an alternative route for the transport of antigen. Whether conduit-mediated antigen delivery has any meaningful impact on the immune response kinetics or immunological outcome has yet to be addressed. The exclusivity of conduit transport to molecules below a specific MW cutoff makes this an intriguing question. However, we have found no evidence that the size of antigen or its transport through PP conduits impacts the resulting immunological response, as blockade of fluid absorption similarly impacts IgA responses to both small and large antigen.

An alternative explanation for decreases in IgA responses following blockade of fluid absorption is that impaired lymphocyte recruitment to the PP restricts the pool of naive lymphocytes locally available to respond to antigen. Recent studies quantifying the primary immune B cell and T cell precursor populations have demonstrated a striking correlation between the size of an antigen-reactive precursor population and the amplitude of primary immune responses to cognate antigen upon immunization - the larger the naive precursor population, the more robust the primary adaptive immune response<sup>1,3,5,9</sup>. By extension, one might infer that the total number of antigen-reactive naive B cells available in the PP at the time of immunization may directly influence the amplitude of resultant immune responses. In line with this concept, we find that the effects of impaired fluid absorption on mucosal antibody responses can be

largely recapitulated in mice in treated systemically with anti-MAdCAM, wherein lymphocyte cellularity of the PP is reduced, but fluid absorption and conduit flow are normal. These data thus suggest a direct relationship between naive lymphocyte recruitment to the PP and mucosal humoral responses.

While disruption of fluid absorption negatively impacts lymphocyte recruitment to the PP, we also note a surprising increase in cellularity of LNs. The nature of this increase remains unclear, though we hypothesize that excess accumulation of lymphocytes in lymph nodes may be secondary to impaired homing of lymphocytes to PPs. Thus far we have not identified any indication that increases in LN cellularity relate to lymphocyte activation or proliferation (data not shown). Rather, we believe these increases result from altered lymphocyte migration from other sites (potentially the PP), as this phenomenon is rapidly reversible and can be prevented by FTY720. Further experimentation is necessary to identify the source of these excess lymphocytes.

Ultimately, however, there is a clear shift in lymphocyte population distribution away from the PPs and towards LNs. We speculate that this effect might broadly impact the nature of immune responses an individual may be prepared to elicit. This raises an intriguing question of whether such shifts in lymphocyte distribution may be biologically beneficial. While reduced lymphocyte cellularity in the PP may limit the initiation of mucosal IgA responses, increased lymphocyte cellularity in peripheral LNs may alternatively enhance systemic responses by preferential induction of IgG responses or cellular immunity. This latter response may in fact be favorable

under conditions of infectious diarrheal diseases where intestinal barrier function may already be compromised and there is risk of systemic dissemination of pathogenic microbes.

Cumulatively, we have shown that, at least in PPs, the conduit network plays an integral role in supporting PP immune homeostasis. The loss of conduit flow not only impacted lymphocyte recruitment and PP cellularity, but culminated in a decreased capacity to mount mucosal immune responses. Due to the unique link between PP conduit flow and intestinal fluid absorption, we anticipate that these processes may be particularly relevant when considering conditions characterized by fluid malabsorption such as inflammatory or infectious diarrheal diseases and chronic laxative use. Ultimately, the contribution of fluid absorption and PP conduit fluid flow within the greater context of mucosal health and disease will ultimately be a topic a great interest for future experimentation.



### 3.4 Materials and methods

**Mice.** Experiments were performed in C57BL/6 mice unless otherwise indicated. C57BL/6J mice and VillinCre mice (021504) were purchased from Jackson Laboratories (Cambridge, Bar Harbor, MA, USA). Rosa26-SSB-BFP mice were generated in the laboratory and previously described<sup>137</sup>. VillinCre mice were crossed to the Rosa26-SSB-BFP line to generate VillinCre-SSB-BFP mice. Mice were maintained under specific pathogen-free conditions in accordance with institutional and National Institute of Health guidelines and used at 6-8 weeks of age. For each of the experiments performed, age-matched mice of both sexes were analyzed. Experiments comparing GF and SPF mice were performed in outbred Swiss Webster mice at 8 weeks of age. GF mice were generously provided by the laboratory of Dr. Eugene Chang at the University of Chicago and housed in their gnotobiotic facility for the duration of treatment. Experiments were approved by the Boston Children's Hospital and Harvard Medical School institutional animal use and care committee in accordance with NIH guidelines for the humane treatment of animals

**Antibodies.** The following antibodies were used:  $\alpha$ CD45 (30-F11),  $\alpha$ CD31 (390),  $\alpha$ PDPN (8.1.1),  $\alpha$ MadCAM-1 (MECA-367),  $\alpha$ B220 (RA3-6B2),  $\alpha$ CD11b (M1/70),  $\alpha$ CD11c (N418),  $\alpha$ CD8a (53-6.7),  $\alpha$ EpCAM (G8.8),  $\alpha$ CD3e (145-2C11),  $\alpha$ TER119 (TER119),  $\alpha$ CR1/CR2 (7E9),  $\alpha$ GL7 (GL7), and  $\alpha$ CD38 (90) from Biolegend,  $\alpha$ Perlecan (A7L6) from ThermoFischer Scientific,  $\alpha$ IgA (C10-3) from bdbioscience,  $\alpha$ Col1 (millipore sigma).

**Disruption of fluid absorption.** Fluid absorption was disrupted by one of two treatments. *Polyethylene glycol (PEG):* PEG was administered to mice through *ad libitum* through drinking

at a concentration of 10% (w/v) for a duration of up to 2 weeks, depending on experiment.

*Amiloride Hydrochloride:* Mice were orally gavaged with amiloride (0.1mg/kg) once daily for up to 3 days, depending on experiment.

**Immunohistochemistry and confocal microscopy.** Isolated tissues were fixed in 4% paraformaldehyde (PFA) for 4 h and placed in 30% sucrose until saturation. Tissue was embedded in OCT medium (Optimal Cutting Temperature), frozen, and cut into 20  $\mu$ m sections. Sections were stained and imaged using Inverted Olympus IX 81 confocal microscope.

**Intravital imaging by multiphoton microscopy.** Mice are anesthetized by inhalation of isoflurane and maintained at physiological temperature with a closed-circuit heated water circulation system. A small loop of intestine is exposed from the anesthetized mouse and immobilized on a heated stage. CMFDA-labeled naive lymphocytes are adoptively transferred, and the blood vasculature is illuminated by intravenous injection with fluorescently labeled vascular-impermeable Qdots (Thermo Fisher Scientific, Q21031MP). Under these conditions, the exposed Peyer's patch can be imaged for a period of at least one hour. Imaging was performed on an Olympus BX 61 WI multiphoton microscope with a Spectra Physics MaiTai DSHP laser.

**GC and FDC quantification.** PP tissue sections were stained for confocal microscopic analysis. Resulting images were analyzed using ImageJ software to identify the perimeter of the FDC network. MFI of GL7+ staining within the FDC network was then quantified.

**Enzymatic digestion of lymphoid organs.** Single cell suspensions of LN, PP, and spleen were prepared for analysis by flow cytometry. *Lymph nodes:* LNs were dissected and incubated at 37 °C in RPMI containing 0.1 mg/ml Dnase I (Invitrogen), 0.2 mg/ml Collagenase P (Roche) and 0.8 mg/ml Dispase (Roche) for 50–60 minutes, as previously described<sup>132</sup>. Cells were collected in medium containing 2% FBS and 5 mM EDTA every 15–20 min and replaced with fresh digestion medium. *Peyer's patches:* Intestines were dissected and washed by lavage with ice cold PBS. PPs were removed from the intestine and washed in a solution 2 mM EDTA and 5% DTT in PBS for 20 minutes at 37°C to remove the epithelium. PPs were then enzymatically digested (as with the LN). *Spleen:* Lymphocyte were extracted from the spleen by mechanical disruption and passage through a 70um cell strainer. Red blood cells were lysed with ACK buffer before analysis by flow cytometry.

**Tissue preparation for TEM.** Segments of intestine roughly 2cm long and containing at least one PP were excised and tied at either end. The lumen of these intestinal "loops" were then filled with FGP fixative (2.5% paraformaldehyde, 5% glutaraldehyde, 0.06% picric acid in 0.2M cacodylate buffer), and the filled loops were then drop-fixed overnight in the same solution. Fixed sections were washed in 0.1M cacodylate buffer and post-fixed with 1% osmium tetroxide (OsO<sub>4</sub>)/1.5% potassium ferrocyanide (K<sub>4</sub>Fe(CN)<sub>6</sub>) for 1h, washed in water three times and incubated in 1% aqueous uranyl acetate for 1h followed by two washes in water and subsequent dehydration in grades of alcohol (10min each; 50%, 70%, 90%, 2× 10min 100%). The samples were then placed in propyleneoxide for 1h subsequently infiltrated overnight in a 1:1 mixture of propyleneoxide and TAAB Epon (Marivac Canada Inc.). The following day the samples were embedded in TAAB Epon and polymerized at 60°C for 48h. Ultrathin sections

(about 60nm) were cut on a Reichert Ultracut-S microtome, placed onto copper grids, stained with uranyl acetate and lead citrate and examined on a JEOL 1200EX microscope. Images were recorded with an AMT 2k CCD camera

**Tissue preparation for SEM.** Samples were fixed for 1-2 days in FGP Fixative as was described for TEM. Fixed PPs were then subjected to alkali-water maceration by immersion in a 10% aqueous solution of NaOH for 5 days at room temperature. Samples were then rinsed twice in distilled water for 1 day each, until they became transparent. The alkali-water macerated specimens were then treated with 0.5-1% tannic acid solution for 2-5 h, washed in distilled water for 1 h, and immersed in 1% OsO<sub>2</sub> solution for several hours. The specimens were dehydrated in a series of graded concentrations of ethanol and transferred to isoamyl acetate. Samples were then briefly frozen in liquid nitrogen and cracked with a razor blade to expose the inside of the PP for imaging before immediately re-immersing in 100% ethanol. Specimens are then dried using a Tousimis 931 GL critical-point dryer. The dried specimens were then affixed on aluminum stubs with adhesives, coated with platinum-palladium using an EMS 300T D dual head sputter coater, and examined by SEM on a Zeiss Ultra55 FESEM.

**Conduit analysis.** Mice were gavage fed with 400ul of FITC-saturated PBS solution 2-4 hours before harvesting the intestine. To examine the effects of blockade of fluid absorption, mice were 1) gavage fed with 400ul of FITC saturated PBS solution with 10% PEG, or 2) gavage fed with FITC in PBS 2 hours following gavage treatment with amiloride (0.1mg/kg). The intestinal lumen was washed by lavage with 10mL of ice cold PBS. Peyer's patches were then excised and fixed in 4% PFA. Fixed tissues were immersed in 30% sucrose for cryoprotection and then

frozen in O.C.T. Thick 100 micron sections were cut using a cryostat. Sections were imaged by multiphoton microscopy.

**Adoptive transfer of lymphocytes.** A single-cell suspension of naive lymphocytes was prepared from spleens from C57Bl/6 donor mice and immediately labeled with CellTracker Green CMFDA dye (ThermoFisher Scientific C2925). Lymphocytes were adoptively transferred to either untreated control, PEG-treated, amiloride-treated recipient mice by retro-orbital injection in 50ul of sterile saline. Alternatively, lymphocytes were adoptively transferred in sterile saline containing 20ug of anti-MAdCAM1 antibody. For comparison of lymphocytes from untreated control and PEG-treated donor mice, donor splenocytes were similarly harvested and labeled, then mixed in a 1 to 1 ratio before adoptive transfer to recipient mice. For all experiments, mice were euthanized 1 hour after adoptive transfer, and PPs and iLNs were harvested for analysis.

**FTY720 treatments.** To prevent cell egress, mice were injected with 1 mg/kg FTY720 (Fingolimod, R&D) i.p. immediately prior to the start of treatment with PEG or amiloride. Mice received an additional dose of FTY720 at 48 h and were sacrificed for analysis at 72 h.

**Antibody blockade of MAdCAM-1.** To block lymphocyte interactions with the PP HEV, mice were injected I.V. with 20ug of anti-MAdCAM (MECA-367). For experiments examining short-term recruitment of adoptively transferred lymphocytes, mice were given a single injection

simultaneous with cell adoptive transfer. For experiments examining long-term effects on PP cellularity and antibody response, mice were injected once daily with 20ug.

***In vivo* labeling of MAdCAM1.** Control or untreated mice received 20ug of anti-MAdCAM1-488 by retro-orbital injection. Mice were euthanized 10 minutes after injection and perfused with ice cold 4% PFA. PPs were harvested and drop-fixed in PFA for an additional 4 hours, immersed in 30% sucrose overnight, and frozen in OCT. Tissue sections were then stained with anti-MAdCAM1-PE and analyzed by confocal microscopy. Images were imported to FlowJo software, and pixel intensity for either 488 or PE channels was assessed for each pixel. Data was quantified as % pixels positive in the 488 channel out of all stained pixels (488+PE).

**Image quantification of HEV-associated lymphocytes.** Confocal imaging was performed on PPs harvested from mice following adoptive transfer of CMFDA labeled lymphocytes. Sections were counterstained with anti-MAdCAM to label HEVs. Masks of HEV staining were created from in ImageJ software and the total number of lymphocytes within the mask were quantified as lymphocytes associated with the HEV.

**Oral immunization and mucosal antibody responses.** For analysis of antigen-specific mucosal antibody responses, control (untreated) or PEG-treated animals received either NP-HEL (100ug) or NP-CGG (20ug) once daily by oral gavage for 2 weeks. Unimmunized controls received PBS once daily by oral gavage for the same duration. All mice were allowed to recover on normal drinking water for 3 days following the final immunization. Stool was collected for fecal IgA titers analysis. Intestinal tissue was harvested for enzymatic digestion and analysis by flow cytometry. Fecal IgA was extracted from stool by vortex in a solution of protease inhibitor

cocktail in PBS for 1 hour at 4°C. Non-soluble fecal material was removed by centrifugation. Supernatant containing soluble fecal-IgA was reserved for analysis by ELISA, while the pellet was allowed to dry and subsequently weighed. Sample volume was normalized to fecal dry weight. ELISA analysis was performed through immobilization of NP-BSA on a high binding plate (Greiner Bio-One, 655081), addition of fecal-IgA preparation at 2-fold serial dilutions, and probing for specific binding of Goat polyclonal anti-IgA-AP (southern biotech) using standard alkaline phosphatase development. For analysis of total fecal IgA, high binding plates were coated with goat polyclonal anti-IgA capture antibody(southern biotech), followed by addition of fecal-IgA preparation, and probing for specific binding of rat anti-IgA-AP (11-44-2) by alkaline phosphatase development.

**Analysis of NP-specific B cells.** Small intestines were harvested from mice following oral immunization against NP-CGG. PPs were removed and fat was carefully dissected away. The intestine was cut into 2-3cm long segments and inverted using forceps. Intestinal segments were then washed twice in 2 mM EDTA and 5% DTT in PBS at 37°C for 20 minutes each to remove epithelium. The remaining lamina propria was enzymatically digested at 37 °C in RPMI containing 0.1 mg/ml Dnase I (Invitrogen), 0.2 mg/ml Collagenase P (Roche) and 0.8 mg/ml Dispase (Roche) for 50–60 minutes. NP-specific B cells were then identified by incubation with NP-PE for 20 minutes on ice, then analyzed by flow cytometry.

**Statistical analysis.** Statistical tests were performed using GraphPad Prism software. Differences were considered to be statistically significant when  $P < 0.05$ . For graphs, data are shown as mean +/- SEM. Statistical significance is indicated with the following: \* ( $p \leq 0.05$ ),

\*\* ( $p \leq 0.01$ ), \*\*\* ( $p \leq 0.005$ ), \*\*\*\* ( $p \leq 0.001$ ). Sample size was not specifically predetermined, but the number of mice used was consistent with prior experience with similar experiments.



## Chapter 4

### Discussion and future directions

#### 4.1 Technological breakthroughs enable an acceleration of stromal cell immunology

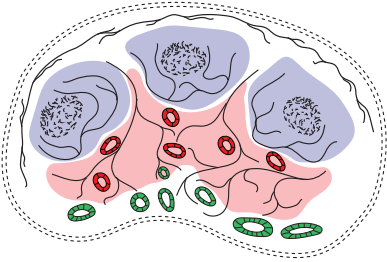
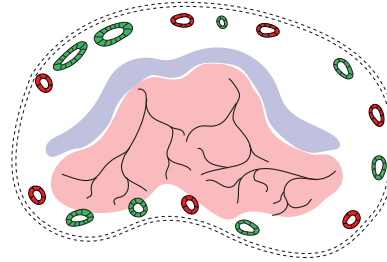
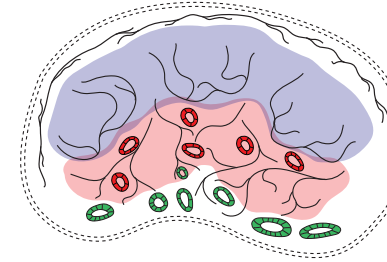
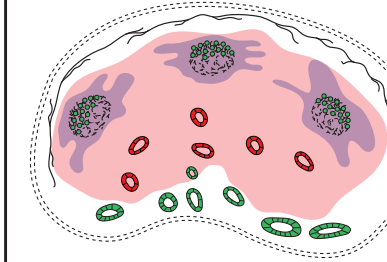
Timely initiation of adaptive immune responses is critically dependent on the efficient surveillance of lymphoid tissues by rare lymphocyte precursors, the exact and strategic positioning of cells within lymphoid organs, the transport of antigen, and the dynamic regulation of microenvironment. These functions are within the purview of lymphoid tissue stromal cells. A general understanding that LN stromal cells contribute to both leukocyte homeostasis and initiation of adaptive immune responses has long been established, yet in many ways the study of stromal cells in immunity may still be considered an emerging field. In comparison to the study of their hematopoietic counterparts, the development of robust tools for both *in vivo* and *in vitro* exploration of stromal cell biology has largely lagged behind.

There are several contributing factors for this slow evolution of the field of stromal cells in immunity. Firstly, stromal cells are simply more difficult to isolate than hematopoietic cells. Secondly, stromal cells comprise a fairly rare population, collectively comprising less than 1% of all lymphoid tissue cellularity. And finally, relatively little has been definitively confirmed regarding the ontogeny of lymphoid tissue stromal cells. Until recently, studies have largely relied on *in situ* imaging to interpret stromal cell function, offering little insight beyond their structural morphology.

However, more sophisticated methods of interrogating stromal biology have been developed in recent years, leading to an exciting acceleration in new findings. One of the most essential advancements to have been made is the establishment of methods for reproducible isolation of primary lymphoid tissue stromal cells<sup>103,132</sup>. Whereas most hematopoietic cells can be obtained from blood or through simple mechanical disruption of tissue, stromal components are firmly embedded in the ECM, requiring a combination of enzymatic and mechanical digestion. Development of these techniques has opened possibilities for several downstream applications. For instance, the ability to isolate stromal populations has enabled informative *in vitro* studies leading to the identification of novel stromal-immune cell interactions<sup>61,69,138-142</sup>. Additionally, transcriptomic analyses of purified primary stromal cell populations has allowed deeper insight into potential functions of known stromal populations<sup>128</sup>. Future studies will likely include the use of single cell RNAseq analyses which we anticipate to be hugely beneficial toward providing a more rapid and specific identification of stromal subpopulations as well as biomarkers to target these populations *in vivo*.

In chapter 2, we discussed what might be considered the first iteration of mouse models for genetic targeting of stromal cells. The recent development of these mouse lines is proving to be a major step forward in the field of stromal cells in immunity. The use of CCL19cre-expressing mice has allowed, for the first time, the *in vivo* targeting of lymph node FRCs<sup>101,113</sup>. Likewise, we believe that the use of CXCL13cre-expressing mice will prove useful for future exploration of B zone FRCs, FDCs, and MRCs. Our own use of these mice as a tool for stromal cell ablation has already provided a wealth of information regarding the contributions of these populations toward maintenance of the LNs, spleen and PPs (Figure 4.1).

**Figure 4.1**

Depletion Model	CXCL13cre - iDTR	CD21cre - iDTR (chimera)	CCL19cre - iDTR	
Original Publication	Unpublished	Wang <i>et al</i> , 2011 (ref 109)	Creiasco <i>et al</i> , 2014 (ref 101)	
Stromal subsets targeted	FDC, MRC, B-zone FRC	FDC	B-zone FRC, T-zone FRC	
Effects on Lymph Node	<i>Loss of B cell homeostasis Loss of follicle identity Loss of GC reactions Redistribution of lymphatics Redistribution of vasculature</i>	<i>Loss of follicle identity Loss of GC reactions Partial loss of B/T separation</i>	<i>Loss of B cell homeostasis Loss of T cell homeostasis Complete loss of B/T separation</i>	
Lymph Node Organization	 <p> <span style="color: blue;">■</span> B cell zone  <span style="color: red;">■</span> T cell zone  <i>Unablated</i> </p>	 <p> <span style="color: blue;">■</span> B cell zone  <span style="color: red;">■</span> T cell zone         </p>	 <p> <span style="color: blue;">■</span> B cell zone  <span style="color: red;">■</span> T cell zone         </p>	 <p> <span style="color: blue;">■</span> B cell zone  <span style="color: red;">■</span> T cell zone         </p>
Effects on Spleen	<i>Loss of B cell homeostasis Loss of T cell homeostasis Decreased follicle size</i>	<i>Disrupted follicle organization Loss of GC reactions (after imm)</i>	<i>Impaired marginal zone humoral immune responses.</i>	
Effects on Peyer's patch	<i>Complete loss of Peyer's patches</i>	<i>Not reported</i>	<i>Moderate loss of B cell homeostasis</i>	

Expanding our knowledge of stromal cell lineage relationships, heterogeneity, and transcriptional identity will allow the generation of new, and potentially more specific genetic models for targeting stromal populations *in vivo*. Of particular use will be the implementation of ligand-dependant inducible Cre recombinases. The ability to temporally control genetic modulation of stromal cells will be an essential advancement, as functional assessment of many signaling pathways of interest requires specific targeting only after the initial stages of lymphoid tissue organogenesis.

Finally, we anticipate that expanding our knowledge of how stromal cells influence the activation, function, and movement of immune cells will ultimately enable both the development of novel therapeutic strategies as well as potentially greater optimization of existing treatments.

#### **4.2 Exploration of conduit networks and moving beyond descriptive research with new experimental approaches.**

Many of the functionally important features of stromal cells are structural in nature and cannot be studied in isolation. As such, many studies centered on lymphoid tissue stromal cells are largely descriptive in nature.

In chapter 3 we attempt to experimentally address the biological function of lymphoid tissue conduit networks. Early descriptions of the FRC reticular networks as support structures of the lymph node date back to early 1960s following the first reported use of electron microscopy to describe the microanatomy of lymphoid tissues <sup>143</sup>. Various descriptions of the reticular

network functioning as a conduit for the transport or distribution of soluble material have been reported over the last several decades <sup>52,131,144</sup>, and many of these studies have gone on to speculate immunologically important roles for conduit-mediated transport of chemokines and antigen <sup>48,50,83,84,133</sup>. However, exploration of LN conduit networks thus far has been largely restricted to interpretation of *in situ* imaging, and thus our understanding of conduit function remains purely descriptive. It has proven far more challenging to move beyond descriptive studies and examine 'how' or 'why' stromal cells form these specific structures. Further scientific advancement in this area is thus dependent on the development of creative new tools for either the manipulation of conduit flow, manipulation of material access to the conduits, or alteration of the conduit-surrounding FRCs. Thus far, manipulation of lymph flow through LN conduits has proven technically challenging.

Here we alternatively sought to gather insight into the biological importance of PP conduit flow, which is uniquely linked with the process of epithelial fluid absorption. As there are a number of ways to disrupt intestinal fluid absorption, conduit flow in the PP is more experimentally pliable than that of LN conduits. We identified a novel role for intestinal fluid absorption and PP conduit flow in the maintenance of HEV structure, PP immune homeostasis, and mucosal antibody responses (Figure 4.2). We hope that our exploration of PP conduit function may additionally provide more general insight into the basic biological functions of reticular conduit networks of other tissues. However, despite many similarities in terms of FRC phenotype and microanatomical structure of PP and LN conduits, we must be cautious about assuming conduit flow to play a similar role in support of LN homeostasis. Alternative approaches must be devised to specifically address the biological role of conduits in lymph nodes.

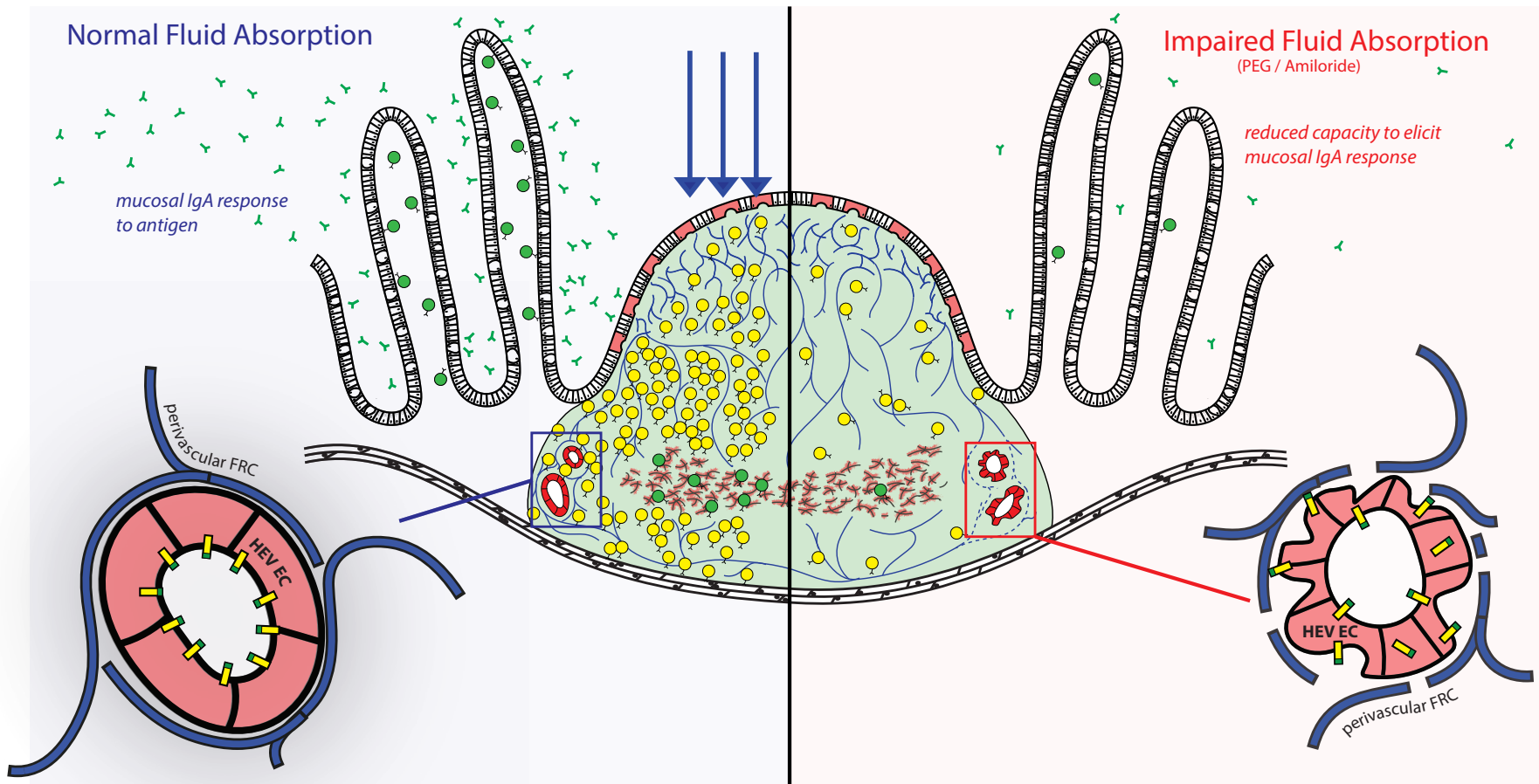


**Figure 4.2:** Intestinal fluid absorption modulates Peyer's patch homeostasis and mucosal antibody responses. *Left:* Directional fluid flow through PP conduits helps maintain normal HEV structure and expression of MAdCAM along the luminal surface of the HEV endothelium. Constitutive recruitment of circulating lymphocytes contributes to the pool of naive lymphocytes within the PP follicle. *Right:* Without fluid absorption and directional fluid flow through the conduits, HEV structure is perturbed, leading to mislocalization of MAdCAM and impaired lymphocyte recruitment to the PP. Resulting decreases in lymphocyte cellularity restricts the PP capacity to generate mucosal IgA antibody responses.

Manipulation of material access to LN conduits may offer one such alternative approach to addressing questions of the conduit networks biological function. A recent study has reported that the protein PLVAP (plasmalemma vesicle-associated protein) plays a critical role in regulating the size-exclusion cut-off of LN conduits<sup>145</sup>. Fibrils of PLVAP appear to form a diaphragm in the transendothelial channels of sinus-lining endothelial cells that overly LN conduits. Knockout of this protein effectively removes the 70-kDa M.W. cutoff restriction, allowing larger molecules entry into the conduit network. This finding offers new opportunities to examine the significance of conduit-mediated transport of antigen in adaptive immune responses. In chapter 3, we describe experiments in which we immunize mice with differently sized NP-conjugated protein antigens: one which is small enough to transport through conduits (NP-HEL) and one that is excluded (NP-CGG). However, a direct comparison between these antigens cannot be made, as immunogenicity may additionally be impacted by differences in carrier protein or NP conjugation ratios. An alternative approach might therefore be to compare adaptive immune responses in WT and PLVAP<sup>-/-</sup> mice when immunized against the same antigen of M.W. greater than the conduit network cutoff. Such an approach may offer new insight into the immunological role of conduit-mediated antigen transport.

Ultimately, the conduit network is a unique and defining feature of the lymphoid tissue reticulum, and yet much of its biological importance to immune function remains largely speculative. The studies reported herein far offer an intriguing first step towards experimentally demonstrating a physiological role for conduit flow. However, additional experimentation and new creative approaches will be necessary to move beyond a descriptive

understanding of conduit structures and fully identify their functional contributions to immune function.



- 1 Moon, J. J. *et al.* Naive CD4(+) T cell frequency varies for different epitopes and predicts repertoire diversity and response magnitude. *Immunity* **27**, 203-213, doi:10.1016/j.immuni.2007.07.007 (2007).
- 2 Kotturi, M. F. *et al.* Naive precursor frequencies and MHC binding rather than the degree of epitope diversity shape CD8+ T cell immunodominance. *Journal of immunology* **181**, 2124-2133 (2008).
- 3 Obar, J. J., Khanna, K. M. & Lefrancois, L. Endogenous naive CD8+ T cell precursor frequency regulates primary and memory responses to infection. *Immunity* **28**, 859-869, doi:10.1016/j.immuni.2008.04.010 (2008).
- 4 Alanio, C., Lemaitre, F., Law, H. K., Hasan, M. & Albert, M. L. Enumeration of human antigen-specific naive CD8+ T cells reveals conserved precursor frequencies. *Blood* **115**, 3718-3725, doi:10.1182/blood-2009-10-251124 (2010).
- 5 Jenkins, M. K. & Moon, J. J. The role of naive T cell precursor frequency and recruitment in dictating immune response magnitude. *Journal of immunology* **188**, 4135-4140, doi:10.4049/jimmunol.1102661 (2012).
- 6 Kwok, W. W. *et al.* Frequency of epitope-specific naive CD4(+) T cells correlates with immunodominance in the human memory repertoire. *Journal of immunology* **188**, 2537-2544, doi:10.4049/jimmunol.1102190 (2012).
- 7 Pape, K. A., Taylor, J. J., Maul, R. W., Gearhart, P. J. & Jenkins, M. K. Different B cell populations mediate early and late memory during an endogenous immune response. *Science* **331**, 1203-1207, doi:10.1126/science.1201730 (2011).
- 8 Weisel, F. J., Zuccarino-Catania, G. V., Chikina, M. & Shlomchik, M. J. A Temporal Switch in the Germinal Center Determines Differential Output of Memory B and Plasma Cells. *Immunity* **44**, 116-130, doi:10.1016/j.immuni.2015.12.004 (2016).
- 9 Abbott, R. K. *et al.* Precursor Frequency and Affinity Determine B Cell Competitive Fitness in Germinal Centers, Tested with Germline-Targeting HIV Vaccine Immunogens. *Immunity* **48**, 133-146 e136, doi:10.1016/j.immuni.2017.11.023 (2018).
- 10 van de Pavert, S. A. *et al.* Chemokine CXCL13 is essential for lymph node initiation and is induced by retinoic acid and neuronal stimulation. *Nature immunology* **10**, 1193-1199, doi:10.1038/ni.1789 (2009).
- 11 Benezech, C. *et al.* Lymphotoxin-beta receptor signaling through NF-kappaB2-RelB pathway reprograms adipocyte precursors as lymph node stromal cells. *Immunity* **37**, 721-734, doi:10.1016/j.immuni.2012.06.010 (2012).
- 12 Vondenhoff, M. F. *et al.* LTbetaR signaling induces cytokine expression and up-regulates lymphangiogenic factors in lymph node anlagen. *Journal of immunology* **182**, 5439-5445, doi:10.4049/jimmunol.0801165 (2009).

- 13 Kim, D. *et al.* Regulation of peripheral lymph node genesis by the tumor necrosis factor family member TRANCE. *The Journal of experimental medicine* **192**, 1467-1478 (2000).
- 14 Benezech, C. *et al.* Ontogeny of stromal organizer cells during lymph node development. *Journal of immunology* **184**, 4521-4530, doi:10.4049/jimmunol.0903113 (2010).
- 15 Cupedo, T. *et al.* Presumptive lymph node organizers are differentially represented in developing mesenteric and peripheral nodes. *Journal of immunology* **173**, 2968-2975 (2004).
- 16 van de Pavert, S. A. & Mebius, R. E. New insights into the development of lymphoid tissues. *Nature reviews. Immunology* **10**, 664-674, doi:10.1038/nri2832 (2010).
- 17 Brendolan, A. & Caamano, J. H. Mesenchymal cell differentiation during lymph node organogenesis. *Frontiers in immunology* **3**, 381, doi:10.3389/fimmu.2012.00381 (2012).
- 18 Koning, J. J. & Mebius, R. E. Interdependence of stromal and immune cells for lymph node function. *Trends in immunology* **33**, 264-270, doi:10.1016/j.it.2011.10.006 (2012).
- 19 Buettner, M. & Lochner, M. Development and Function of Secondary and Tertiary Lymphoid Organs in the Small Intestine and the Colon. *Frontiers in immunology* **7**, 342, doi:10.3389/fimmu.2016.00342 (2016).
- 20 Gowans, J. L. The recirculation of lymphocytes from blood to lymph in the rat. *J Physiol* **146**, 54-69 (1959).
- 21 Gowans, J. L. & Knight, E. J. The Route of Re-Circulation of Lymphocytes in the Rat. *Proc R Soc Lond B Biol Sci* **159**, 257-282 (1964).
- 22 Springer, T. A. Traffic signals for lymphocyte recirculation and leukocyte emigration: the multistep paradigm. *Cell* **76**, 301-314 (1994).
- 23 von Andrian, U. H. & Mempel, T. R. Homing and cellular traffic in lymph nodes. *Nature reviews. Immunology* **3**, 867-878, doi:10.1038/nri1222 (2003).
- 24 Mionnet, C. *et al.* High endothelial venules as traffic control points maintaining lymphocyte population homeostasis in lymph nodes. *Blood* **118**, 6115-6122, doi:10.1182/blood-2011-07-367409 (2011).
- 25 Bai, Z. *et al.* Constitutive lymphocyte transmigration across the basal lamina of high endothelial venules is regulated by the autotaxin/lysophosphatidic acid axis. *Journal of immunology* **190**, 2036-2048, doi:10.4049/jimmunol.1202025 (2013).
- 26 Nakasaki, T. *et al.* Involvement of the lysophosphatidic acid-generating enzyme autotaxin in lymphocyte-endothelial cell interactions. *The American journal of pathology* **173**, 1566-1576, doi:10.2353/ajpath.2008.071153 (2008).
- 27 Hendriks, H. R., Duijvestijn, A. M. & Kraal, G. Rapid decrease in lymphocyte adherence to high endothelial venules in lymph nodes deprived of afferent lymphatic vessels. *European journal of immunology* **17**, 1691-1695, doi:10.1002/eji.1830171203 (1987).

- 28 Hendriks, H. R. & Eestermans, I. L. Disappearance and reappearance of high endothelial venules and immigrating lymphocytes in lymph nodes deprived of afferent lymphatic vessels: a possible regulatory role of macrophages in lymphocyte migration. *European journal of immunology* **13**, 663-669, doi:10.1002/eji.1830130811 (1983).
- 29 Mebius, R. E. *et al.* Expression of GlyCAM-1, an endothelial ligand for L-selectin, is affected by afferent lymphatic flow. *Journal of immunology* **151**, 6769-6776 (1993).
- 30 Hendriks, H. R., Eestermans, I. L. & Hoefsmit, E. C. Depletion of macrophages and disappearance of postcapillary high endothelial venules in lymph nodes deprived of afferent lymphatic vessels. *Cell Tissue Res* **211**, 375-389 (1980).
- 31 Moussion, C. & Girard, J. P. Dendritic cells control lymphocyte entry to lymph nodes through high endothelial venules. *Nature* **479**, 542-546, doi:10.1038/nature10540 (2011).
- 32 Browning, J. L. *et al.* Lymphotoxin-beta receptor signaling is required for the homeostatic control of HEV differentiation and function. *Immunity* **23**, 539-550, doi:10.1016/j.immuni.2005.10.002 (2005).
- 33 Onder, L. *et al.* Endothelial cell-specific lymphotoxin-beta receptor signaling is critical for lymph node and high endothelial venule formation. *The Journal of experimental medicine* **210**, 465-473, doi:10.1084/jem.20121462 (2013).
- 34 Tomei, A. A., Siegert, S., Britschgi, M. R., Luther, S. A. & Swartz, M. A. Fluid flow regulates stromal cell organization and CCL21 expression in a tissue-engineered lymph node microenvironment. *Journal of immunology* **183**, 4273-4283, doi:10.4049/jimmunol.0900835 (2009).
- 35 Herzog, B. H. *et al.* Podoplanin maintains high endothelial venule integrity by interacting with platelet CLEC-2. *Nature* **502**, 105-109, doi:10.1038/nature12501 (2013).
- 36 Grigorova, I. L., Panteleev, M. & Cyster, J. G. Lymph node cortical sinus organization and relationship to lymphocyte egress dynamics and antigen exposure. *Proceedings of the National Academy of Sciences of the United States of America* **107**, 20447-20452, doi:10.1073/pnas.1009968107 (2010).
- 37 Grigorova, I. L. *et al.* Cortical sinus probing, S1P1-dependent entry and flow-based capture of egressing T cells. *Nature immunology* **10**, 58-65, doi:10.1038/ni.1682 (2009).
- 38 Matloubian, M. *et al.* Lymphocyte egress from thymus and peripheral lymphoid organs is dependent on S1P receptor 1. *Nature* **427**, 355-360, doi:10.1038/nature02284 (2004).
- 39 Pham, T. H., Okada, T., Matloubian, M., Lo, C. G. & Cyster, J. G. S1P1 receptor signaling overrides retention mediated by G alpha i-coupled receptors to promote T cell egress. *Immunity* **28**, 122-133, doi:10.1016/j.immuni.2007.11.017 (2008).
- 40 Schwab, S. R. *et al.* Lymphocyte sequestration through S1P lyase inhibition and disruption of S1P gradients. *Science* **309**, 1735-1739, doi:10.1126/science.1113640 (2005).

- 41 Pappu, R. *et al.* Promotion of lymphocyte egress into blood and lymph by distinct sources of sphingosine-1-phosphate. *Science* **316**, 295-298, doi:10.1126/science.1139221 (2007).
- 42 Pham, T. H. *et al.* Lymphatic endothelial cell sphingosine kinase activity is required for lymphocyte egress and lymphatic patterning. *The Journal of experimental medicine* **207**, 17-27, doi:10.1084/jem.20091619 (2010).
- 43 Lee, M. J. *et al.* Sphingosine-1-phosphate as a ligand for the G protein-coupled receptor EDG-1. *Science* **279**, 1552-1555 (1998).
- 44 Lo, C. G., Xu, Y., Proia, R. L. & Cyster, J. G. Cyclical modulation of sphingosine-1-phosphate receptor 1 surface expression during lymphocyte recirculation and relationship to lymphoid organ transit. *The Journal of experimental medicine* **201**, 291-301, doi:10.1084/jem.20041509 (2005).
- 45 Tomura, M. *et al.* Monitoring cellular movement in vivo with photoconvertible fluorescence protein "Kaede" transgenic mice. *Proceedings of the National Academy of Sciences of the United States of America* **105**, 10871-10876, doi:10.1073/pnas.0802278105 (2008).
- 46 Cyster, J. G. & Schwab, S. R. Sphingosine-1-phosphate and lymphocyte egress from lymphoid organs. *Annual review of immunology* **30**, 69-94, doi:10.1146/annurev-immunol-020711-075011 (2012).
- 47 Hall, J. G. & Morris, B. The immediate effect of antigens on the cell output of a lymph node. *British journal of experimental pathology* **46**, 450-454 (1965).
- 48 Baekkevold, E. S. *et al.* The CCR7 ligand elc (CCL19) is transcytosed in high endothelial venules and mediates T cell recruitment. *The Journal of experimental medicine* **193**, 1105-1112 (2001).
- 49 Gretz, J. E., Norbury, C. C., Anderson, A. O., Proudfoot, A. E. & Shaw, S. Lymph-borne chemokines and other low molecular weight molecules reach high endothelial venules via specialized conduits while a functional barrier limits access to the lymphocyte microenvironments in lymph node cortex. *The Journal of experimental medicine* **192**, 1425-1440 (2000).
- 50 Stein, J. V. *et al.* The CC chemokine thymus-derived chemotactic agent 4 (TCA-4, secondary lymphoid tissue chemokine, 6CKine, exodus-2) triggers lymphocyte function-associated antigen 1-mediated arrest of rolling T lymphocytes in peripheral lymph node high endothelial venules. *The Journal of experimental medicine* **191**, 61-76 (2000).
- 51 Gretz, J. E., Anderson, A. O. & Shaw, S. Cords, channels, corridors and conduits: critical architectural elements facilitating cell interactions in the lymph node cortex. *Immunological reviews* **156**, 11-24 (1997).
- 52 Anderson, A. O. & Shaw, S. T cell adhesion to endothelium: the FRC conduit system and other anatomic and molecular features which facilitate the adhesion cascade in lymph node. *Seminars in immunology* **5**, 271-282, doi:10.1006/smim.1993.1031 (1993).

- 53 Shiow, L. R. *et al.* CD69 acts downstream of interferon-alpha/beta to inhibit S1P1 and lymphocyte egress from lymphoid organs. *Nature* **440**, 540-544, doi:10.1038/nature04606 (2006).
- 54 Soderberg, K. A. *et al.* Innate control of adaptive immunity via remodeling of lymph node feed arteriole. *Proceedings of the National Academy of Sciences of the United States of America* **102**, 16315-16320, doi:10.1073/pnas.0506190102 (2005).
- 55 Kumar, V., Chyou, S., Stein, J. V. & Lu, T. T. Optical projection tomography reveals dynamics of HEV growth after immunization with protein plus CFA and features shared with HEVs in acute autoinflammatory lymphadenopathy. *Frontiers in immunology* **3**, 282, doi:10.3389/fimmu.2012.00282 (2012).
- 56 Webster, B. *et al.* Regulation of lymph node vascular growth by dendritic cells. *The Journal of experimental medicine* **203**, 1903-1913, doi:10.1084/jem.20052272 (2006).
- 57 Chyou, S. *et al.* Fibroblast-type reticular stromal cells regulate the lymph node vasculature. *Journal of immunology* **181**, 3887-3896 (2008).
- 58 Chyou, S. *et al.* Coordinated regulation of lymph node vascular-stromal growth first by CD11c+ cells and then by T and B cells. *Journal of immunology* **187**, 5558-5567, doi:10.4049/jimmunol.1101724 (2011).
- 59 Kumar, V. *et al.* Global lymphoid tissue remodeling during a viral infection is orchestrated by a B cell-lymphotoxin-dependent pathway. *Blood* **115**, 4725-4733, doi:10.1182/blood-2009-10-250118 (2010).
- 60 Yang, C. Y. *et al.* Trapping of naive lymphocytes triggers rapid growth and remodeling of the fibroblast network in reactive murine lymph nodes. *Proceedings of the National Academy of Sciences of the United States of America* **111**, E109-118, doi:10.1073/pnas.1312585111 (2014).
- 61 Acton, S. E. *et al.* Dendritic cells control fibroblastic reticular network tension and lymph node expansion. *Nature* **514**, 498-502, doi:10.1038/nature13814 (2014).
- 62 Astarita, J. L. *et al.* The CLEC-2-podoplanin axis controls the contractility of fibroblastic reticular cells and lymph node microarchitecture. *Nature immunology*, doi:10.1038/ni.3035 (2014).
- 63 Kamath, A. T., Henri, S., Battye, F., Tough, D. F. & Shortman, K. Developmental kinetics and lifespan of dendritic cells in mouse lymphoid organs. *Blood* **100**, 1734-1741 (2002).
- 64 Steinman, R. M. The dendritic cell system and its role in immunogenicity. *Annual review of immunology* **9**, 271-296, doi:10.1146/annurev.iy.09.040191.001415 (1991).
- 65 Gregory, J. L. *et al.* Infection Programs Sustained Lymphoid Stromal Cell Responses and Shapes Lymph Node Remodeling upon Secondary Challenge. *Cell Rep* **18**, 406-418, doi:10.1016/j.celrep.2016.12.038 (2017).
- 66 Baluk, P. *et al.* Functionally specialized junctions between endothelial cells of lymphatic vessels. *The Journal of experimental medicine* **204**, 2349-2362, doi:10.1084/jem.20062596 (2007).

- 67 Schmid-Schonbein, G. W. Microlymphatics and lymph flow. *Physiological reviews* **70**, 987-1028 (1990).
- 68 von der Weid, P. Y. Review article: lymphatic vessel pumping and inflammation--the role of spontaneous constrictions and underlying electrical pacemaker potentials. *Alimentary pharmacology & therapeutics* **15**, 1115-1129 (2001).
- 69 Acton, S. E. *et al.* Podoplanin-rich stromal networks induce dendritic cell motility via activation of the C-type lectin receptor CLEC-2. *Immunity* **37**, 276-289, doi:10.1016/j.immuni.2012.05.022 (2012).
- 70 Randolph, G. J., Angeli, V. & Swartz, M. A. Dendritic-cell trafficking to lymph nodes through lymphatic vessels. *Nature reviews. Immunology* **5**, 617-628, doi:10.1038/nri1670 (2005).
- 71 Teijeira, A., Russo, E. & Halin, C. Taking the lymphatic route: dendritic cell migration to draining lymph nodes. *Seminars in immunopathology* **36**, 261-274, doi:10.1007/s00281-013-0410-8 (2014).
- 72 Schumann, K. *et al.* Immobilized chemokine fields and soluble chemokine gradients cooperatively shape migration patterns of dendritic cells. *Immunity* **32**, 703-713, doi:10.1016/j.immuni.2010.04.017 (2010).
- 73 Tal, O. *et al.* DC mobilization from the skin requires docking to immobilized CCL21 on lymphatic endothelium and intralymphatic crawling. *The Journal of experimental medicine* **208**, 2141-2153, doi:10.1084/jem.20102392 (2011).
- 74 Weber, M. *et al.* Interstitial dendritic cell guidance by haptotactic chemokine gradients. *Science* **339**, 328-332, doi:10.1126/science.1228456 (2013).
- 75 Hoogewerf, A. J. *et al.* Glycosaminoglycans mediate cell surface oligomerization of chemokines. *Biochemistry* **36**, 13570-13578, doi:10.1021/bi971125s (1997).
- 76 Lee, K. M. *et al.* D6 facilitates cellular migration and fluid flow to lymph nodes by suppressing lymphatic congestion. *Blood* **118**, 6220-6229, doi:10.1182/blood-2011-03-344044 (2011).
- 77 Lee, K. M., Nibbs, R. J. & Graham, G. J. D6: the 'crowd controller' at the immune gateway. *Trends in immunology* **34**, 7-12, doi:10.1016/j.it.2012.08.001 (2013).
- 78 de Paz, J. L. *et al.* Profiling heparin-chemokine interactions using synthetic tools. *ACS chemical biology* **2**, 735-744, doi:10.1021/cb700159m (2007).
- 79 Ulvmar, M. H. *et al.* The atypical chemokine receptor CCRL1 shapes functional CCL21 gradients in lymph nodes. *Nature immunology* **15**, 623-630, doi:10.1038/ni.2889 (2014).
- 80 Heinzl, K., Benz, C. & Bleul, C. C. A silent chemokine receptor regulates steady-state leukocyte homing in vivo. *Proceedings of the National Academy of Sciences of the United States of America* **104**, 8421-8426, doi:10.1073/pnas.0608274104 (2007).

- 81 Ulvmar, M. H., Hub, E. & Rot, A. Atypical chemokine receptors. *Experimental cell research* **317**, 556-568, doi:10.1016/j.yexcr.2011.01.012 (2011).
- 82 Roozendaal, R., Mebius, R. E. & Kraal, G. The conduit system of the lymph node. *International immunology* **20**, 1483-1487, doi:10.1093/intimm/dxn110 (2008).
- 83 Roozendaal, R. *et al.* Conduits mediate transport of low-molecular-weight antigen to lymph node follicles. *Immunity* **30**, 264-276, doi:10.1016/j.immuni.2008.12.014 (2009).
- 84 Sixt, M. *et al.* The conduit system transports soluble antigens from the afferent lymph to resident dendritic cells in the T cell area of the lymph node. *Immunity* **22**, 19-29, doi:10.1016/j.immuni.2004.11.013 (2005).
- 85 Nossal, G. J., Abbot, A., Mitchell, J. & Lummus, Z. Antigens in immunity. XV. Ultrastructural features of antigen capture in primary and secondary lymphoid follicles. *The Journal of experimental medicine* **127**, 277-290 (1968).
- 86 Carrasco, Y. R. & Batista, F. D. B cells acquire particulate antigen in a macrophage-rich area at the boundary between the follicle and the subcapsular sinus of the lymph node. *Immunity* **27**, 160-171, doi:10.1016/j.immuni.2007.06.007 (2007).
- 87 Junt, T. *et al.* Subcapsular sinus macrophages in lymph nodes clear lymph-borne viruses and present them to antiviral B cells. *Nature* **450**, 110-114, doi:10.1038/nature06287 (2007).
- 88 Phan, T. G., Grigorova, I., Okada, T. & Cyster, J. G. Subcapsular encounter and complement-dependent transport of immune complexes by lymph node B cells. *Nature immunology* **8**, 992-1000, doi:10.1038/ni1494 (2007).
- 89 Drinker, C. K., Field, M. E. & Ward, H. K. The Filtering Capacity of Lymph Nodes. *The Journal of experimental medicine* **59**, 393-405 (1934).
- 90 Iannacone, M. *et al.* Subcapsular sinus macrophages prevent CNS invasion on peripheral infection with a neurotropic virus. *Nature* **465**, 1079-1083, doi:10.1038/nature09118 (2010).
- 91 Gonzalez, S. F. *et al.* Capture of influenza by medullary dendritic cells via SIGN-R1 is essential for humoral immunity in draining lymph nodes. *Nature immunology* **11**, 427-434, doi:10.1038/ni.1856 (2010).
- 92 Tamburini, B. A., Burchill, M. A. & Kedl, R. M. Antigen capture and archiving by lymphatic endothelial cells following vaccination or viral infection. *Nature communications* **5**, 3989, doi:10.1038/ncomms4989 (2014).
- 93 Itano, A. A. *et al.* Distinct dendritic cell populations sequentially present antigen to CD4 T cells and stimulate different aspects of cell-mediated immunity. *Immunity* **19**, 47-57 (2003).
- 94 Bleul, C. C., Fuhlbrigge, R. C., Casasnovas, J. M., Aiuti, A. & Springer, T. A. A highly efficacious lymphocyte chemoattractant, stromal cell-derived factor 1 (SDF-1). *The Journal of experimental medicine* **184**, 1101-1109 (1996).

- 95 Gunn, M. D. *et al.* A B-cell-homing chemokine made in lymphoid follicles activates Burkitt's lymphoma receptor-1. *Nature* **391**, 799-803, doi:10.1038/35876 (1998).
- 96 Gunn, M. D. *et al.* A chemokine expressed in lymphoid high endothelial venules promotes the adhesion and chemotaxis of naive T lymphocytes. *Proceedings of the National Academy of Sciences of the United States of America* **95**, 258-263 (1998).
- 97 Ngo, V. N., Tang, H. L. & Cyster, J. G. Epstein-Barr virus-induced molecule 1 ligand chemokine is expressed by dendritic cells in lymphoid tissues and strongly attracts naive T cells and activated B cells. *The Journal of experimental medicine* **188**, 181-191 (1998).
- 98 Forster, R. *et al.* CCR7 coordinates the primary immune response by establishing functional microenvironments in secondary lymphoid organs. *Cell* **99**, 23-33 (1999).
- 99 Bajenoff, M. *et al.* Stromal cell networks regulate lymphocyte entry, migration, and territoriality in lymph nodes. *Immunity* **25**, 989-1001, doi:10.1016/j.immuni.2006.10.011 (2006).
- 100 Forster, R. *et al.* A putative chemokine receptor, BLR1, directs B cell migration to defined lymphoid organs and specific anatomic compartments of the spleen. *Cell* **87**, 1037-1047 (1996).
- 101 Cremasco, V. *et al.* B cell homeostasis and follicle confines are governed by fibroblastic reticular cells. *Nature immunology* **15**, 973-981, doi:10.1038/ni.2965 (2014).
- 102 Denton, A. E., Roberts, E. W., Linterman, M. A. & Fearon, D. T. Fibroblastic reticular cells of the lymph node are required for retention of resting but not activated CD8+ T cells. *Proceedings of the National Academy of Sciences of the United States of America* **111**, 12139-12144, doi:10.1073/pnas.1412910111 (2014).
- 103 Link, A. *et al.* Fibroblastic reticular cells in lymph nodes regulate the homeostasis of naive T cells. *Nature immunology* **8**, 1255-1265, doi:10.1038/ni1513 (2007).
- 104 Estes, J. D., Haase, A. T. & Schacker, T. W. The role of collagen deposition in depleting CD4+ T cells and limiting reconstitution in HIV-1 and SIV infections through damage to the secondary lymphoid organ niche. *Seminars in immunology* **20**, 181-186, doi:10.1016/j.smim.2008.04.002 (2008).
- 105 Zeng, M. *et al.* Cumulative mechanisms of lymphoid tissue fibrosis and T cell depletion in HIV-1 and SIV infections. *The Journal of clinical investigation* **121**, 998-1008, doi:10.1172/JCI45157 (2011).
- 106 Mionnet, C. *et al.* Identification of a new stromal cell type involved in the regulation of inflamed B cell follicles. *PLoS biology* **11**, e1001672, doi:10.1371/journal.pbio.1001672 (2013).
- 107 Bannard, O. *et al.* Germinal center centroblasts transition to a centrocyte phenotype according to a timed program and depend on the dark zone for effective selection. *Immunity* **39**, 912-924, doi:10.1016/j.immuni.2013.08.038 (2013).
- 108 Cyster, J. G. *et al.* Follicular stromal cells and lymphocyte homing to follicles. *Immunological reviews* **176**, 181-193 (2000).



- 109 Wang, X. *et al.* Follicular dendritic cells help establish follicle identity and promote B cell retention in germinal centers. *The Journal of experimental medicine* **208**, 2497-2510, doi:10.1084/jem.20111449 (2011).
- 110 Katakai, T. Marginal reticular cells: a stromal subset directly descended from the lymphoid tissue organizer. *Frontiers in immunology* **3**, 200, doi:10.3389/fimmu.2012.00200 (2012).
- 111 Katakai, T. *et al.* Organizer-like reticular stromal cell layer common to adult secondary lymphoid organs. *Journal of immunology* **181**, 6189-6200 (2008).
- 112 Jarjour, M. *et al.* Fate mapping reveals origin and dynamics of lymph node follicular dendritic cells. *The Journal of experimental medicine* **211**, 1109-1122, doi:10.1084/jem.20132409 (2014).
- 113 Chai, Q. *et al.* Maturation of lymph node fibroblastic reticular cells from myofibroblastic precursors is critical for antiviral immunity. *Immunity* **38**, 1013-1024, doi:10.1016/j.immuni.2013.03.012 (2013).
- 114 Benedict, C. A. *et al.* Specific remodeling of splenic architecture by cytomegalovirus. *PLoS pathogens* **2**, e16, doi:10.1371/journal.ppat.0020016 (2006).
- 115 Cadman, E. T. *et al.* Alterations of splenic architecture in malaria are induced independently of Toll-like receptors 2, 4, and 9 or MyD88 and may affect antibody affinity. *Infection and immunity* **76**, 3924-3931, doi:10.1128/IAI.00372-08 (2008).
- 116 Glatman Zaretsky, A. *et al.* Infection with *Toxoplasma gondii* alters lymphotoxin expression associated with changes in splenic architecture. *Infection and immunity* **80**, 3602-3610, doi:10.1128/IAI.00333-12 (2012).
- 117 John, B. *et al.* Dynamic Imaging of CD8(+) T cells and dendritic cells during infection with *Toxoplasma gondii*. *PLoS pathogens* **5**, e1000505, doi:10.1371/journal.ppat.1000505 (2009).
- 118 Mueller, S. N. *et al.* Regulation of homeostatic chemokine expression and cell trafficking during immune responses. *Science* **317**, 670-674, doi:10.1126/science.1144830 (2007).
- 119 Mueller, S. N. *et al.* Viral targeting of fibroblastic reticular cells contributes to immunosuppression and persistence during chronic infection. *Proceedings of the National Academy of Sciences of the United States of America* **104**, 15430-15435, doi:10.1073/pnas.0702579104 (2007).
- 120 St John, A. L. & Abraham, S. N. Salmonella disrupts lymph node architecture by TLR4-mediated suppression of homeostatic chemokines. *Nature medicine* **15**, 1259-1265, doi:10.1038/nm.2036 (2009).
- 121 Scandella, E. *et al.* Restoration of lymphoid organ integrity through the interaction of lymphoid tissue-inducer cells with stroma of the T cell zone. *Nature immunology* **9**, 667-675, doi:10.1038/ni.1605 (2008).

- 122 Katakai, T. *et al.* A novel reticular stromal structure in lymph node cortex: an immuno-platform for interactions among dendritic cells, T cells and B cells. *International immunology* **16**, 1133-1142, doi:10.1093/intimm/dxh113 (2004).
- 123 Groom, J. R. *et al.* CXCR3 chemokine receptor-ligand interactions in the lymph node optimize CD4+ T helper 1 cell differentiation. *Immunity* **37**, 1091-1103, doi:10.1016/j.immuni.2012.08.016 (2012).
- 124 Woodruff, M. C. *et al.* Trans-nodal migration of resident dendritic cells into medullary interfollicular regions initiates immunity to influenza vaccine. *The Journal of experimental medicine* **211**, 1611-1621, doi:10.1084/jem.20132327 (2014).
- 125 Luther, S. A., Tang, H. L., Hyman, P. L., Farr, A. G. & Cyster, J. G. Coexpression of the chemokines ELC and SLC by T zone stromal cells and deletion of the ELC gene in the plt/plt mouse. *Proceedings of the National Academy of Sciences of the United States of America* **97**, 12694-12699, doi:10.1073/pnas.97.23.12694 (2000).
- 126 Hase, H. *et al.* BAFF/BLyS can potentiate B-cell selection with the B-cell coreceptor complex. *Blood* **103**, 2257-2265, doi:10.1182/blood-2003-08-2694 (2004).
- 127 Schmidt, T. H., Bannard, O., Gray, E. E. & Cyster, J. G. CXCR4 promotes B cell egress from Peyer's patches. *The Journal of experimental medicine* **210**, 1099-1107, doi:10.1084/jem.20122574 (2013).
- 128 Malhotra, D. *et al.* Transcriptional profiling of stroma from inflamed and resting lymph nodes defines immunological hallmarks. *Nature immunology* **13**, 499-510, doi:10.1038/ni.2262 (2012).
- 129 Girard, J. P., Moussion, C. & Forster, R. HEVs, lymphatics and homeostatic immune cell trafficking in lymph nodes. *Nature reviews. Immunology* **12**, 762-773, doi:10.1038/nri3298 (2012).
- 130 von Andrian, U. H. Intravital microscopy of the peripheral lymph node microcirculation in mice. *Microcirculation* **3**, 287-300 (1996).
- 131 Anderson, A. O. & Anderson, N. D. Studies on the structure and permeability of the microvasculature in normal rat lymph nodes. *The American journal of pathology* **80**, 387-418 (1975).
- 132 Fletcher, A. L. *et al.* Reproducible isolation of lymph node stromal cells reveals site-dependent differences in fibroblastic reticular cells. *Frontiers in immunology* **2**, 35, doi:10.3389/fimmu.2011.00035 (2011).
- 133 Sainte-Marie, G. & Peng, F. S. Diffusion of a lymph-carried antigen in the fiber network of the lymph node of the rat. *Cell Tissue Res* **245**, 481-486 (1986).
- 134 Berg, E. L., McEvoy, L. M., Berlin, C., Bargatze, R. F. & Butcher, E. C. L-selectin-mediated lymphocyte rolling on MAdCAM-1. *Nature* **366**, 695-698, doi:10.1038/366695a0 (1993).

- 135 Li, J. *et al.* Piezo1 integration of vascular architecture with physiological force. *Nature* **515**, 279-282, doi:10.1038/nature13701 (2014).
- 136 Ranade, S. S. *et al.* Piezo1, a mechanically activated ion channel, is required for vascular development in mice. *Proceedings of the National Academy of Sciences of the United States of America* **111**, 10347-10352, doi:10.1073/pnas.1409233111 (2014).
- 137 Degn, S. E., Alicot, E. & Carroll, M. C. B cell tolerance to epidermal ribonuclear-associated neo-autoantigen in vivo. *Clin Exp Immunol* **191**, 151-165, doi:10.1111/cei.13066 (2018).
- 138 Astarita, J. L. *et al.* The CLEC-2-podoplanin axis controls the contractility of fibroblastic reticular cells and lymph node microarchitecture. *Nature immunology* **16**, 75-84, doi:10.1038/ni.3035 (2015).
- 139 Cohen, J. N. *et al.* Lymph node-resident lymphatic endothelial cells mediate peripheral tolerance via Aire-independent direct antigen presentation. *The Journal of experimental medicine* **207**, 681-688, doi:10.1084/jem.20092465 (2010).
- 140 Fletcher, A. L. *et al.* Lymph node fibroblastic reticular cells directly present peripheral tissue antigen under steady-state and inflammatory conditions. *The Journal of experimental medicine* **207**, 689-697, doi:10.1084/jem.20092642 (2010).
- 141 Katakai, T., Hara, T., Sugai, M., Gonda, H. & Shimizu, A. Lymph node fibroblastic reticular cells construct the stromal reticulum via contact with lymphocytes. *The Journal of experimental medicine* **200**, 783-795, doi:10.1084/jem.20040254 (2004).
- 142 Lukacs-Kornek, V. *et al.* Regulated release of nitric oxide by nonhematopoietic stroma controls expansion of the activated T cell pool in lymph nodes. *Nature immunology* **12**, 1096-1104, doi:10.1038/ni.2112 (2011).
- 143 Moe, R. E. Fine Structure of the Reticulum and Sinuses of Lymph Nodes. *Am. J. Anat.* **110**, 217-257 (1963).
- 144 Gretz, J. E., Kaldjian, E. P., Anderson, A. O. & Shaw, S. Sophisticated strategies for information encounter in the lymph node: the reticular network as a conduit of soluble information and a highway for cell traffic. *Journal of immunology* **157**, 495-499 (1996).
- 145 Rantakari, P. *et al.* The endothelial protein PLVAP in lymphatics controls the entry of lymphocytes and antigens into lymph nodes. *Nature immunology* **16**, 386-396, doi:10.1038/ni.3101 (2015).